



Terms and Conditions of Use of Digitised Theses from Trinity College Library Dublin

Copyright statement

All material supplied by Trinity College Library is protected by copyright (under the Copyright and Related Rights Act, 2000 as amended) and other relevant Intellectual Property Rights. By accessing and using a Digitised Thesis from Trinity College Library you acknowledge that all Intellectual Property Rights in any Works supplied are the sole and exclusive property of the copyright and/or other IPR holder. Specific copyright holders may not be explicitly identified. Use of materials from other sources within a thesis should not be construed as a claim over them.

A non-exclusive, non-transferable licence is hereby granted to those using or reproducing, in whole or in part, the material for valid purposes, providing the copyright owners are acknowledged using the normal conventions. Where specific permission to use material is required, this is identified and such permission must be sought from the copyright holder or agency cited.

Liability statement

By using a Digitised Thesis, I accept that Trinity College Dublin bears no legal responsibility for the accuracy, legality or comprehensiveness of materials contained within the thesis, and that Trinity College Dublin accepts no liability for indirect, consequential, or incidental, damages or losses arising from use of the thesis for whatever reason. Information located in a thesis may be subject to specific use constraints, details of which may not be explicitly described. It is the responsibility of potential and actual users to be aware of such constraints and to abide by them. By making use of material from a digitised thesis, you accept these copyright and disclaimer provisions. Where it is brought to the attention of Trinity College Library that there may be a breach of copyright or other restraint, it is the policy to withdraw or take down access to a thesis while the issue is being resolved.

Access Agreement

By using a Digitised Thesis from Trinity College Library you are bound by the following Terms & Conditions. Please read them carefully.

I have read and I understand the following statement: All material supplied via a Digitised Thesis from Trinity College Library is protected by copyright and other intellectual property rights, and duplication or sale of all or part of any of a thesis is not permitted, except that material may be duplicated by you for your research use or for educational purposes in electronic or print form providing the copyright owners are acknowledged using the normal conventions. You must obtain permission for any other use. Electronic or print copies may not be offered, whether for sale or otherwise to anyone. This copy has been supplied on the understanding that it is copyright material and that no quotation from the thesis may be published without proper acknowledgement.

**SYNTHETIC AMORPHOUS SILICA NANOPARTICLES
INDUCE HUMAN ENDOTHELIAL CELL INFLAMMATION
AND PLATELET AGGREGATION: ROLE OF NF- κ B AND
REACTIVE NITROGEN SPECIES**

by

Juan José Corbalán-Peñas

Being a thesis submitted for the degree of
Doctor of Philosophy (Pharmacology)

at

**University of Dublin
Trinity College**



Under the supervision and direction of

Dr Carlos Medina and Professor Marek W. Radomski

School of Pharmacy and Pharmaceutical Sciences

Trinity College Dublin

Thursday, August 26th, 2010 (Submission)

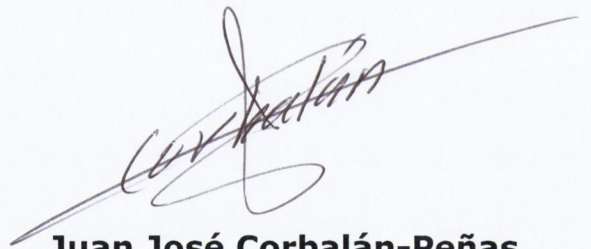
Thursday, October 7th, 2010 (Viva voce)



Thesis 9349

DECLARATION

This thesis is submitted by the undersigned to the University of Dublin, Trinity College, for examination for the degree of Doctor of Philosophy. It has not been submitted as an exercise for a degree at this or any other University. I have carried out all the practical work except where duly acknowledged. I agree that the library may lend or copy this thesis upon request.

A handwritten signature in black ink, appearing to read 'Juan José Corbalán-Peñas', written in a cursive style with a long horizontal stroke extending to the right.

Juan José Corbalán-Peñas

*To my wife, Isabel María Morales-Gabarrón, for leaving
everything in Spain and moving with me first to England
(County Norfolk), later to Scotland (Edinburgh), and
finally to Ireland (Dublin) in chase of my dream: science
and teaching. I love you Isabella!*

*In loving memory of my grandma, Concepcion García-
Pérez (1925 - 2005), and my grandpa, Juan Corbalán-
Paco (1919 - 2010)*

*'The most important thing is not to stop
questioning' Albert Einstein (1897 - 1955)*

'It matters if you just don't give up' Stephen

Williams Hawking

TABLE OF CONTENTS

ACKNOWLEDGEMENTS.....	i
SUMMARY	iv
LIST OF ABBREVIATIONS.....	vi
INTRODUCTION	1
NANOTECHNOLOGY, NANOMEDICINE, AND NANOTOXICOLOGY.....	1
EXPOSURE OF HUMANS TO NANOPARTICLES	6
INHALATION.....	8
INGESTION AND SKIN APPLICATION.....	11
OVERVIEW OF DIFFERENT CLASSES OF NANOPARTICLES	12
SILICA.....	15
PROPERTIES OF AMORPHOUS SILICA NANOPARTICLES.....	24
EYJAFJALLAJÖKULL VOLCANIC SYSTEM.....	24
LEGISLATION ON AMORPHOUS SILICA.....	25
ENDOTHELIUM.....	27
INFLAMMATION AND IMMUNITY	29
INNATE IMMUNITY IN BRIEF	29
ADAPTATIVE IMMUNITY IN BRIEF	32
INFLAMMATORY RESPONSE.....	34
NUCLEAR FACTOR κ B (NF- κ B).....	41
INTERCELLULAR ADHESION MOLECULE I (ICAM1).....	42
VASCULAR CELL ADHESION MOLECULE I (VCAM1).....	43
SELECTINS.....	44
MATRIX METALLOPROTEINASES (MMPs).....	45
PROSTAGLANDIN H SYNTHASES (PTGS) OR CYCLOOXIGENATES (COX).....	46

COAGULATION FACTOR 3 (F3, TISSUE FACTOR).....	47
INTERLEUKIN 6 (IL6).....	48
INTERLEUKIN 8 (IL8).....	49
PLATELETS	50
OXIDATIVE STRESS.....	55
THE [NO]/[ONOO-] BALANCE.....	56
ATHEROSCLEROSIS.....	57
AIMS OF THE PROJECT	61
MATERIALS AND METHODS	63
REAGENTS.....	63
SILICA NANOPARTICLES	63
NANOPARTICLE CHARACTERIZATION	63
CELL CULTURE.....	64
EXPOSURE OF CELLS TO NANOPARTICLES.....	64
PHASE-CONTRAST MICROSCOPY.....	65
PLATELET AGGREGATION STUDIES	65
TRANSMISSION ELECTRON MICROSCOPY (TEM).....	67
CYTOTOXICITY	70
FREE RADICAL DETECTION	72
NITRIC OXIDE (NO) AND PEROXYNITRITE (ONOO ⁻) DETECTION BY NANOSENSORS	73
NANOSENSOR DESIGN	73
STUDIES IN CELLS.....	75
STUDIES IN PLATELETS.....	76

NUCLEAR FACTOR $\kappa\beta$ (NF- $\kappa\beta$) ACTIVITY MEASUREMENT.....	76
NUCLEAR PROTEIN EXTRACTION	76
MEASUREMENT OF NF- κ B (p65) DNA BINDING ACTIVITY	77
REAL-TIME QUANTITATIVE PCR (qPCR).....	78
CYTOMETRIC BEAD ARRAY (CBA)	80
FLOW CYTOMETRY	81
SELECTIN P (SELP) ANALYSES	82
GPIIb/IIIa ANALYSES	82
STATISTICAL ANALYSES	83

RESULTS	84
CHARACTERIZATION OF AMORPHOUS SILICA NANOPARTICLES	84
AMORPHOUS SILICA NANOPARTICLES INDUCE MORPHOLOGY CHANGES IN HUVEC PRIMARY CELLS.....	86
UPTAKE OF AMORPHOUS SILICA NANOPARTICLES BY HUVEC PRIMARY CELLS.....	87
AMORPHOUS SILICA NANOPARTICLES INDUCE CYTOTOXICITY.....	89
AMORPHOUS SILICA NANOPARTICLES INDUCE HUVEC PRIMARY CELLS TO PRODUCE FREE RADICALS	92
AMORPHOUS SILICA NANOPARTICLES STIMULATE HUVEC PRIMARY CELLS TO RELEASE NO AND ONOO ⁻	94
AMORPHOUS SILICA NANOPARTICLES INDUCE NF- κ B BINDING ACTIVITY IN HUVEC PRIMARY CELLS.....	98
AMORPHOUS SILICA NANOPARTICLES INDUCE GENE EXPRESSION OF ICAM1, VCAM1, SELE, MMP9, PTGS2, F3, IL6, and IL8.....	100
AMORPHOUS SILICA NANOPARTICLES INDUCE RELEASE OF THE CYTOKINES IL6 AND IL8.....	111
UPTAKE OF AMORPHOUS SILICA NANOPARTICLES BY HUMAN PLATELETS.....	115

AMORPHOUS SILICA NANOPARTICLES INDUCE GPIIb/IIIa ACTIVATION IN WASHED PLATELETS	117
AMORPHOUS SILICA NANOPARTICLES INDUCE SELP EXPRESSION IN WASHED PLATELETS	118
AMORPHOUS SILICA NANOPARTICLES INDUCE PLATELET AGGREGATION IN WASHED PLATELETS	120
EFFECTS OF AMORPHOUS SILICA NANOPARTICLES ON SELP IN PRP	122
EFFECTS OF AMORPHOUS SILICA NANOPARTICLES ON PLATELET AGGREGATION IN PRP	123
AMORPHOUS SILICA NANOPARTICLES STIMULATE HUMAN PLATELETS TO RELEASE NO AND ONOO ⁻ IN PRP	124
DISCUSSION	128
EFFECTS OF AMORPHOUS SILICA NANOPARTICLES IN HUMAN ENDOTHELIAL CELLS	132
EFFECTS OF AMORPHOUS SILICA NANOPARTICLES IN HUMAN PLATELETS	145
PHYSIOLOGICAL SIGNIFICANCE: A HYPOTHESIS	149
CONCLUSIONS	154
FUTURE DIRECTIONS	158
REFERENCES	160

ACKNOWLEDGEMENTS

I would like to express my sincere gratitude to both my supervisors **Professor Marek Radomski** and **Dr Carlos Medina** for giving me the great opportunity of launching my career in science working under their guidance. Thank you both very much for taking me on as your PhD student and for your willingness to teach me everything you know to make me a better scientist. Also, thanks a lot for giving me the opportunity to be involved in other projects of the group. I am very lucky to have had you both as my supervisors.

To **Professor Marek Radomski**, thanks a million for always having the door of your office open for me, for treating me always kindly, and for your wise advices and direction of my studies in the interesting and challenging field of the nanotoxicology. Also, thanks very much for suggesting Professor Tadeusz Malinski to take me on as a Post Doctoral Research Fellow for his lab.

To **Dr Carlos Medina**, thank you so much for all your help, wise advices, guidance, and support during my studies. Thank you also for always having your door open for me and treating me always kindly.

I would like to show my appreciation to **Professor Tadeusz Malinski** and **Dr Adam Jacoby** (Ohio University, Athens, Ohio, USA) for collaborating on our studies performing silica nanoparticle stimulate endothelial cells and platelets to release NO and ONOO⁻.

To **Professor Tadeusz Malinski**, thank you so much for always being very kind with me and answering as many questions as I had on your work. Also, thanks a lot for offering me a position of Post Doctoral Research Fellow for your lab.

A big thank you to **Dr Lidia Tajber** (Trinity College Dublin) for allowing me to use her zetasizer and helping me perform and understand my measurements.

Thanks a lot to **Dr Lorraine O'Driscoll** (Trinity College Dublin) for allowing me to use her NanoDrop® ND-1000 spectrophotometer and providing me with wise advices on my real-time qPCR studies.

I would like to thank **Mr Neal Leddy** (Centre for Microscopy and Analysis, Trinity College Dublin) for his advice and help with my transmission electron microscopy studies.

A big thank you to my fellow PhD students and friends **Dr Johannah McCarthy, Dr Aneta Radziwon-Balicka, Dr Maria Jose**

Santos-Martínez, and **Dr Alan Gaffney** for all their help, chats, tea breaks, and brainstorming. Also thanks to my lab mates and friends **Dr Ania Radomska**, **Dr Shona Harmon**, and **Dr Sibylle Endter**. Thank you all for making an incredible atmosphere in the lab!

Thanks to my summer student (2009), **Mr Dino Muravek**, and my SS project students (2009), **Ms Sinead Marie McManus** and **Mr Cormac Gearoid Spooner** for their hard work in the lab and for being so interested in my group's research. Good luck guys!

A big thank you to my parents, **Soledad Peñas-García** and **José Corbalán-Pérez**, and my sister, **María Cristina Corbalán-Peñas**, for their support and love from Spain. I would also like to mention the birth of my first niece **Laura Morales-Gallardo** (June 21st, 2010); congratulations to **Rosa** and **José**!

Finally, I would like to show my appreciation to **everybody in the School of Pharmacy and Pharmaceutical Sciences at Trinity College Dublin** for making me feel at home.

SUMMARY

Background and purpose: The human population has been exposed to nanoparticles (particles with nano-dimensions) throughout all its evolutionary process; however, this exposure has been increased since the industrial revolution in the XIX century. Indeed, engineered nanoparticles are already used in many industries (e.g. computing engineering, aerospace) and in a wide range of applications, from cosmetics and food to paints and batteries. Therefore, humans are being increasingly more exposed to different types of nanoparticles. Furthermore, purposeful use of nanoparticles in humans is also growing as drug delivery systems and other nanomedical and nanopharmaceutical applications are being developed. Amorphous silica nanoparticles are one of the most frequently used group of engineered nanoparticles. However, interactions of these nanoparticles with human cells and tissues as well as their pharmacological and toxicological effects have not been elucidated yet. Inhalation is the main portal of entry of nanoparticles to the body and this is followed by translocation of particles to the vascular system and to possible interactions with endothelial cells and platelets. Therefore, the main objective of my PhD research was to investigate the pharmacological and toxicological effects of amorphous silica nanoparticles on platelet and endothelial cell function.

Experimental approach: Human umbilical vein endothelial primary cells (HUVEC primary cells) were exposed to 10-nm, 50-nm, 150-nm, and 500-nm amorphous silica nanoparticles. Nanoparticle-endothelial cell interaction was studied by both phase-contrast microscopy and transmission electron microscopy (TEM). Cytotoxicity induced by nanoparticles was measured using a standard LDH assay procedure. Free radical production stimulated by nanoparticles was detected by a flourometric assay and nitric oxide (NO) and peroxynitrite (ONOO^-) specifically quantified by nanosensors. Nuclear factor κB (NF- κB) activity was measured by enzyme-linked immunosorbent assay (ELISA). Pro-inflammatory responses to nanoparticles were examined by real-time qPCR and flow cytometry. In addition, human platelets were also exposed to amorphous silica nanoparticles and their interaction studied

by TEM. Aggregation and platelet receptor expression as a response to nanoparticles were measured by aggregometry and flow cytometry.

Key results: I have demonstrated that synthetic amorphous silica nanoparticles (10 nm) are up-taken by HUVEC primary cells and localized mainly in vesicles in the endothelial cytoplasm. Moreover, 10-nm silica nanoparticles are cytotoxic for endothelial cells. The mechanism of this cytotoxicity may be related to high nitrosative stress as shown by massive production of ONOO⁻. This appears to severely damage cells and trigger off the induction of NF- κ B activity in those which survive. The increased activity of this transcription factor is associated with the inflammatory and coagulation responses as evidenced by up-regulation of intercellular adhesion molecule I (ICAM1), vascular cell adhesion molecule I (VCAM1), selectin E (SELE), matrix metalloproteinase 9 (MMP9), cyclooxygenase 2 (COX2), interleukin 6 (IL6), interleukin 8 (IL8), and tissue factor. Release of IL6 and IL8 from endothelial cells was also detected. In addition, I have shown that human platelets have the capacity to uptake silica nanoparticles leading to up-regulation of platelet receptors (GPIIb/IIIa and selectin-P) and stimulation of platelet aggregation, an effect also associated with increased generation of ONOO⁻. All noxious effects of amorphous silica nanoparticles in both endothelial cells and platelets seemed to be nanoparticle-size dependent.

Conclusions and implications: The exposure of endothelial cells and platelets to amorphous silica nanoparticles results in endothelial inflammation and platelet aggregation. These effects may contribute to potential toxicological effects of engineered amorphous silica nanoparticles in the vascular system.

LIST OF ABBREVIATIONS

Å	Angstrom (1 Å = 0.1 nm)
µm	micrometre(s) = 10 ⁻⁶ m, 10 ³ nm
10SiNP(s)	10-nm silica nanoparticle(s)
50SiNP(s)	50-nm silica nanoparticle(s)
150SiNP(s)	150-nm silica nanoparticle(s)
500SiNP(s)	500-nm silica nanoparticle(s)
AP1	Activator protein 1
APC(s)	Antigen-presenting cell(s)
Carboxy-H ₂ DFFDA	5-(and-6)-carboxy-2',7'- difluorodihydrofluorescein diacetate
cDNA	Complementary deoxyribonucleic acid
COX1	Cyclooxygenase 1; also, PTGS1
COX2	Cyclooxygenase 2; also, PTGS2
CP(s)	Coarse particle(s)
cPLA ₂	Cellular phospholipase A ₂
DNA	Deoxyribonucleic acid
eNOS	Endothelial nitric-oxide synthase; also, NOS3
ER	Endoplasmic reticulum
EU	European Union
F3	Coagulation factor 3; also, tissue factor
FP(s)	Fine Particle(s); also, PM _{2.5}
GPCR(s)	G-protein-coupled receptor(s)
HUVEC	Human umbilical vein endothelial cells
ICAM1	Intercellular adhesion molecule 1
IDL(s)	Intermediate-density lipoprotein(s)
IL(s)	Interleukin(s)
Ig	Immunoglobulin
iNOS	Inducible nitric-oxide synthase; also, NOS2
LDH	Lactate dehydrogenase
LDL(s)	Low-density lipoprotein(s)

LPC	Lysophosphatidylcholine
LPS	Lipopolysaccharide
MHC	Major histocompatibility complex
MMAD	Mass median aerodynamic diameter
MMP(s)	Matrix metalloproteinase(s)
MSR	Macrophage scavenger receptor
MWCNT(s)	Multi-walled carbon nanotube(s)
NF- κ B	Nuclear factor κ B
nm	nanometre(s) = 10^{-9} metres (m), 10^{-3} μ m
NNI	National Nanotechnology Initiative
nNOS	Neural nitric-oxide synthase; also, NOS1
NO	Nitric oxide
NOS1	Nitric-oxide synthase 1; also, nNOS
NOS2	Nitric-oxide synthase 2; also, iNOS
NOS3	Nitric-oxide synthase 3; also, eNOS
ONOO ⁻	Peroxynitrite
PAF	Platelet-activating factor
PAMP(s)	Pathogen-associated molecular pattern(s)
PC	Phosphatidylcholine
PGI ₂	Prostaglandin I ₂ ; also, prostacyclin
PM _{0.1}	Particulate matter < 0.1 μ m in MMAD; also, UFPs
PM _{2.5}	Particulate matter < 2.5 μ m in MMAD; also, FPs
PM ₁₀	Particulate matter < 10 μ m in MMAD; also, thoracic particles
PPP	Platelet-poor plasma
PRP	Platelet-rich plasma
PRR(s)	Pattern-recognition receptor(s)
PTGS1	Prostaglandin H synthase 1; also, COX1
PTGS2	Prostaglandin H synthase 2; also, COX2
qPCR	Quantitative polymerase chain reaction
RNA	Ribonucleic acid
RNS	Reactive nitrogen species
ROS	Reactive oxygen species

rRNA18S	ribosomal ribonucleic acid 18S
SELE	Selectin E; also, E selectin (ESEL), CD62E
SELP	Selectin P; also, P selectin (PSEL), CD62P
SEM	Standard error of the mean
SiO ₂	Silica, silicon (IV) oxide, silicon dioxide
SWCNT(s)	Single-walled carbon nanotube(s)
T-25 flask	25-cm ² -50-ml tissue culture flask
T-75 flask	75-cm ² -250-ml tissue culture flask
T _c	Cytotoxic T (cell)
TCR(s)	T-cell receptor(s)
TEM	Transmission electron microscopy
T _H	T helper (cell)
TLR(s)	Toll-like receptor(s)
TNF	Tumour necrosis factor
UFP(s)	Ultrafine particle(s); also, PM _{0.1}
UK	United Kingdom
USA	United States of America
UC	Untreated control (without nanoparticles)
VCAM1	Vascular cell adhesion molecule 1
vWF	von Willebrand factor
WHO	World Health Organization
WPB(s)	Weibel-Palade body (-ies)

INTRODUCTION

NANOTECHNOLOGY, NANOMEDICINE, AND NANOTOXICOLOGY

Nanotechnology [Greek *νᾶνος* (*nanos*) dwarf + Greek *τεχνολογία* (*tekhnologia*) systematic treatment] is defined by the United States of America (USA) National Nanotechnology Initiative (NNI) ¹ as 'the understanding and control of matter at dimensions between approximately 1 and 100 nanometres (nm), where unique phenomena enable novel applications'. A similar definition is given by the Community Research and Development Information Service (CORDIS) of the European Union (EU) ², which defines nanotechnology as 'the study of phenomena and fine-tuning of materials at atomic, molecular, and macromolecular scales, where properties differ significantly from those at a larger scale'. Nanotechnology is a scientific field encompassing many scientific disciplines such as chemistry, physics, engineering, and life sciences.

It is mostly accepted that the recent history of nanotechnology began with the speech 'There's Plenty of Room at the Bottom' ³, delivered by the American physicist Richard Phillips Feynman (**Figure 1**) in the California Institute of Technology (USA), on December 29th, 1959. In his talk, Professor Feynman, who received the Nobel Prize in Physics in 1965, recognized the great importance of miniaturization and strongly pointed out the need to explore 'the world at the bottom'. This beginning is not supported by everybody, as some

people believe than Professor Feynman's speech arose little enthusiasm as presented, and only became famous in the 1990s, when Kim Eric Drexler unearthed it to give credence to his own ideas⁴. Anyway, the idea of exploration of 'the world at the bottom' was under way.



Figure 1 | History of nanotechnology. Upper line, from left to right: Richard Phillips Feynman, born: 1918 (USA) – died: 1988; Gordon Earle Moore, born: 1929 (USA); Norio Taniguchi, born: 1912 (Japan) – died: 1999; Gerd Binnig, born: 1947 (Germany); Heinrich Rohrer, born: 1933 (Switzerland). Lower line, from left to right: Calvin F. Quate, born: 1923 (USA); Christoph Gerber (Switzerland); Kim Eric Drexler, born: 1955 (USA).

Miniaturization was seen as the future of computing engineering by Gordon Earle Moore (**Figure 1**), the co-founder of Intel Corporation. He observed that silicon chips (also known as integrated circuits, IC, or microchips) were undergoing a continual process of scaling downward, and made the prediction that 'the number of

transistors, and hence the processing power, that can be built onto a single silicon chip of a given area would double every 18 months for the next 10 years'. This prediction, which later was known as Moore's law, was published on April 19th, 1965 ⁵. Moore's law has continued far past the predicted 10 years, going from just over 2,250 transistors, and millimetres in size, in the original Intel 4004 (1971), which is considered the first microprocessor, to over 700,000,000 transistors, and 45 – 65 nm in size, in the Intel Core 2 (2006) ⁶.

The term nanotechnology was first coined by Professor Norio Taniguchi (**Figure 1**) in his article 'On the Basic Concept of 'Nano-Technology'' (1974) ⁷. He wrote: "Nano-technology' mainly consists of the processing of separation, consolidation, and deformation of materials by one atom or one molecule'. This initial concept of nanotechnology has suffered profound modifications until its current definition ⁴.

One of the most important boost for the development of nanotechnology was the invention of the atomic force microscope by Gerd Binnig, Calvin F. Quate and Christoph Gerber (1986) ⁸ (**Figure 1**). This type of microscopy enables the detection of atomic scale topographical features (from angstroms (Å) to 100 µm) on a wide range of insulating surfaces that include ceramic materials, biological samples, and polymers. This form of scanning probe microscopy, is an improvement of the original scanning tunneling microscope ⁹, which was first designed in 1982 by Gerd Binnig and Heinrich Rohrer

(**Figure 1**), who received the Nobel Prize in Physics in 1986 for its development.

The idea of nanotechnology was explored deeply by the American engineer Kim Eric Drexler (**Figure 1**), who promoted the technological significance of nano-scale phenomena and devices through several speeches and two books 'Engines of Creation: The Coming Era of Nanotechnology' (1986) ¹⁰ and 'Nanosystems: Molecular Machinery, Manufacturing, and Computation' (1992) ¹¹. Afterwards, nanotechnology acquired its current sense.

In 2001, President William Jefferson 'Bill' Clinton's administration (USA) raised nanotechnology to the level of a federal initiative. Today, the NNI, which gathers 25 nanotechnology-related federal agencies, has got a range of research, regulatory roles and responsibilities in nanotechnology. The proposed NNI budget for the fiscal year 2011 of \$1.76 billion will bring the cumulative investment of the USA government in nanotechnology since 2001 to nearly \$14 billion ¹.

In 2004, the EU proposed an integrated and responsible nanotechnology strategy for Europe. An action plan on nanoscience and nanotechnology was adopted in 2005. The budget of the EU for nanotechnology under the seventh framework programme (FP7) for research and technological development, running from 2007 to 2013, is €3.5 billion ¹².

In 2006, it was projected that nanotechnology worldwide would become a \$1 trillion market by 2015 ¹³.

A dynamic growth of nanotechnology and development of nanoparticles promise substantial societal benefits that may have a global economical and medical impact. Medicine may be a major beneficiary of nanotechnology, and **nanomedicine** (applications of nanotechnology in medicine) has become a very fast-growing and promising medical discipline. In its flagship document 'Nanomedicine: Nanotechnology for Health' (2006) ¹⁴ the EU envisages and encourages the development of nanomedicine particularly in the areas of diagnostics and imaging, targeted drug delivery systems (nanopharmacology and nanopharmaceutics) and regenerative medicine. To achieve these aims, nanotechnology strives to develop and combine new materials by precisely engineered atoms and molecules to yield new molecular assemblies on the scale of individual cells, organelles, or even smaller components, providing a personalized medicine ¹⁵⁻¹⁶. Personalized medicine is individualized or individual-based therapy, which allows the prescription of precise treatments best suited for a single patient ¹⁷. However, like most new technologies, including all nascent medicine and medical devices, there is a rising debate concerning the possible side effects derived from the use of particles at the nano-level.

The rapidly growing field studying the noxious consequences of the life matter-nanoparticle interaction is called **nanotoxicology**

[Greek *νᾶνος* (*nanos*) dwarf + Greek *τοξικός* (*toxicos*) poisonous + Greek *λόγος* (*logos*) reason]. Studies on toxicity of nanoparticles began as soon as a part of the scientific community realized the potential negative issues that the full introduction of nanoparticles in a daily bases, without precisely understanding their behaviour, might have for the health and the environment. Nanotoxicology is becoming increasingly important as nanotechnology is already applied in many disciplines and used in many applications; and consequently, exposure of humans and the environment to nanoparticles is a real issue. Moreover, nano-size allows nanoparticles potentially to reach any cell in the body. Furthermore, the same characteristics, which make nanoparticles desirable for their use in nanotechnology applications, also make them very reactive in the biological environment. However, consequences derived from live matter-nanoparticle interactions are not fully understood. All these concerns have led to general scientific thinking that nanoparticle use, as well as the applicability of nanotechnology, may ultimately be limited due to toxicity concerns ^{13,18-20}.

EXPOSURE OF HUMANS TO NANOPARTICLES

Humans have been exposed to nanoparticles throughout their evolution process. However, this exposure has been increased to a significant extent in the past two centuries because of the industrial revolution.

Nanoparticles may be formed in many natural processes such as volcanic emissions, sea spray and erosion (**nano-objects**), and/or as by-products of combustion, industrial manufacturing, construction and demolition activities, farming, and other human activities (**incidental nanoparticles**), and/or they are purposefully manufactured with nano-dimensions (**engineered nanoparticles**). Using the classical nanotechnology definition, engineered nanoparticles are such categorized, when at least one of their dimensions is between 1 and 100 nm. However, from the pharmaceutical point of view, particles are categorized as nanoparticles when at least one of their dimensions is less than 1000 nm. Nanoparticles have specific physicochemical properties different to bulk materials of the same composition and such properties make them very attractive for commercial and medical development ¹⁸.

Today, exposure of the human population to engineered nanoparticles may occur during production, storage, transportation, and consumer use ²¹. As nanotechnology is already being applied in aerospace, computing, robotic, and electronics, the release of high amounts of nanoparticles in an enclosed environment may be of great concern for workers ²². Engineered nanoparticles are already added to medicines, food, and cosmetics to improve their properties ²³, and they are being developed to be used as drug delivery systems ²⁴, and other medicine-related uses. Therefore, humans are exposed to

nanoparticles via **inhalation**, **ingestion** or **skin application**. This exposure may be unintended or purposeful.

INHALATION: The exposure of humans to pollutants via inhalation has been studied for years. Today, inhalation is the most studied route of entry of nanoparticles in the human body. Nanoparticles, including engineered nanoparticles, constitute a part of ambient airborne particulate matter (PM), which along with carbon monoxide, oxides of nitrogen, sulphates, sulphur dioxide, and lead are notably important environmental air pollutants. Humans, especially those inhabiting metropolitan and industrial areas, are exposed to them on a daily bases.

Ambient airborne PM, with a mass median aerodynamic diameter (MMAD) of less than 10 μm (PM_{10}), can be classified into 3 categories: **coarse particles** (CPs), with a MMAD between 2.5 and 10 μm ; **fine particles** (FPs), < 2.5 μm ($\text{PM}_{2.5}$) in MMAD; and **ultra-fine particles** (UFPs), < 0.1 μm ($\text{PM}_{0.1}$) in MMAD ²⁵ (**Figure 2**). Airborne PM_{10} is also known as '**thoracic particles**' because of the ability of these particles to deposit in the thoracic region of the respiratory system. In contrast, larger particles demonstrate a greater fractional deposition in the extrathoracic and upper tracheobronchial regions ²⁵. On the other hand, FPs are capable to deposit deep in the lung ^{18,25} and reach extrapulmonary tissues. It has been stated that a typical urban atmosphere can contain in the

region of 10^7 particles per cm^3 of air and that these particles in turn are less than 300 nm in MMAD ¹⁸.

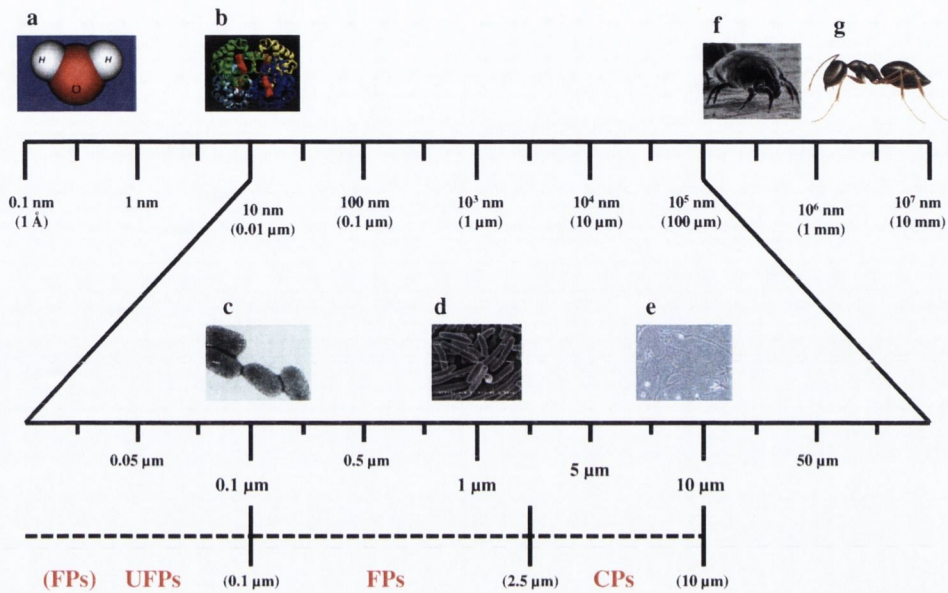


Figure 2 | Particle size on the ruler. The size ranges of the three categories of thoracic particles (UFPs, FPs, CPs) are compared with the sizes of well-known molecules, macromolecules, viruses, microorganisms, and organisms: **a**, water molecule ($\approx 3 \text{ \AA}$ in diameter); **b**, haemoglobin A ($\approx 6 \text{ nm}$ in diameter); **c**, rabies virus ($\approx 0.18 \times 0.075 \text{ }\mu\text{m}$); **d**, *Escherichia coli* ($\approx 0.5 \times 2 \text{ }\mu\text{m}$); **e**, endothelial cells ($\approx 8 - 12 \text{ }\mu\text{m}$); **f**, *Dermatophagoides pteronyssinus* (house dust mite; $\approx 420 \text{ }\mu\text{m}$ long); and **g**, ant ($\approx 2 - 25 \text{ mm}$ long).

The respiratory risks associated with severe air pollution exposure have long been known. Examples of effects of extreme exposure of the human population to ambient airborne PM are provided by the smog episodes in Meuse Valley, Belgium (1930) ²⁶; Donora, Pennsylvania, USA (1948) ²⁷; London, UK (1952) ²⁸; and World Trade Centre, New York, USA (2001) ²⁹. Especially in the last decade, there have been growing epidemiological, toxicological and clinical evidences that the exposure of the human population to fine

and ultra-fine particulate matter air pollution is a risk factor for the development of cardiac arrhythmia and arrest; as well as, for ischemic and thrombotic cardiovascular events, via exacerbation of atherosclerotic disease leading to myocardial infarction ³⁰⁻³³. Particulate matter exposure exacerbates cardiovascular diseases, as demonstrated by Mills, N.L. *et al.* (2007) ³⁴. In this study men, with stable coronary heart disease, were briefly exposed to diesel-exhaust particulate matter and an increased myocardial ischemia and impaired endogenous fibrinolytic capacity was observed. Interestingly, changes in the concentration of FPs in the respirable air affect life expectancy as shown by Pope, C.A. *et al* (2009) ³⁵. This epidemiological study showed that a 10- $\mu\text{g}/\text{m}^3$ reduction in the concentration of fine particulate matter in the respirable air was associated with an increased expectancy of 0.77 years. These results are in agreement with previous studies ³⁶⁻³⁸, in other countries, showing that a 10- $\mu\text{g}/\text{m}^3$ increase in FP concentration in the respirable air reduces life expectancy between approximately 0.80 and 1.37 years.

It is important to note that there is a great variability in the chemical composition of fine and ultra-fine particles in the air in both space and time, which is breathed daily by modern populations. Particles derived from combustion sources such as motor vehicles, e.g. carbon particles, will be in higher proportion in urban areas;

while, this ratio may change in rural or industrial areas. Therefore, it is crucial to know how different classes of particles affect humans.

INGESTION AND SKIN APPLICATION: Although, nanoparticles are being introduced in the food chain and added to cosmetics, very little is known on the exposure of humans to nanoparticles via ingestion and skin application. In 2008, a report by the Food Safety Authority of Ireland Scientific Committee ³⁹ concluded that nanomaterials are present in foods which are currently available on the market, mostly through internet trading. Main forms are inorganic nanoparticles (e.g. silica) to improve the properties of the final product and simple nanoscale encapsulated functional ingredients. Also, titanium dioxide and silica, but not carbon nanotubes, are used in packaging and may potentially migrate into food.

In 2008, other report (translated to English in 2009) ⁴⁰ this time by the Dutch National Institute for Public Health and the Environment reviewed the risks of use of engineered nanoparticles in medical applications and food production. As a specific nanoparticle may be hazardous, but if the level of exposure is very small, the ultimate risk will always be limited, they proposed that 'RISK = EXPOSURE x TOXICITY', where a number of factors determined both exposure (e.g. physicochemical properties and likelihood of contact) and toxicity (e.g. behaviour in the cellular environment and ability to

pass through certain physiological barriers). They also concluded that nanotechnology and nanoparticles, especially those which are tried to be applied in life sciences, were still largely in development; and in general, not yet applied on large scale, with the exception of carbon black, titanium dioxide and silica.

OVERVIEW OF DIFFERENT CLASSES OF NANOPARTICLES

Liposomes are nanoparticles comprising lipid bilayer membranes surrounding an aqueous interior (**Figure 3**). The amphiphilic molecules used for the preparation of these compounds are similar to biological membranes and have been used for improving the efficacy and safety of different drugs ⁴¹. Usually, liposomes are classified into three categories on the basis of their size and lamellarity (number of bilayers): small unilamellar vesicles or oligolamellar, large unilamellar vesicles and multilamellar vesicles. The active compound can be located either in the aqueous spaces, if it is water-soluble, or in the lipid membrane, if it is lipid-soluble. Recently, a new generation of liposomes called 'stealth liposomes' have been developed. Stealth liposomes have the ability to evade the interception by the immune systems, and therefore, have longer half-life ⁴².

Emulsions comprise oil-in-water type mixtures that are stabilized with surfactants to maintain their size and shape. The lipophilic material can be dissolved in a water organic solvent that is

emulsified in an aqueous phase. Like liposomes, emulsions have been used for improving the efficacy and safety of diverse compounds ⁴³.

Polymers such as polysaccharide chitosan nanoparticles (**Figure 3**) have been used for some time now as drug delivery systems ⁴⁴. Recently, water-soluble polymer hybrid constructs have been developed. These are polymer-protein conjugates or polymer-drug conjugates. Polymer conjugation to proteins reduces immunogenicity, prolongs plasma half-life and enhances protein stability. Polymer-drug conjugation promotes tumour targeting through the enhanced permeability and retention effect and, at the cellular level following endocytic capture, allows lysosomotropic drug delivery ⁴⁵.

Ceramic nanoparticles (**Figure 3**) are porous and non-porous potential biocompatible particles, such as silica, titania and alumina, that can be used in many applications in the nanotechnology field. Inorganic systems with porous characteristics have recently emerged as drug vehicles ⁴⁶. However, one of the main concerns is that these particles are non-biodegradable, as they can accumulate in the body, thus causing undesirable effects.

Metallic particles such as iron oxide nanoparticles (15 to 60 nm) generally comprise a class of superparamagnetic agents that can be coated with dextran, phospholipids, or other compounds to inhibit aggregation and enhance stability. The particles are used as passive or active targeting agents ⁴⁷.

Gold shell nanoparticles, other metal-based agents, are a novel category of spherical nanoparticles consisting of a dielectric core covered by a thin metallic shell, which is typically gold (**Figure 3**). These particles possess highly favourable optical and chemical properties for biomedical imaging and therapeutic applications ⁴⁸.

Carbon nanomaterials include fullerenes and nanotubes (**Figure 3**). Fullerenes are novel carbon allotrope with a polygonal structure made up exclusively by 60 carbon atoms. These nanoparticles have numerous points of attachment whose surfaces also can be functionalized for tissue binding ⁴⁹. Nanotubes have been one of the most extensively used types of nanoparticles because of their high electrical conductivity and excellent strength. Carbon nanotubes can be structurally visualised as a single sheet of graphite rolled to form a seamless cylinder. There are two classes of carbon nanotubes: single-walled (SWCNT) and multi-walled (MWCNT). MWCNT are larger and consist of many single-walled tubes stacked one inside the other. Functionalised carbon nanotubes are emerging as novel components in nano-formulations for the delivery of therapeutic molecules ⁵⁰.

Quantum dots are nanoparticles made of semiconductor materials with fluorescent properties. Crucial for biological applications quantum dots must be covered with other materials allowing dispersion and preventing leaking of the toxic heavy metals ⁵¹ (**Figure 3**).

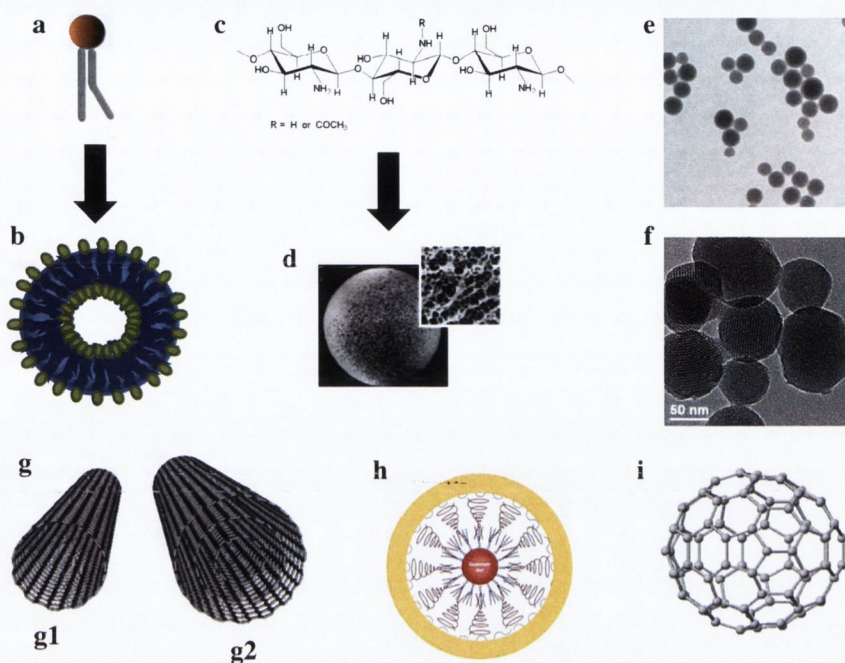


Figure 3 | Types of nanoparticles with applications in nanotechnology. Amphiphilic phospholipids (a) are used to synthesise liposomes (b) and polymers such as chitosan (i.e. chains of $\beta(1-4)$ -linked D-glucosamine and N-acetyl-D-glucosamine) (c) are used to make biodegradable porous nanoparticles (d). These and other classes of nanoparticles such as non-porous (e) and mesoporous porous (f) silica nanoparticles (ceramic nanoparticles), single- (g1) and multi-walled (g2) carbon nanotubes⁵², quantum dot (red) encapsulated in a gold shell⁵³ (h), and a fullerene (i) are important for nanotechnology applications.

SILICA

'Silica' is used as a short convenient designation for 'silicon dioxide' (also known as silicon (IV) oxide; chemical formula: SiO_2) in all its crystalline and amorphous forms. As deduced from its chemical formula, silica is formed by the metalloid or semimetal element silicon (Si) and the non-metal element oxygen (O). Silicon is the second most abundant component of the Earth's crust after oxygen, basically because it is in the composition of silica, which in

turn is by far the most abundant component. Silicon is essential for computing, electronic and hi-tech manufacturing. Pure silicon is employed to produce silicon wafers, doped with other elements such as boron and phosphorus, which are the base for transistor, integrated circuit, and microprocessor manufacturing. Pure silicon crystals are very rarely found in nature. Consequently, silicon used in industrial applications is obtained from high-purity silica. This fact makes silica highly appreciated and used in technology manufacturing. Silicon is produced in two grades of purity: ultra-pure silicon ($> 99.9\%$)⁵⁴ and highly purified or metallurgical grade silicon ($\geq 98\%$)⁵⁵.

Silicon normally occurs in various forms of silicon dioxide. Silica may have a crystalline or a non-crystalline (amorphous) structure. **Crystalline silica** may be found naturally in more than one form, depending of the orientation of its basic structural unit silicon tetrahedron (SiO_4) (**Figure 4**), which gives them specific crystal parameters. In crystalline silica, each silicon atom, within each tetrahedron, shares electrons with four oxygen atoms forming single covalent bonds; each oxygen atom is common to two tetrahedra, and the overall chemical formula is SiO_2 .

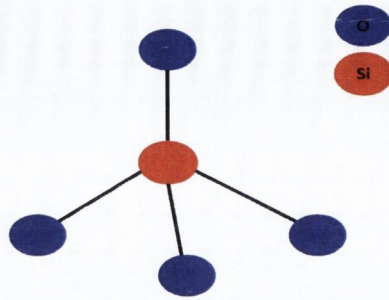


Figure 4 | Ball-and-stick model of silicon tetrahedron. Schematic representation of the silicon tetrahedron, which is characteristic of the silica crystalline structure.

By far the commonest crystalline silica form found in nature is quartz (**Figure 5**), which is the main constituent of common sand. Others naturally found forms are for example tridymite and cristobalite. Moreover, there are polymorphic forms of quartz, tridymite, and cristobalite, which are transformed spontaneously with temperature. Keatite, coesite, and stishovite are more crystalline silica forms, created under conditions of high temperature and pressure ⁵⁶. Silicon tetrahedron is also present in silicates minerals (e.g. olivine, micas minerals, clay, talc, feldspars), which are formed when elements such as sodium, potassium, calcium, magnesium, iron, and aluminium are substituted into the crystalline silica matrix.

The silicon tetrahedral unit, characteristic of crystalline silica, is not present in amorphous silica. **Amorphous silica** has also an overall chemical formula SiO_2 ; but its silicon and oxygen atoms are randomly linked, forming non-repeating patterns and therefore non-crystalline structure (**Figure 5**).

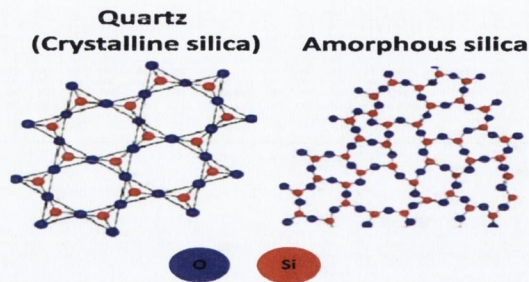


Figure 5 | Ball-and-stick representation comparing the crystalline and amorphous silica structure. Silicon tetrahedra, which are present in the crystalline silica structure, are not observed in the amorphous structure; this is crucial for their different structural characteristics.

Amorphous silica is naturally present in diatomite (also known as diatomaceous earth or kieselgur), a sedimentary rock composed of frustules (diatom cell walls); in turn, made of silica. It is also present in minerals such as flint and opal.

Synthetic (man-made) amorphous silica particles may be broadly divided into three types ⁵⁶:

- a. **Vitreous silica** (also known as **fused silica glass**), made by fusing quartz.
- b. **Silica M**, which is an amorphous silica formed when either amorphous or crystalline silica are irradiated with high speed neutrons.
- c. **Microamorphous silica**, which includes sols, gels, powders, and porous glasses, which generally consists of ultimate particles less than a micron in size or have a specific surface area greater than about $3 \text{ m}^2 \text{ g}^{-1}$. Silica sol may refer broadly either to polysilicic acid (oligomers)

or colloidal silica. The term 'colloidal silica' refers to stable dispersions, or sols, of discrete amorphous silica particles. By arbitrary definition, the term excludes solutions of polysilicic acid in which the polymer molecules or particles are so small (smaller than 1 – 2 nm) that they are not stable.

Basically, colloidal particles are an intrinsic part of systems in which finely matter (particles) is dispersed in a liquid or gas. Their size usually ranges from 1 nm to several tens of micrometres, thus covering a broad size domain ⁵⁷.

Microamorphous silica may be divided into three types ⁵⁶:

- i. **Microscopic sheets, ribbons, and fibre-like forms** obtained by special processes.
- ii. **Common amorphous forms** consist of ultimate spherical particles of SiO₂ less than 1 μm in diameter, the surface of which consists of anhydrous SiO₂ or SiOH groups (surface-hydrated silica). The term 'silanol' is used for any OH group attached to silicon (Si-OH) on the particle surface.
- iii. **Highly hydrated amorphous silica** in which most, if not all, of the silicon atoms each retains one or more hydroxyl group (OH) in the silica structure. This type, which is generally stable up to

60°C, seems to differ in solubility from the anhydrous or only surface-hydrated amorphous silica forms.

Two broad classes of common amorphous forms exist⁵⁶:

a. **Anhydrous amorphous silica** particles (e.g. 'pyrogenic' or 'fumed' silicas) are formed at very high temperature and recovered from the gas phase as voluminous, extremely finely divided powders. When water vapour is present in the surface of these particles, their surfaces may be partly hydrated as SiOH groups. For fumed silica, the fraction of the surface silicon atoms that bear the OH groups falls between 0.25 and 0.5 (every second or third atom)⁵⁸ (**Figure 6**). These particles are made in one of the following ways:

- i. Vaporizing silicon dioxide in an arc or plasma jet and condensing it in a stream of dry inert gas.
- ii. Oxidizing the more volatile silicon monoxide in the vapour phase with air and condensing the SiO₂.
- iii. Oxidizing silicon compounds (e.g. SiH₄, SiCl₄, HSiCl₃) in the vapour state with dry oxygen or a hydrocarbon flame.

The so-called Aerosil particles are made by condensation of silica from the vapour phase at elevated temperature.

b. **Surface-hydroxylated amorphous silica** particles are nucleated and grown from aqueous solution supersaturated with monosilicic acid (also known as orthosilicic acid; chemical formula: $\text{Si}(\text{OH})_4$). If the concentration of $\text{Si}(\text{OH})_4$ exceeds about 2×10^{-3} M, condensation to polysilicic acids ('active' silica) occurs and colloidal particles are formed. This form of silica presents fully hydroxylated surfaces (**Figure 6**).

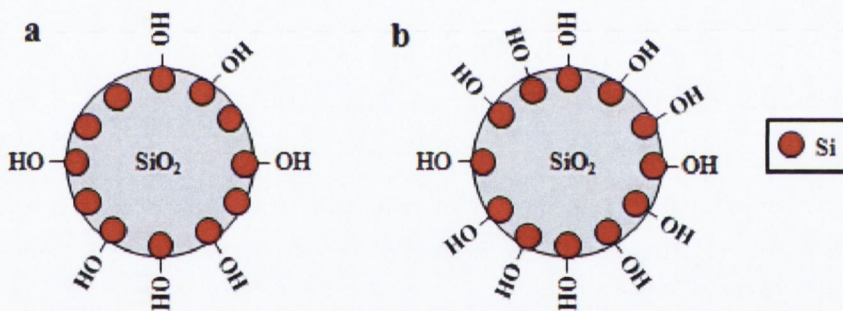


Figure 6 | Amorphous silica particles with hydroxylated surfaces. Representative surfaces of fumed (a) and surface-hydroxylated (b) of amorphous silica particles. Distribution of silicon and oxygen atoms into the amorphous structure of these particles is represented in figure 5.

The very weak monosilicic acid, which exists only in dilute aqueous solution, has never been isolated, since it polymerizes when it is concentrated. However, it can be prepared by dissolving amorphous or crystalline silica in acid, hydrolysing monomeric silicon compounds, and dissolving silicates in acid.

In summary, non-porous precipitated silica particles are synthesized by acidifying amorphous or crystalline silica. In nearly all commercial processes, sulfuric acid is used as the acid source. Under standard conditions, silica solution and the acid are fed simultaneously in a stirred vessel containing water. This is followed by precipitation, which is performed under alkaline conditions. The choice of agitation during precipitation, the addition rate of reactants, the temperature and the pH can vary the properties of the silica. In the next stage, the precipitated silica slurry is washed to remove soluble salts and other contaminants. The resultant filter cake is then dried commonly by spray drying and rotary drying. The dried silica is now subject to milling and classifying steps to obtain a specific particle size distribution. Precipitated amorphous silica particles may commercialize as dried powders or in watery suspensions.

Except for fused silica glass, the common forms of amorphous silica consist of extremely small particles of amorphous silicon dioxide, the surface of which is partly or totally hydrated as OH groups; the presence of which increase particle solubility.

Primary amorphous silica particles obtained are generally non-porous if formed or grown in alkaline solution and especially if formed

at elevated temperature, either above 60°C in aqueous solution or condensing from the gas phase at very high temperature.

Once synthesized, particles are quantified and characterized. It is important to note that any particle submerged in water has a hydration layer surrounding its surface. On the other hand, a particle submerged in a protein solution presents a 'protein corona', constituted by proteins around its surface⁵⁹ (**Figure 7**). These layers hydrodynamically move with the particle and are responsible for some effects observed in particle behaviour (e.g. aggregation). They must be taken into account when particles are characterized, for instance when particles properties (e.g. size) are measured by certain techniques (e.g. zetasizer).

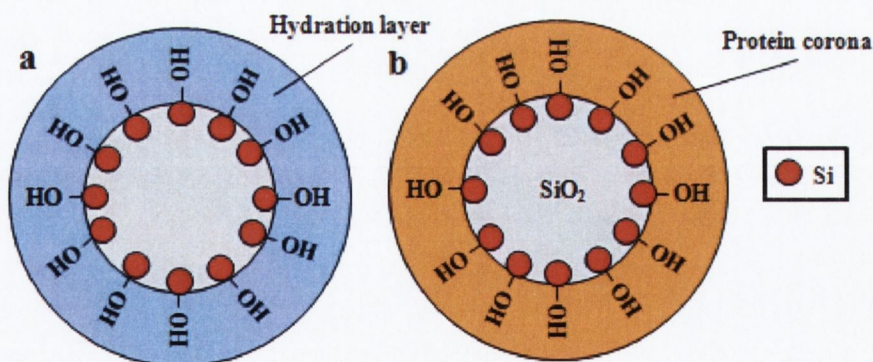


Figure 7 | Hydration layer and protein corona on the surface of particles submerged in water or a protein solution respectively. This figure shows a representative hydration layer (a) and protein corona (b) surrounding the surface of surface-hydroxylated amorphous silica particles.

PROPERTIES OF AMORPHOUS SILICA NANOPARTICLES:

Amorphous silica nanoparticles, especially those with dimensions between 1 to 100 nm, show high surface-area-to-volume ratio, large negative surface charge under both neutral and basic conditions, relatively high solubility in water, silanol surface groups (if it is not modified), and very small ultimate particle size. They also have a relatively low cost of preparation. All these striking characteristics make them very attractive to be used in many industries, such as computing, pharmaceutical, and food; and are available for various applications such as cellophane film, paper, textiles, tyres, footwear, printing ink, grass fibre, paints, cosmetics (beauty cream and sunscreen), condoms, batteries, toothpaste, desiccant, glass-ceramic hobs, and polishing. Modification of final surface characteristics and other physicochemical properties allow the use of synthetic amorphous silica nanoparticles in even a larger range of applications.

EYJAFJALLAJÖKULL VOLCANIC SYSTEM: A recent case of high exposure to natural amorphous silica particles (including nanoparticles) is provided by the eruptions of the Eyjafjöll volcano. In nature, amorphous silica nanoparticles can either be condensing from the vapour phase ejected in volcanic eruptions or deposited from supersaturated solution in natural waters or living organisms ⁵⁶. In the late evening of March 20th, 2010, a volcanic eruption occurred in southern Iceland at the Eyjafjallajökull volcanic system (also

known as Eyjafjöll volcano; Global Volcanism Program Volcano number 1702-02=). The volcanic ash cloud, produced as consequence of this volcano activation, caused the biggest disruptions and economical lost in European aerospace history. This cloud also meant important health concerns derived from the exposure of humans (especially Icelandic people) to the ash particulate component. On April 16th, 2010, the World Health Organization (WHO) Regional Office for Europe stated that 'the volcanic PM₁₀, which constitutes about 25% of the volcanic ash, could be expected to have health effects, which are likely to be minimal, if ash reaches ground level from the upper atmosphere; people with chronic respiratory conditions such as asthma, emphysema or bronchitis may be more susceptible to irritation'. Chemical studies of the volcano by the Icelandic Institute of Earth Sciences showed that silica was present in high proportion in volcanic ash, scoria, and rocks; as well as in lava. Therefore, it is most likely that the ambient airborne was enriched in amorphous silica particles after this volcanic eruption.

LEGISLATION ON AMORPHOUS SILICA: There is not an international legislation regulating exposure of humans to amorphous silica particles. However, due to its potential to cause health effects, a number of guidelines were established for the various forms of amorphous silica by various United States (US) agencies. The

American Conference of Governmental Industrial Hygienists (1993) imposed a threshold limit value (TLV) of 10 mg/m³ for a time-weighted average (TWA) of 8 hours (as total dust containing <1% crystalline silica) for precipitated and gel amorphous silica. So did a TLV of 0.1 mg/m³ (as respirable free silica) and 2 mg/m³ for 8-h TWA respectively for fused and fumed amorphous silica.

A report (1996) by the US-Environmental Protection Agency (EPA) ⁶⁰ on 'Ambient Level and Non-cancer Health Effects of Inhaled Crystalline and Amorphous Silica' concluded that no data on ambient air concentrations of amorphous silica were available, principally because methods of measurement used were not designed to deal with the large amounts of non-silica particles in ambient air. This report, along with another one by Merget *et al.* (2002) ⁶¹, also reported that few experimental toxicological studies were available to ensure whether amorphous silica was or was not toxic to human.

In 2004, the United Nation's Organization for Economic Co-operation and Development released the 'Screening Information Data Set for synthetic amorphous silica', and concluded that it had a low priority for further study. On the basis of this report, the US-EPA (2004) assumed that synthetic amorphous silica was not toxic. However, very soon this view was challenged with a number of contributions showing that synthetic amorphous silica nanoparticles exert noxious cardiopulmonary effects ⁶²⁻⁶³.

Humans are likely to be exposed to amorphous silica nanoparticles at least in close environments due to their high worldwide production volume and uses. Moreover, it is known that FPs show a great deposition in the deep lung ²⁵ and reach extrapulmonary tissues. Furthermore endothelium, blood, and other elements of the cardiovascular system have been shown to be targeted by nanoparticles ¹⁸.

ENDOTHELIUM

The **endothelium** (Greek *ἔνδον* (*endo*) within + Greek *θῆλῆ* nipple) is a simple squamous epithelium lining the interior surface of blood vessels. In an adult human being, approximately 10,000 billion endothelial cells constitute the endothelial tissue, which covers a surface area between 1 and 7 m², and weighs approximately 1 kilogram ⁶⁴. Endothelial cells comprise a continuous, but in some capillary vessels, layer of cells that is in direct contact with the blood components. Blood circulates into the human body through a network of different types of blood vessels (arteries, arterioles, capillaries, venules, and veins). Each blood vessel type has a specific vessel wall structure; but, the innermost layer of all of them is formed by a monolayer of endothelial cells. Arteries and veins are constituted by 3 morphologically distinct layers or 'tunicas': intima, media, and adventitia (**Figure 8**).

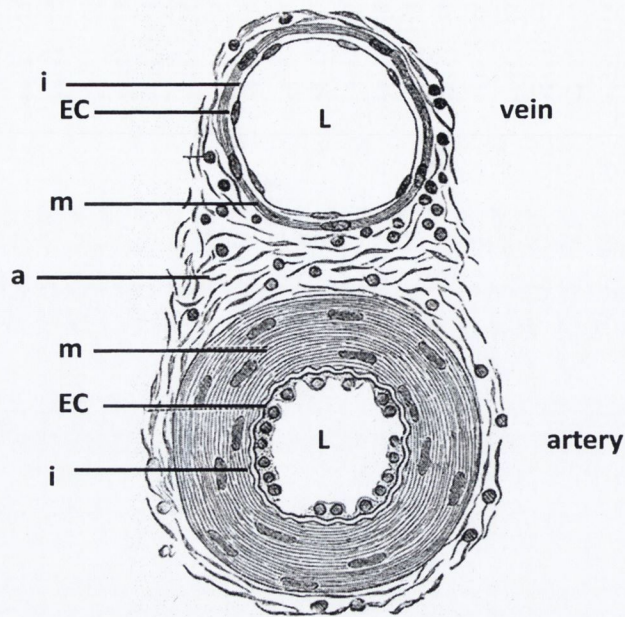


Figure 8 | Structure of a normal large vein and artery. Endothelium is in direct contact with blood components, followed by three layers that form the vessel wall (tunica intima, media, and adventitia). **EC**, endothelial cell; **i**, tunica intima; **m**, tunica media; **a**, tunica adventitia; **L**, blood vessel lumen. Adapted from Gray's Anatomy of the Human Body (1918).

The innermost layer, **tunica intima**, is bounded by the endothelium, on the luminal side and the internal elastic lamina, a sheet of elastic fibres, on the peripheral side. The normal intima is a very thin region and consists of an extracellular connective tissue matrix, primary proteoglycans and collagen. Infoldings of this tunica form the vein valves, which are necessary to keep blood flowing towards the heart, sometimes against the force of gravity; these valves are not present in arteries. The muscular middle layer, the **tunica media**, consists of smooth muscle cells. Arteries, mainly near the heart, have to bear by far higher pressure than veins without breaking apart; therefore, they pose a larger tunica media. The

tunica adventitia, the outer layer, consists of connective tissue with interspersed fibroblasts and smooth muscle cells.

Endothelial cells play a vital role in physiology and pathophysiology of the cardiovascular system; they are involved in maintenance of blood fluidity, control of vessel wall permeability, regulation of platelet activation, vascular contractility, and inflammation ⁶⁵.

INFLAMMATION AND IMMUNITY

Inflammation is a response of the body against infectious microbes or injured tissues, which can be acute (over a period of hours) or chronic, and involves recruitment of immune cells.

The **immune system** recognizes and destroys infectious pathogens. Vertebrates have two types of immunity: **innate** and **adaptive** (also known as acquired).

INNATE IMMUNITY IN BRIEF: Innate immune system is constituted by different types of cells: macrophages, dendritic cells, granulocytes (neutrophils, basophils, and eosynophils), natural killers, and mast cells; as well as, acellular elements: the complement system.

White and red cells differentiate from a common multi-potent haematopoietic stem cell progenitor in the bone marrow in a process called **haematopoiesis** ⁶⁶ (**Figure 9**).

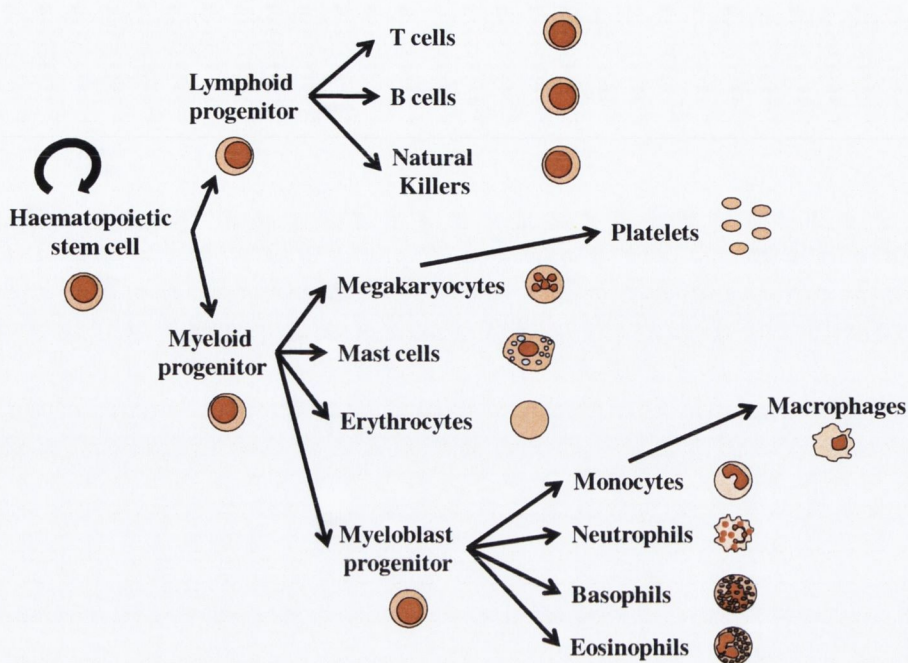


Figure 9 | Schematic representation of the haematopoiesis. Multi-potent hematopoietic stem cells, in the bone marrow, divide and differentiate into a common lymphoid or myeloid progenitor, which in turn differentiate into white and red cells. Platelets are formed from megakaryocytes. In tissue, macrophages differentiate from circulating peripheral-blood mononuclear cells (monocytes). Adapted from Rosmarin, A.G. *et al* (2005) ⁶⁶.

Innate immunity is mediated by pattern-recognition receptors (PRRs) that bind to pathogen-associated molecular patterns (PAMPs), which are present on and are unique to both pathogenic and non-pathogenic microorganisms. Each PRR has broad specificities for PAMPs and is germ-line encoded ⁶⁷. The best characterized PRRs are Toll-like receptors (TLRs) ⁶⁸. An extracellular leucine-rich repeat domain and an intracellular Toll/IL1 receptor domain characterize this family of receptors ⁶⁹⁻⁷⁰. These PRRs recognize, among other molecules, viral nucleic acids, Gram-negative cell wall component lipopolysaccharide (LPS), and Gram-positive cell wall component lipoteichoic acids. The first characterized mammalian TLR was TLR4,

which associates with MD2 (lymphocyte antigen 96) and CD14 to form a high affinity receptor for LPS. Beforehand, LPS must bind to the serum protein LPS-binding protein, which functions by transferring LPS monomer to CD14⁶⁸. Other examples of PRRs are Dectin 1, which recognizes the fungal cell wall component β -glucan, and the macrophage scavenger receptor (MSR), which recognizes LPS, double-stranded RNA, and oxidized lipoproteins; and is involved in atherosclerosis⁶⁸ (**Figure 10**).

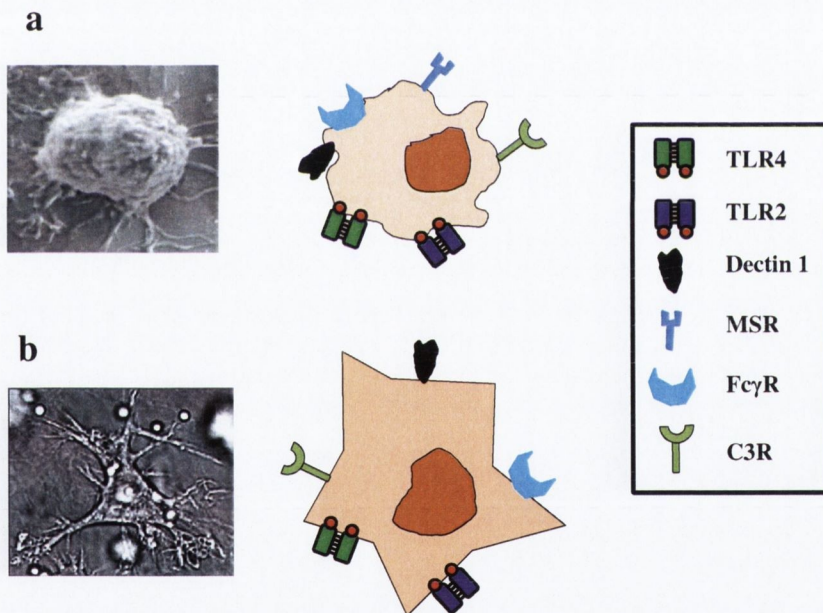


Figure 10 | Some important receptors of macrophages and dendritic cells. Pattern-recognition receptors (TLR4, TLR2, Dectin 1, and MSR) and other receptors (Immunoglobulin G (Ig G) γ receptor (Fc γ R); and C3a complement protein receptor, C3R) involved in responses of macrophages (**a**) and dendritic cells (**b**) to infection are shown.

Other cellular elements of the innate immune system such as natural killers are specialized in defence against intracellular pathogens, mainly viruses; while, eosinophils and basophils form a

host-defence module involved in protection against multicellular parasites, such as helminths ⁷¹.

It is important to note that pathogen discrimination by the innate immune system is not perfect and under certain conditions can result in development of autoimmune diseases ⁷².

ADAPTATIVE IMMUNITY IN BRIEF: Adaptive immune system, which is formed by T cells and B cells, is modulated by antigen receptors. Gene segments, encoding these receptors in the germ line, suffer a process of recombination-activating gene-protein-mediated somatic recombination, which enables the generation of a diverse repertoire of receptors with narrow specificities. Antigen receptors are clonally distributed on T and B lymphocytes allowing clonal selection of pathogen-specific receptors and is the basis for immunological memory ⁷³.

Conventional T cells, which have T-cell receptors (TCRs) constituted by α and β subunits, may be divided into: T helper (T_H) cells, which are marked by the co-receptor CD4 on the cell surface (**Figure 11**); and cytotoxic T (T_C) cells, which express CD8 (**Figure 12**); therefore, T_H cells are $CD4^+CD8^-$ and T_C cells are $CD8^+CD4^-$. Tolerant naive T cells from the thymus ⁷⁴ may differentiate to T_{H1} or T_{H2} (**Figure 11**).

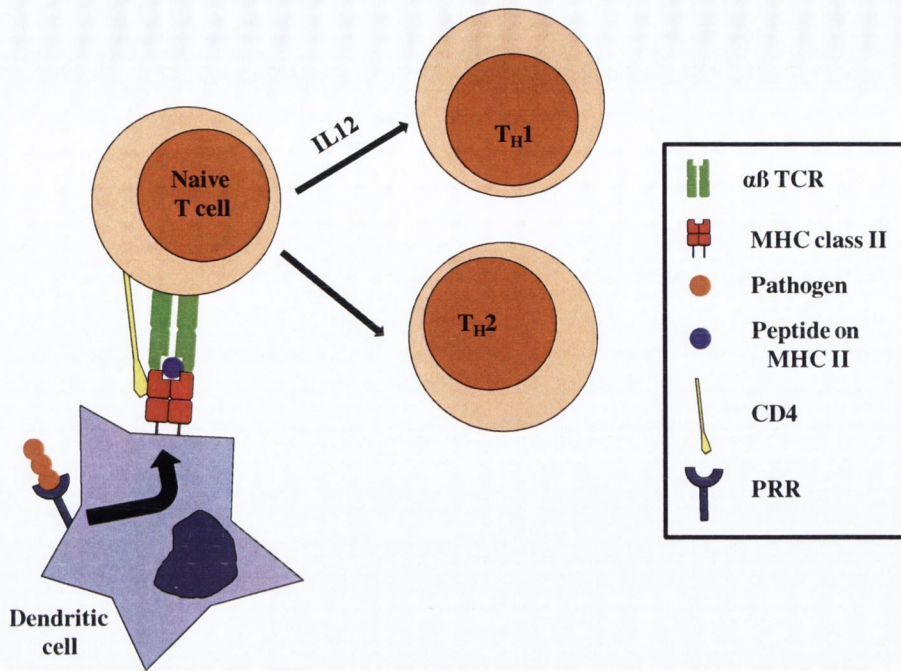


Figure 11 | Differentiation of naive T cells to T_H1 or T_H2 . After a PAMP is sensed via PRRs by a professional antigen-presenting cells (APCs) (e.g. dendritic cells or macrophages), it is internalized and processed. Some peptides from the pathogen are loaded on major histocompatibility complex (MHC) class II molecules and then expressed on the APC cell surface. Recognition by tolerant naive T cells, involving the TCR and CD4, induces differentiation to T_H1 or T_H2 depending of the protection needed. Certain cytokines are also involved. More receptors of APCs and T_H cells are involved in this differentiation. Adapted from Medzhitov, R. (2001) ⁶⁸.

T_H1 cells are involved in the protection against prokaryotic, viral and protozoan pathogens, while T_H2 cells are involved in protection against multicellular eukaryotic parasites, such as helminths. T_H1 cells synthesize IFN- γ and tumour-necrosis factor α (TNF- α), which potent the action of macrophages and activate endothelial cells ⁶⁸.

Cytotoxic T cells are involved in the protection against viruses and other cytoplasmatic pathogens ⁷⁵ (**Figure 12**).

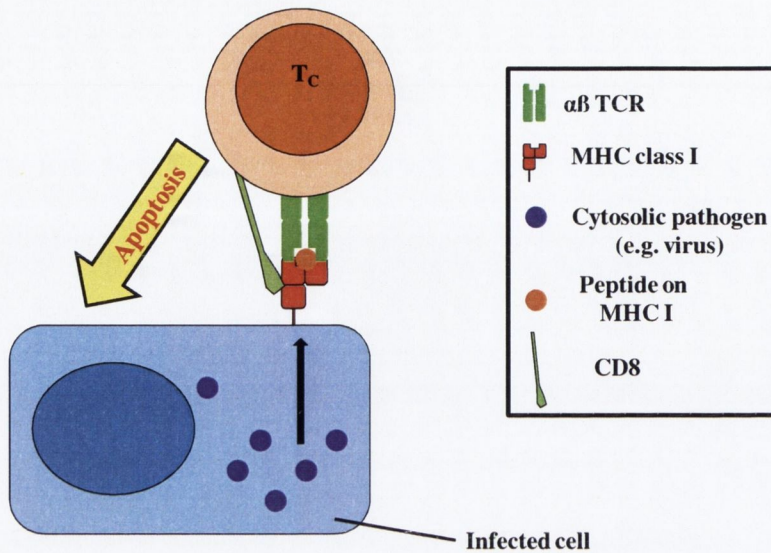


Figure 12 | Recognition and destruction of infected cells by T_C cells. Peptides from viruses or other cytoplasmic pathogens are presenting to T_C cells loaded on MHC class I molecules. These molecules are present in all nucleated cells of the human body. Recognition by T_C cells, involving TCR and CD8 receptors, induces apoptosis of the infected cell. More receptors are involved in this process.

Antigen recognition by B cells, and their activation, happens in secondary lymphoid organs (lymph nodes and spleen) ⁷⁶. B cell activation leading to antibody secretion occurs when B cells recognize peptide antigens presented on MCH class II by professional APCs macrophages and dendritic cells. B cells also are activated by recognition of soluble antigens and by the complement system ⁷⁶⁻⁷⁷.

INFLAMMATORY RESPONSE: In terms of inflammatory response, recognition of invading pathogens and/or altered host cells by components of the complement system initiate a proteolytic

cascade leading to generation of pro-inflammatory fragments such as C3a and C5a; as well as, the opsonization of the invaders by other fragments such as C3b, C4b and C5b ⁷⁷. This leads to elimination of the invader by cell lysis due to formation of membrane-attack complexes or phagocytosis (and elimination); as well as, mast cell stimulation. Activation or degranulation of mast cells, which have an effective sentinel role in the tissue, leads to release of cytokines TNF- α ⁷⁸⁻⁷⁹ and/or biogenic amine histamine ⁷⁹ (**Figure 13**).

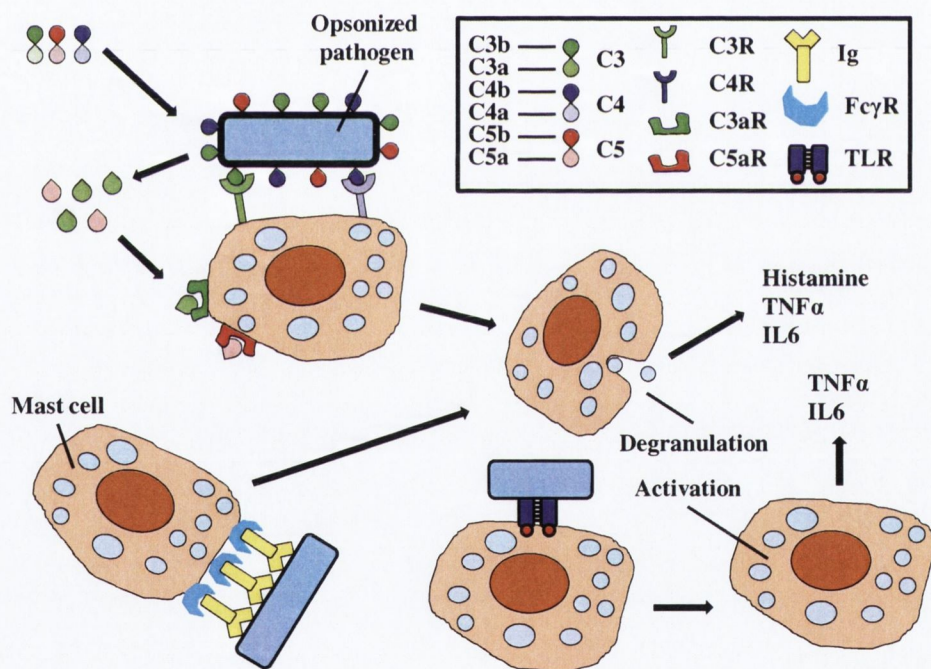


Figure 13 | Mast-cell responses. C3a and C5a (C3aR and C5aR respectively) as well as C3b and C4b (C3R and C4R respectively) bind their receptors on the surface of mast cells. This results in cell degranulation and release of cytokines and histamine. Degranulation is also produced by Fc-receptor-mediated activation. Cell activation, which leads to cytokine release rather than cell degranulation, is produced as mast cells sense pathogens via TLRs. Adapted from Marshall, J.S. (2004) ⁷⁹.

Macrophages are present in virtually all tissues. They differentiate from monocytes, which migrate into tissue in the steady state or in response to inflammation⁸⁰. Macrophages can sense pathogens via recognition of PAMPs by TLRs and/or other PRRs. This recognition induces macrophage activation leading to synthesis and release of TNF- α , interleukin-1 β (IL-1 β), interleukin-8 (IL-8) and interleukin-6 (IL-6)^{71,78}.

Histamine (from mast cells) and cytokines (from mast cells and macrophages) induce inflammatory responses in local endothelial cells, leading to leukocyte recruitment from the bloodstream to the site of infection to eliminate the stimulus, which triggered the inflammatory response. An inflammatory reaction (acute) is triggered when for instance histamine binds to the external domain of heterotrimeric G-protein-coupled receptors (GPCRs) histamine H1 on local endothelial cells. This leads to a cascade of events that produces expression of selectin P (SELP), von Willebrand factor (vWF), and platelet-activating factor (PAF) on the endothelial surface membrane; as well as, release of nitric oxide (NO) and prostaglandin I₂ (PGI₂; also known as prostacyclin) (**Figure 14**).

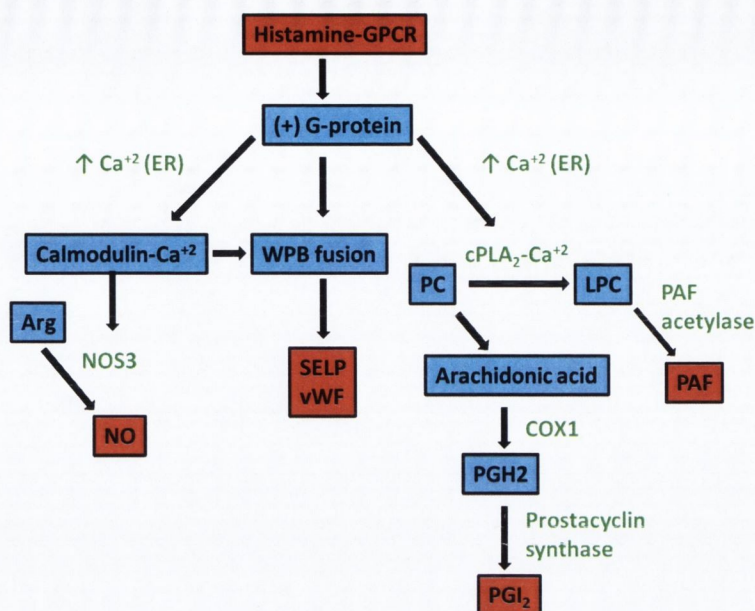


Figure 14 | Involvement of GPCRs in acute inflammation.

Mechanistically, histamine-GPCR binding induces G-protein activation leading to a transient increase of cytoplasmic Ca^{+2} from the endoplasmic reticulum (ER). A series of enzymatic reactions, initiated by the Ca^{+2} -calmodulin and G-proteins, ultimately leads to fusion of Weibel-Palade bodies (WPBs) ⁸¹ with the endothelial luminal membrane. This fusion results in expression of SELP and vWF. The Ca^{+2} -calmodulin also activates nitric-oxide synthase 3 (NOS3) which is the major form in endothelial cells. The NOS3 is one of the three forms of nitric-oxide synthases in cells: endothelial (eNOS or NOS3), inducible (iNOS or NOS2), and neural (nNOS or NOS1). The nNOS and eNOS are constitutively expressed and activated by calcium. The iNOS is calcium-independent and its synthesis is induced in endothelial cells during inflammation and other cell types by stimuli such as endotoxin and proinflammatory cytokines ⁸². The eNOS, which localizes primarily in the Golgi complex and plasma membrane caveolae, catalyzes NO synthesis from arginine (Arg). On the other hand, calcium-activated cellular phospholipase A_2 (cPLA₂) catalyzes the conversion of phosphatidylcholine (PC) into arachidonic acid and lysophosphatidylcholine (LPC). Then, the enzyme PAF acetylase catalyzes the conversion of LPC into PAF. Arachidonic acid, in a reaction catalyzed by cyclooxygenase 1 (COX1; also known as prostaglandin H (PGH) synthase 1 (PTGS1)), is converted into PGH₂. Finally, prostaglandin synthase transforms PGH₂ into PGI₂. Adapted from Pober, J.S. & Sessa, W.C. (2007) ⁶⁵.

Nitric oxide and PGI_2 , which are potent vasodilators, synergistically relax the smooth muscle vascular tone which allows a larger amount of blood reach this area. Histamine and IL8 ⁷⁸ attract neutrophils to the place of infection via chemotaxis. The combined display of SELP and PAF on the luminal endothelial membrane is involved in neutrophil tethering, rolling, and extravasation (diapedesis) into the infected tissue⁸³ (**Figure 15**). IL-6 is also involved in the recruitment of leukocytes⁸⁴. Signals by GPCRs last for 10–20 minutes, after which the receptors become desensitized, preventing restimulation⁸⁵. This is a quick response since it is independent of new gene expression.

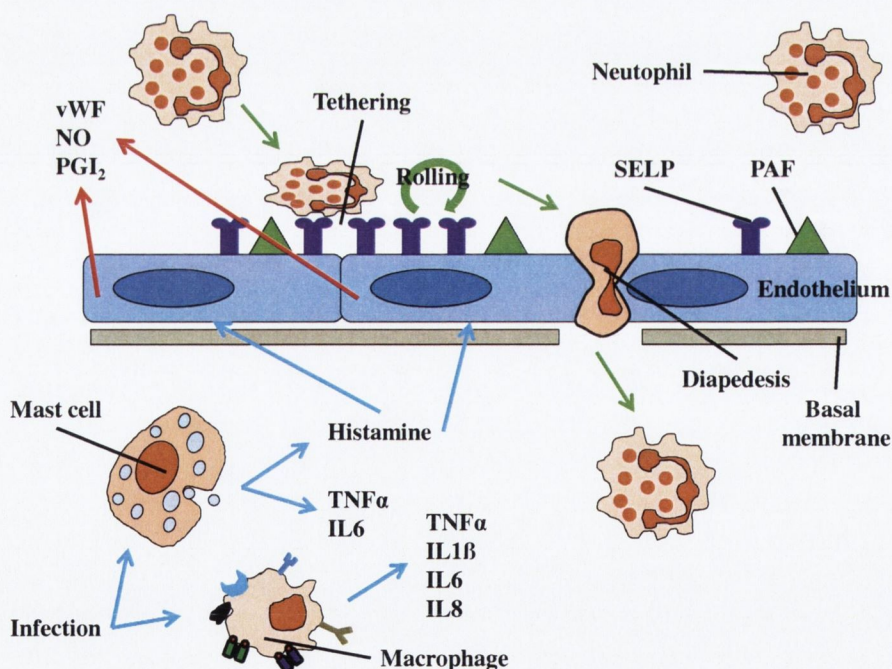


Figure 15 | Quick recruitment of neutrophils to the site of infection. Degranulation of mast cells leads to release of histamine and cytokines (**blue lines**). Binding of histamine to GPCRs induces release of NO , PGI_2 and vWF (**red lines**). SELP and PAF are expressed on the surface of endothelial cells leading to tethering, rolling, and extravasation of neutrophils from the bloodstream to the infectious tissue (**green lines**).

The cytokines TNF- α and IL-1 β , released from cells such as macrophages and mast cells, bind to their receptors on the plasma membrane of local endothelial cells triggering gene expression-dependent responses, which are slower than those of histamine. However, these responses are more sustained and programmed to evolve over time. Via a complex molecular mechanism, which involves activation of the transcription factors nuclear factor κ B (NF- κ B) and activator protein 1 (AP-1), ligand-receptor binding leads to gene expression of several genes such as intercellular adhesion molecule 1 (ICAM1), vascular cell adhesion molecule 1 (VCAM1), selectin E (SELE), matrix metalloproteinase 9 (MMP9), cyclooxygenase 2 (COX2; also known as prostaglandin H synthase 2 (PTGS2)), coagulation factor 3 (F3; also known as tissue factor), IL-6, and IL-8⁶⁵ (**Figure 16**).

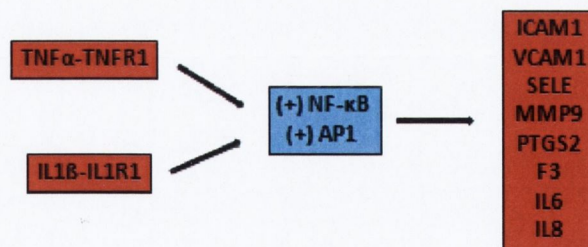


Figure 16 | Involvement of transcription factors in acute inflammation. TNF α -TNFR1 and IL1 β -IL1R binding produce, via NF- κ B and AP-1 activation, transcription of several genes such as *ICAM1*, *VCAM1*, *SELE*, *MMP9*, *PTGS2*, *F3*, *IL6*, and *IL8*. Messenger RNA (mRNA), obtained as a result of the transcription, is translated to proteins in the ribosomes. Adapted from Pober, J.S. & Sessa, W.C. (2007)⁶⁵.

Expression of inflammatory mediators leads to an exacerbation of the acute inflammatory response initiated by histamine allowing the innate immunity to eliminate the triggering stimulus (**Figure 17**).

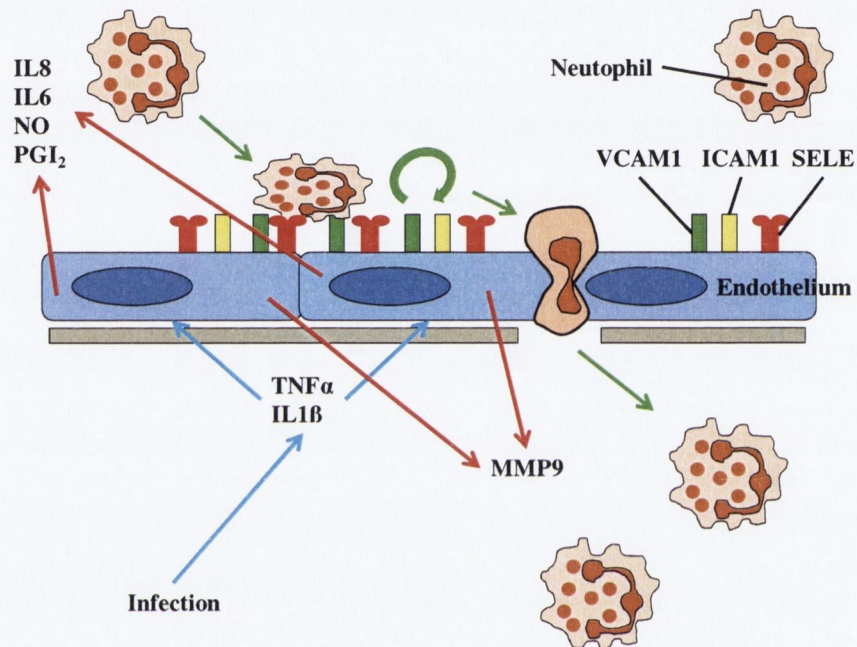


Figure 17 | An interplay of various factors to trigger off and sustain the inflammatory reactions. $TNF\alpha$ and $IL1\beta$, produce as a consequence of an infection, bind their receptors on the local endothelial cell surface (**blue lines**). Inflammatory mediators thus expressed (**red lines**) increase neutrophil recruitment to the site of infection (**green lines**).

If it is successful, acute inflammation is resolved, restoring normal tissue architecture or forming a connective tissue scar. If the stimulus is not eliminated (over a period of hours) the inflammatory process will persist and evolve and finally lead to chronic inflammation. T cells will infiltrate into the infected tissue to help eliminate the infectious microorganism. Concomitantly, the inflammatory stimulus changes from one sensed by PRRs of innate

immune cells to one recognized as an antigen by activating receptors on T and B cells of adaptive immunity.

All the events shown above underpinned the four cardinal signs of inflammation: rubor (redness), due to increased local blood flow; calor (warmth); tumor (swelling), due to extravasation of cells and plasma-protein-rich fluid; and dolor (pain), due to leukocyte mediator on C-type sensory nerve fibres ⁶⁵.

NUCLEAR FACTOR κ B (NF- κ B): The NF- κ B belongs to the Rel/NF- κ B family of transcription factors, which includes a collection of proteins related through a highly conserved DNA-binding/dimerization domain: the Rel homology (RH) domain ⁸⁶. Members of the mammalian Rel/NF- κ B family are p50 (also known as NF- κ B1), p52, c-Rel, p65 (also known as RelA) and RelB ⁸⁷. All these proteins can form homo- or heterodimers, except for RelB which can only form homodimers ⁸⁶. Typically, NF- κ B is a heterodimer composed by p65 and p50 subunits. The mechanism of activation of NF- κ B has been carefully studied ⁸⁶⁻⁸⁸ (**Figure 18**). The NF- κ B activation underpins transcription of several genes involved in inflammation and coagulation to mRNA, among of which are *ICAM1*, *VCAM1*, *SELE*, *MMP9*, *PTGS2*, *F3*, *IL6*, and *IL8* ⁸⁹. Transcription factor NF- κ B activity appears to be oxidative-stress sensitive ⁹⁰.

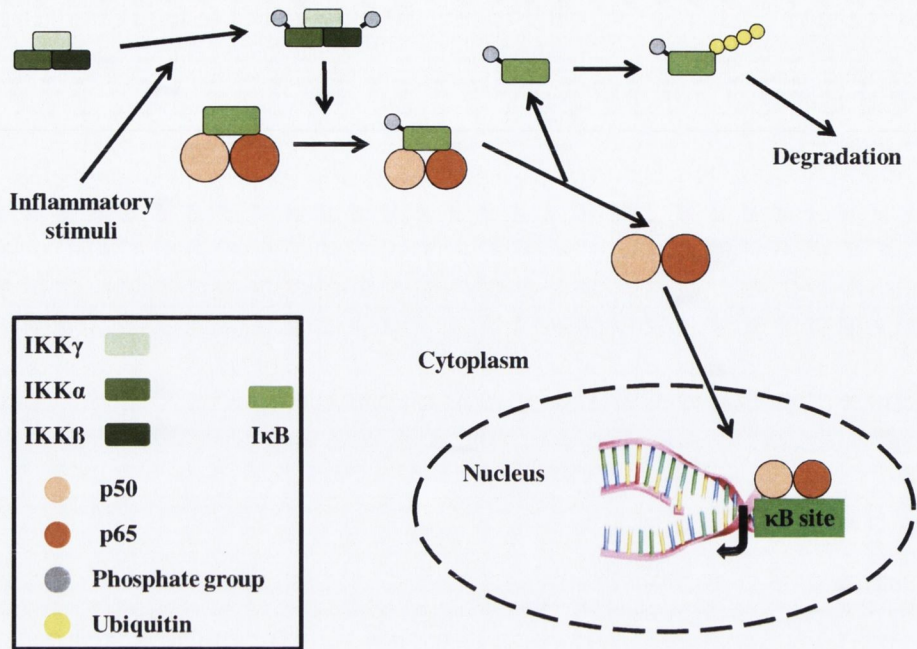


Figure 18 | The NF- κ B activation. Inhibitor of NF- κ B (I κ B) normally binds to and sequesters NF- κ B. This interaction blocks the ability of NF- κ B to enter the nucleus and bind to DNA in κ B sites. In the simplest model of NF- κ B activation, inflammatory stimuli (e.g. TNF α and IL-1 β) activate signal transduction pathways that induce the activation of the IKK (inhibitor of NF- κ B kinase) complex (IKK α , IKK β , and IKK γ). This results in the phosphorylation of I κ B, following by ubiquitination, and consequently degradation in the proteasome. Released NF- κ B dimers translocate to the nucleus and bind κ B sites in the promoters or enhancers of target genes, which leads to their transcription.

INTERCELLULAR ADHESION MOLECULE 1 (ICAM1): This adhesion molecule belongs to the immunoglobulin (Ig) superfamily. Members of this superfamily are characterized by the presence of structural motifs (Ig-like domains), which in turn have a distinguished immunoglobulin fold⁹¹ built up of a sandwich of two β -sheets containing antiparallel strands. Disulfide bonds links the two β -sheets⁹²; however, they are not essential for the structure of the domain⁹³.

The human *ICAM1* gene is located in the chromosome 19 (19p13.3-p13.2). The receptor ICAM1, which is also known as CD54, P3.58, and BB2, is critical for the recruitment of leukocytes from the bloodstream into the tissues. Although constitutively expressed, interleukin 1 β (IL-1 β) and tumour-necrosis factor α (TNF- α) greatly increase their expression on the plasma membrane of endothelial cells.

The type I transmembrane protein ICAM1, which is present in endothelial cells and leukocytes, has a molecular weight of 80-114 kDa depending of its level of glycosylation (60 kDa unglycosylated). The human ICAM1 is composed of a total of 505 amino acids. It has five Ig-like domains in its extracellular region (453 amino acids in total), each of which contains 90-100 amino acids consisting of two β -sheets of antiparallel strands. These five domains are stabilized by disulfide bonds and each of them is codified by a separate exon. The transmembrane region has 24 amino acids and the cytoplasmatic tail 28 amino acids. Its main leukocyte ligand is lymphocyte function associated molecule 1. The endothelial expression of ICAM1 is increased in atherosclerotic and transplant-associated atherosclerotic tissue and in animal models of atherosclerosis. Additionally, ICAM1 has been implicated in the progression of autoimmune diseases⁹⁴⁻⁹⁵.

VASCULAR CELL ADHESION MOLECULE I (VCAM1):

Adhesion molecule VCAM1, which gene is located in the human

chromosome 1 (1p32-p31), is also known as CD106 and INCAM-100. It is a member of the Ig superfamily critical for the recruitment of leukocytes from the blood to the site of infection. Its main ligand is the β -1 integrin very late antigen 4, which is present in mononuclear leukocytes, eosinophils, and basophils. In vivo, VCAM1 is expressed in inflamed vascular endothelium, as well as in circulating monocytes and dendritic cells in both normal and inflamed tissue ⁹⁶.

The molecule ICAM1 has seven extracellular Ig-like domains in its major form. Two forms of VCAM1 with either six or seven extracellular domains, although with the longer form predominant, are present in HUVEC cells via alternative splicing ⁹⁷⁻⁹⁸.

SELECTINS: Type I transmembrane selectin E (in endothelial cells) is a member of the selectin family along with selectin P (in endothelial cells and platelets) and selectin L (in leukocytes). The genes *SELE* and *SELP* are located in the human chromosome 1 (1q22-q25).

Member of the selectin family pose (from N- to C-terminal): (i) N-terminal extracellular domain, with structural homology to calcium-dependent lectins; (ii) a domain homologous to epidermal growth factor; (iii) two to nine consensus repeats, similar to sequences found in complement regulatory proteins; (iv) a hydrophobic transmembrane region inserted in the plasma membrane; and (v) a short cytoplasmic tail ⁹⁹. Selectin P is synthesized and stored in WPBs

along with vWF. This allows a quickly expression after the inflammatory response is triggered. Whereas, SELE expression on the endothelial surface membrane is slower since it must be synthesized de novo. Selectin P is also stored in α -granules of platelets and rapidly expressed after platelet activation.

MATRIX METALLOPROTEINASES (MMPs): Due to its involvement in the extracellular matrix (ECM) breakdown, proteinase MMP9 (EC 3.4.24.25), which is also known as gelatinase B, belongs to a family of enzymes known as matrix metalloproteinases (MMPs) or matrixins. Members of this family are characterized by the presence of a cysteine (Cys, C) switch motif PRCGXPD in the propeptide that maintains MMPs in their zymogen form, and/or the zinc-binding motif HEXGHXXGXXH in the catalytic domain. Under physiological conditions, the activities of MMPs are precisely regulated at the level of transcription, activation of the precursor zymogens, interaction with specific ECM components, and inhibition by endogenous inhibitors (TIMPs). Members of this family are usually divided into subfamilies collagenases, gelatinases, stromelysins, matrilysins, membrane-type MMPs, and other MMPs. Proteinase MMP9, along with MMP2 (also known as gelatinase A), belong to the gelatinase subfamily, which is characterized by the ability of these enzymes to digest denatured collagens, gelatines. These enzymes have three repeats of a type II fibronectin domains inserted in the catalytic

domain, which bind to gelatine, collagens, and laminin. Type I, II, and III collagens are digested by MMP2, but not by MMP9. 92-kDa MMP9 readily digests the components of the ECM: collagen (type IV, V, XI, XIV), gelatin I, elastin, aggrecan, laminin, and decorin¹⁰⁰⁻¹⁰¹.

The *MMP9* gene is located in the human chromosome 20 (20q11.2-q13.1). Apart from being crucial for the physiological ECM turnover, ECM digestion, performed by MMP9, allows the accommodation of leukocytes after diapedesis.

PROSTAGLANDIN H SYNTHASES (PTGS) OR CYCLOOXYGENASES (COX): There are two isoenzymes of COX (EC 1.14.99.1): a constitutive COX1 and an inducible COX2, which differ in their regulation of expression and tissue distribution. Inhibition of these enzymes, by non-steroidal anti-inflammatory drugs (NSAIDs) (e.g. aspirin, ibuprofen, naproxen), inhibits the formation of prostanoids. The *PTGS1* gene (22 kilobases in size) is located in the human chromosome 9 (9q32-q33.3), whereas *PTGS2* (8 kilobases in size) is located in chromosome 1 (1q25.2-q25.3); their mRNAs are also quite different respectively 2.8 kilobases and 4 kilobases in size. However, substrate-binding sites and catalytic regions in protein tertiary structures are almost identical. A splice variant of COX1 retaining intron 1 in its mRNA, COX3, has also been identified. An exchange of isoleucine in COX1 for valine in COX2 at position 434 and

523 allows COX2 to catalyze the conversion of arachidonic acid to PGH₂ but at a much higher level of throughput¹⁰².

Isoenzyme COX1 is predominately produced by endothelial cells; however, COX2 becomes readily expressed at sites where inflammatory processes (e.g. atherosclerosis), vascular injury or infection are taking place. In this condition, endothelium is able to produce, apart from prostacyclin, non-prostacyclin prostanoids (e.g. prostaglandin E₂, PGH₂)¹⁰².

COAGULATION FACTOR 3 (F3, TISSUE FACTOR): The F3 gene, which is located in the human chromosome 1, codifies a 47-kDa protein (tissue factor) constitutively expressed in subendothelial cells (e.g. vascular smooth muscle cells), but not in endothelial cells, under physiological conditions¹⁰³. In endothelial cells, IL-1 β and TNF- α induce the synthesis of tissue factor¹⁰⁴, but this factor is normally sequestered within the endothelial cell and unable to start the coagulation cascade⁶⁵. Various stimuli, such as vessel injury¹⁰⁵, induce tissue factor activity on the endothelial surface¹⁰³.

Although soluble tissue factor, generated through alternative splicing, can also be found in the circulation¹⁰⁶, it cannot trigger coagulation because it fails to act as a cofactor for coagulation factor VIIa¹⁰⁷. In non-inflamed tissues, endothelial cells express tissue factor pathway inhibitor that prevents the initiation of coagulation by blocking the actions of the factor-VIIa-tissue-factor complex⁶⁵.

The foremost initiator of the coagulation cascade in vivo is tissue factor ¹⁰⁸⁻¹⁰⁹ through the so-called **extrinsic pathway**. Tissue factor participate as a cofactor in the activation of the coagulation factor VII to its active form, factor VIIa. The factor VIIa-tissue factor complex initiates a series of enzymatic reactions which lead to activation of prothrombin to thrombin on the platelet membrane surface. Thrombin converts soluble fibrinogen to insoluble fibrin to form the blood clot. Thrombin not only converts fibrinogen to fibrin but also activates platelets ¹¹⁰. The second classic pathway of initiation of the coagulation cascade, the **intrinsic pathway**, begins with the activation of coagulation factor XII to XIIa, which is promoted by certain surfaces such as glass or collagen. Factor XIIa also initiate a series of enzymatic reactions which lead to activation of prothrombin to thrombin on the platelet membrane surface ¹¹⁰. However, this pathway is not required for initiation of haemostasis in vivo.

It has been also proposed that tissue factor can exist in a latent (or "encrypted") form that lacks of coagulant activity or in an active form that initiates blood coagulation; and inactive tissue factor can be enzymatically activated by an enzyme produced in activated platelets and endothelial cells ¹⁰⁵.

INTERLEUKIN 6 (IL6): Human IL-6 is a monomeric multifunctional cytokine consisting of 184 amino acids with two

potential N-glycosylation sites and four cysteine residues ¹¹¹. Secretion of IL6, which is produced by a wide spectrum of cell types in the cardiovascular system, is upregulated in response to inflammation, angiotensin II, oxidative stress, and cardiovascular injury. Human IL6 is a marker of the vascular inflammation. Angiotensin II, IL-1 β , TNF- α , and viral infection highly induce IL6 levels in blood. Transcription factor NF- κ B underpins inducible IL6 expression ¹¹². IL-6 (23.7 kDa) has a pro-atherogenic effect on endothelial cells and B cells; as well as is involved in proliferation and differentiation of B cells into plasma cells and antibody secretion; it is also involved in acute phase response ⁷⁸. Interactions between IL-6 and endothelial cells regulate recruitment of leukocytes and expression of chemokines ⁸⁴.

INTERLEUKIN 8 (IL8): Human IL8 is generated as a precursor of 99 amino acids and is secreted after cleavage of a signal sequence of 20 residues. N-terminal extracellular processing of the mature form yields several biologically active variants (77, 72, 70, and 69 amino acids). The predominant variant consists of 72 amino acids and has a molecular weight of 8,383. It is a basic protein (pI 8.3) and contains four cysteines that form two disulfide bridges ¹¹³. IL8 forms dimers in solution ¹¹⁴, but it is unknown if it acts as a dimer or monomer in vivo ¹¹⁵.

Normally, IL8 protein is barely secreted from noninduced cells, but its production is rapidly induced by a very wide range of stimuli encompassing proinflammatory cytokines such as tumour necrosis factor (TNF) or IL-1, bacterial, or viral products, and cellular stress¹¹⁶; NF-κB is involved.

Endothelial cells, monocytes, and macrophages produce IL8 which acts on monocytes, macrophages, and T cells promoting chemotaxis and leukocyte arrest; as well as has pro-atherogenic and pro-inflammatory actions⁷⁸.

PLATELETS

Platelets are anucleated blood elements in the order of 2 to 4 μm in size that derived from megakaryocytes⁶⁶ in a process called thrombopoiesis. Thrombopoietin is the main regulator; but IL3, IL6, IL11, and stem cell factor are also involved¹¹⁷. Platelets contain granules (α-granules and dense δ-granules), lysosomes, mitochondria, and endoplasmic reticulum. Platelet granules stored numerous crucial factors for platelet function. In humans, the physiological range for platelets is 150 - 400 x 10⁶ per millilitre; frequently, females have higher platelet count than males. The lifespan of circulating platelets is 7 to 10 days¹¹⁷. Old platelets are eliminated in the spleen and in Kupffer cells (in the liver).

In the absence of any activating stimulus, resting platelets circulate in a quiescent state being discoid in shape; however, when

they become activated, they change their shape, extending pseudopodia in many directions, and platelet degranulation takes place (**Figure 19**).

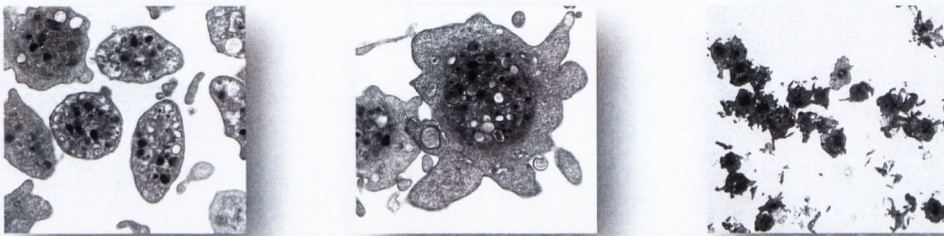


Figure 19 | Transmission electron microscopy of platelets. Discoid shape resting platelets (left), activated platelet with the formation of pseudopodia (centre), and aggregated platelets forming different plugs (right).

In the absence of vascular damage, endothelial cells synthesize and release NO and prostacyclin, which along with the expression of CD39 (ectonucleoside triphosphate diphosphohydrolase 1) on the endothelial luminal plasma membrane, inhibit platelet activation. The CD39, an ADPase, hydrolyzes any small amount of ADP that might cause platelet activation ¹¹⁷.

Platelets play a crucial role in vascular haemostasis. After vessel-wall damage, platelets adhere to the site of vascular damage, activate and aggregate (primary haemostasis) ¹¹⁸. Simultaneously, coagulation factors react in a complex cascade of events (coagulation cascade or secondary haemostasis) that culminates in the activation of thrombin and generation of fibrin. All these events lead to the

formation of a stable platelet plug (also known as clot or thrombus) that ensues wound healing. Afterwards, this platelet plug is gradually dissolved by enzymes of the fibrinolytic system. An imbalance in the formation (e.g. excess of platelet aggregation) or degradation (e.g. fibrinolytic system deficiencies) of the platelet plug may lead to breakage and release of various sizes of thrombus which travel free in the bloodstream. Free thrombi are known as emboli and if they block bloodstream in large arteries (thromboembolism) eventually result in pathologies such as heart attack and stroke. In addition to their role in haemostasis and thrombosis, accumulated evidence also indicates the role of platelets in non-haemostatic processes such as wound repair, angiogenesis, innate immune response, and carcinogenesis¹¹⁹⁻¹²¹.

Under physiologic conditions, loss of endothelial barrier, after vessel wall damage, results in exposure of subendothelial collagen and vWF to flowing blood. Binding of these proteins to platelet receptors triggers platelet adhesion and activation that eventually leads to a local platelet plug formation to arrest haemorrhage and guarantee wound vessel healing. Platelet collagen receptors glycoprotein (GP) GPIa/IIa complex and GPVI, as well as platelet vWF receptor GPIb/IX/V complex, play an important role on activating platelets in an early stage¹²². Soluble vWF does not bind to platelets to prevent aggregation; however, immobilized vWF onto collagen is highly reactive toward flowing platelets. The binding of vWF and

collagen to their receptors on the platelet surface membranes induces release and activation of GPIIb/IIIa receptors. The activation (a change from the low- to high-affinity conformation) of the GPIIb/IIIa complex is crucial for platelet aggregation to occur ¹²³ (**Figure 20**).

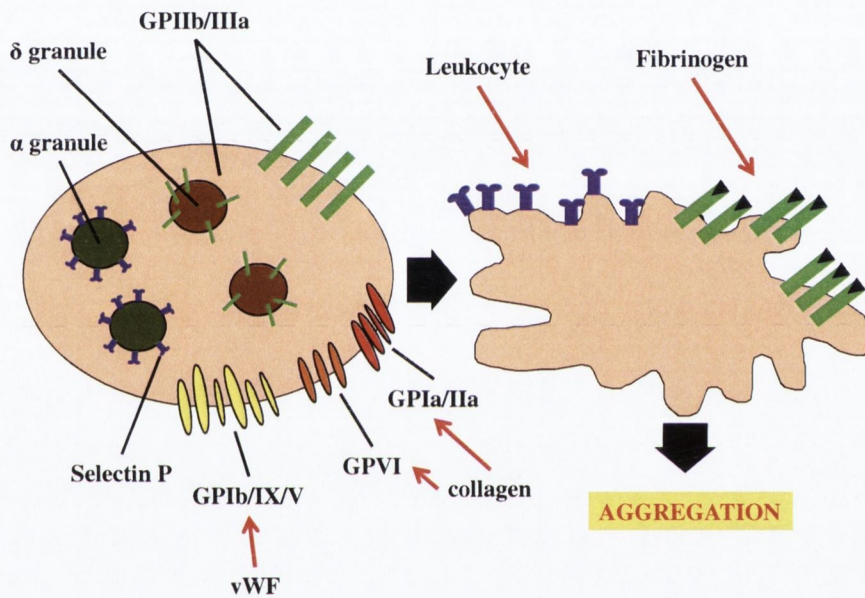


Figure 20 | Platelet aggregation. In resting platelets, GPIIb/IIIa has no ligand-binding activity and SELP is stored in a granules; this prevents platelet aggregation. The binding of vWF (GPIb/IX/V) and collagen (GPIa/IIa and GPVI) to their receptors lead to activation of GPIIb/IIIa on the platelet surface membrane. A conformational change in GPIIb/IIIa structure results in exposure of high affinity-binding sites that facilitate the recognition of circulating soluble fibrinogen. Also, more GPIIb/IIIa receptors translocate to the platelet surface membrane and activate. In addition, upon platelet activation SELP translocate to the platelet surface membrane.

GPIIb/IIIa receptors are platelet specific surface receptors that belong to the integrin superfamily ($\alpha_{Ib}\beta_3$ integrin). It is the most abundant receptor on platelet surface; as many as 80,000 copies of GPIIb/IIIa are expressed on the surface of resting platelets with

additional pools in the membranes of δ -granules ¹²⁴. **Selectin P** receptors on the platelet surface membrane underlies platelet-leukocyte aggregation ¹²⁵. Selectin P is involved in the recruitment of leukocytes from the blood into the damage tissue to eliminate the potential infection associate with the injury. This recruitment occurs in a similar way than that in endothelial cells (see figure 15). Platelet-leukocyte aggregation is also observed in the embolus.

Early adhesion and platelet activation results in the formation of a monolayer of platelets on the exposed collagen and vWF where the loss of endothelial barrier occurred. Afterwards, platelets accumulate on the initial platelet monolayer and activated thrombin, on activated platelet surface, catalyzes the conversion of soluble fibrinogen into insoluble fibrin. This establishes fibrin bridges between platelets, which results in the formation of a local stable platelet plug, which ensures vessel wound healing. The activation and recruitment of additional platelets to form the platelet aggregate is mediated by diffusible mediators such as ADP and thromboxane A₂ (TXA₂) which are released upon platelet degranulation and act via GPCRs. These platelet activators further increase their own formation and release from activated platelet, thus acting as positive-feedback mediators that amplify the initial signals to ensure the rapid activation and recruitment of platelets into a growing thrombus. The MMP2 release from platelet during their activation is also involved in platelet aggregation and extension of the clot ¹²⁶.

Regulation of adhesion, activation, and platelet aggregation result from the balance between the action of platelet activators (collagen, vWF, TXA₂¹²⁷, ADP¹²⁸, and MMP2¹²⁶) and inhibitors¹²⁵ (prostacyclin, ADPase, and NO).

OXIDATIVE STRESS

Oxygen is vital in the cellular metabolism. Its high redox potential allows it to easily accept electrons from reduced substrates. Free partially reduced forms of oxygen, or free radicals, are known as reactive oxygen species (**ROS**). Superoxide anion (O₂^{•-}), hydrogen peroxide (H₂O₂), and hydroxyl radical (OH[•]) are ROS. Excess of ROS can affect the redox state levels of glutathione and thioredoxin, which are antioxidant enzyme cofactors; as well as, oxidize and damage lipids, nucleic acids, proteins, and polysaccharides. Superoxide can interact with NO to form peroxynitrite (ONOO⁻), a strong oxidant. Free radicals derived from nitric oxide are known as reactive nitrogen species (**RNS**). Excess RNS affect the nitrosation or nitration of cellular targets, including proteins and glutathione; as well as, oxidizes proteins and nucleic acids. This is referred as **nitrosative stress**. Collectively, excessive accumulation of ROS or RNS, and the uncontrolled oxidation of cellular components are referred to as **oxidative stress**. Oxidative and nitrosative stress accompany aging and several diseases, including hypertension, atherosclerosis, Alzheimer's disease and a variety of dementias¹²⁹.

Enzymes such as NAD(P)H oxidases, xanthine oxidase, NOS, cyclooxygenase, and lipoxygenase¹³⁰, and also the mitochondrion¹³¹⁻¹³², have been showed as free radical generators.

The antioxidant enzymes superoxide dismutase (SOD), catalase, and glutathione peroxidase (GPx) maintain reactive oxygen species level low by detoxification of ROS, that in turn maintain RNS also low, to avoid their undesirable effects. The expression of these enzymes is induced by H₂O₂¹³³. When free radical production over saturated the protective enzymatic mechanism, the cell suffers the catastrophic consequences of the oxidative stress. However, ROS and RNS in low levels are involved in regulations of certain physiological functions.

THE [NO]/[ONOO⁻] BALANCE: Endothelial cells and platelets release NO which inhibits platelet aggregation. However, the reaction of NO with O₂^{•-}, and production of ONOO⁻, leads to impairments in NO bioavailability⁸². This reaction takes place under physiological conditions in both platelets and endothelial cells. Essentially, NO is produced but it is not available to perform its functions. This is correlated with the reduction of the vasodilator and platelet-regulatory functions of endothelium during the course of vascular disorders such as atherosclerosis, essential hypertension, and preeclampsia¹³⁴. Therefore, a high [NO]/[ONOO⁻] ratio is crucial for platelet function under physiologic conditions. A high [NO]/[ONOO⁻]

balance leads to inhibition of platelet adhesion and aggregation as well as an increase in disaggregation of platelet aggregates. On the other hand, a reduced $[NO]/[ONOO^-]$ ratio conduces to an increased platelet aggregation, SELP expression, MMP activation; and finally, to platelet and endothelial cell dysfunction⁸² (**Figure 21**).

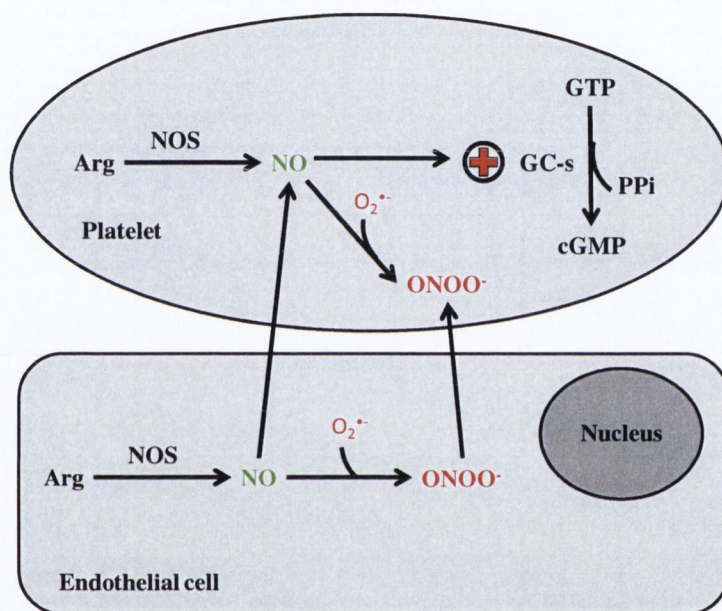


Figure 21 | The $[NO]/[ONOO^-]$ balance. As $[NO]/[ONOO^-]$ ratio is high, NO activates the platelet soluble guanylate cyclase (GC-s) to increase the levels of cyclic guanosine monophosphate (cGMP). The cGMP induces activation of protein kinase G (PKG), inhibition of cGMP-inhibited cyclic adenosine monophosphate (cAMP) phosphodiesterase, and inhibition of the opening of ion channels regulating calcium flux and producing a reduction in platelet cytosolic Ca^{+2} . As $[NO]/[ONOO^-]$ ratio is low, NO is not available to perform its functions. Adapted from Alonso, D. & Radomski, M.W. (2003)⁸².

ATHEROSCLEROSIS

High fat diet, inflammatory diseases, elevated low-density lipoprotein (LDL) and intermediate-density lipoprotein (IDL) levels, obesity, and smoking are all classic risk factors for atherosclerosis¹³⁵.

It is increasingly recognized that fine and ultra-fine particulate matter are also risk factors ^{25,30,32,136}.

Atherosclerosis is a progressive disease whereby modified lipoproteins, macrophages, T cells and the normal cellular and fibrous elements of the arterial wall interact with each other in the subendothelial space (tunica intima) of medium-sized or large arteries, and ultimately leads to the formation of atherosclerotic plaque or atheroma. Atheroma rupture derives most likely in heart attack or stroke.

Arterial branching or curvatures are preferential sites for atherosclerotic lesion formation ¹³⁷. These areas are especially prone to the passive permeation of apolipoprotein B-containing lipoproteins, LDLs and IDLs, through endothelial cell junctions and subendothelial accumulation ¹³⁸. These lipoproteins are retained in the tunica intima by interaction between the apoB-100, in their surface, and proteoglycans of the extracellular matrix ¹³⁹ (**Figure 22**).

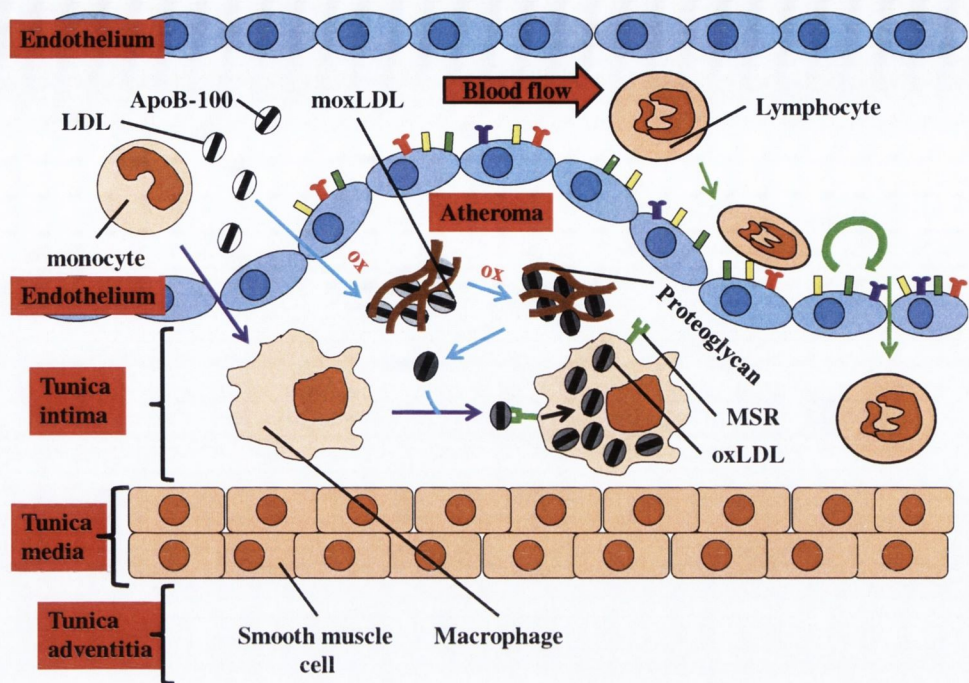


Figure 22 | Arterial atheroma formation. Circulating LDLs diffuse to the tunica intima and are retained. Trapped LDLs become minimally oxidized LDLs (moxLDLs) by exposure to free radicals released from local endothelial cells or enzymes of the extracellular matrix (**blue lines**). For reasons that are not completely understood, but involved moxLDLs, shear stress and disturbed blood flow¹⁴⁰, the local overlying endothelium is activated to secrete chemokines and express adhesion molecules (ICAM1, yellow; VCAM1, green; SELE, red; and SELP, purple)^{135,141-142}. This leads to tethering, rolling and extravasation of lymphocytes (**green line**) and monocytes (**purple line**). In the intima, monocytes differentiate to macrophages. Also, moxLDLs become highly oxidized LDLs (oxLDLs). Macrophages recognize oxLDLs, via scavenger receptors, engulf them and activate. Lipoprotein IDLs may suffer similar modification than LDL and promote atherosclerosis.

Atherosclerosis shares some characteristic with inflammation; however, this disease is characterized by the recruitment of monocytes and lymphocytes, but not neutrophils. Activated macrophages induce the differentiation of T cells to T_H1 via MHC class II. Activated macrophages and T_H1 (CD40 and CD40 ligand are involved) release a cocktail of cytokines (e.g. INF- γ , TNF- α) and

growth factors. This increases the recruitment of more monocytes and lymphocytes; as well as, smooth muscle cell and extracellular matrix proliferation ¹³⁵. In parallel, macrophages continue engulfing oxLDLs and become foam cells, and finally die via necrosis or apoptosis ¹³⁵. All these events lead to atheroma growth to the lumen of the blood vessel and development of a fibrous cap. Atheroma vulnerability is a critical factor in the formation of a blood thrombus. Vulnerable plaques generally have thin fibrous caps and increased numbers of inflammatory cells; and therefore, break easily. The rupture of the atheroma leads to thrombosis and embolus formation.

AIMS OF THE PROJECT

As nanoparticles have been shown to interact with biological components and induce noxious effects ¹⁴³, I was interested in studying the interactions of silica nanoparticles with the cardiovascular system, since this has been shown to be targeted by nanoparticles ¹⁸. I selected silica nanoparticles for my studies because the exposure of the human population to them may be very important due to their very high production volume worldwide and their number of applications. Moreover, there are not enough studies available to ensure silica nanoparticle safety or toxicity. I specifically focused on endothelial cells and platelets since interferences with their normal physiological functions bring catastrophic consequences. For my studies on endothelial cells, I selected human umbilical vein endothelial primary cells (HUVEC primary cells). This cell line has been used for many years as a standard for physiological and pharmacological studies of endothelial cells. For my studies on platelets, I used human platelets isolated in the same day that I performed my experiments. All my studies were in vitro.

Specific aims:

1. To demonstrate if amorphous silica nanoparticles induce noxious effects in human endothelial cells and human platelets.

2. To study the consequences derived from the exposure of endothelial cells to amorphous silica nanoparticles in terms of inflammatory response.
3. If amorphous silica nanoparticles induce noxious effects on human endothelial cells, to understand how this happens mechanistically.
4. To investigate the consequences derived from the exposure of human platelets to amorphous silica nanoparticles in terms of platelet activation (receptors activation and expression), aggregation, and free radical production.

MATERIALS AND METHODS

REAGENTS

Foetal bovine serum (FBS), endothelial cell growth supplement, tri-sodium citrate, Tyrode's salt solution, glutaraldehyde, KH_2PO_4 , K_2HPO_4 , osmium tetroxide, propylene oxide, agar 100 epoxy resin, DDSA hardener, MNA hardener, BDMA accelerator, uranyl acetate, and Reynold's lead citrate were all purchased from Sigma-Aldrich (Arklow, Ireland). Phosphate-buffered saline (PBS), 5-(and-6)-carboxy-2',7'-dichlorodihydrofluorescein diacetate (carboxy- H_2DFFDA) (Invitrogen, Paisley, UK).

SILICA NANOPARTICLES

10-nm (10SiNPs), 50-nm (50SiNPs), 150-nm (150SiNPs), and 500-nm silica nanoparticles (500SiNPs) were all purchased from Polysciences Europe GmbH (Eppelheim, Germany). Nanoparticles suspensions were maintained refrigerated (4°C) while my studies lasted.

NANOPARTICLE CHARACTERIZATION

The hydrodynamic sizes and ζ potentials (zeta potentials) of all silica nanoparticles were determined by a Zetasizer Nano ZS (Malvern Instruments Ltd, Malvern, UK). Sixtuplicate measurements of hydrodynamic size and zeta potential were performed on each commercial particle size suspended in deionised ultra-pure water H_2O

at 25 °C. All measurements were conducted using silica nanoparticles at a concentration of 100 µg/ml. Malvern folded capillary cells were used to fulfil all measurements.

CELL CULTURE

Pre-screened human umbilical vein endothelial primary cells were purchased from the Health Protection Agency Culture Collections (ECACC, Salisbury, UK). Cells were cultured in 75-cm²-250-ml tissue culture flasks (T-75 flasks) and in the recommended ECACC complete endothelial cell growth medium. Cells were maintained in a 37°C, 5% CO₂ humidified incubator. Cells were supplied with fresh medium every two days, and propagated using the recommended ECACC subculture kit, for a maximum of 16 population doublings.

EXPOSURE OF CELLS TO NANOPARTICLES

Immediately before use, commercial silica nanoparticle suspensions were sonicated in a sonic bath for 10 minutes to ensure dispersity. When cells reached 80% confluence, they were exposed to nanoparticles, which were suspended in basal media (ECACC complete media without serum or growth factors) supplemented with 2% FBS and 0.03-mg/ml endothelial cell growth supplement. Nanoparticle concentrations in culture media to be tested were prepared by serial dilution from the sonicated suspensions and mixed by vortexing. Untreated controls (without nanoparticles) were

incubated in an equivalent volume of basal media supplemented with 2% FBS and 0.03-mg/ml endothelial cell growth supplement. For each experiment untreated cells served as a control.

PHASE-CONTRAST MICROSCOPY

When HUVEC primary cells, growing in 25-cm²-50-ml tissue culture flasks (T-25 flasks), reached 80% confluence, they were washed twice with basal media; and then, incubated with 10- μ g/ml and 50- μ g/ml 10SiNPs for 15 hours. Untreated control cells (without nanoparticles) were also prepared. Cells were examined by an OLYMPUS CKX41 inverted microscope (Olympus UK Ltd., Southend on Sea, UK). Micrographs were taken by an Altra₂₀ Soft Imaging System (Olympus UK Ltd., Southend on Sea, UK).

PLATELET AGGREGATION STUDIES

Blood was obtained from healthy volunteers, who had not taken any drugs known to affect platelet function for 2 weeks prior to the study. **Washed platelets** and **platelet-rich plasma (PRP)** was obtained as previously described¹⁴⁴. Briefly, blood was collected and anticoagulated using tri-sodium citrate (3.15% w/v; 9:1 v/v). The citrated blood was centrifuged at 250 x g for 20 minutes at room temperature to prepare PRP. Washed platelets were prepared by centrifugation of PRP, containing prostacyclin (1 μ M), a further 10 minutes at 900 x g at room temperature. Prostacyclin was used to

protect platelets from activation during differential centrifugation, washing and isolation from blood. Following isolation, platelets were resuspended in prostacyclin-free Tyrode's salt solution. The samples of PRP and washed platelets were adjusted using Tyrode's salt solution to a final concentration of 2.5×10^8 platelets per millilitre.

The ability of nanoparticles to stimulate platelet aggregation of unstimulated (resting) platelets was studied. Immediately before use, nanoparticle suspensions were sonicated for 10 minutes in a sonic bath to ensure dispersity. Then, nanoparticle suspensions in Tyrode's salt solution were prepared by serial dilution from the commercial suspensions and mixed by vortexing. A maximum of 10 μ l of particle suspensions in Tyrode's salt solution were added to either Tyrode's salt solution containing platelets or PRP in the aggregometer.

Platelet aggregation was studied against a Tyrode's salt solution blank, for washed platelets; and poor-platelet plasma (PPP) (with or without Tyrode's salt solution), for PRP. Blanks contained the same particle concentration than the test tubes. Final volumes into all test and blank tubes were the same.

Platelets were incubated for 2 minutes at 37°C in a four-channel whole blood/optical lumi-aggregometer (model 700) (Chrono-Log, Manchester, UK), prior to the addition of silica nanoparticles (1–200- μ g/ml of 10SiNPs, 50SiNPs, 150SiNPs, and 500SiNPs) and the reaction was measured for up to 15 minutes.

Collagen (5 µg per millilitre of either PRP or washed platelets) was used as a positive control for platelet aggregation studies. Aggregation in control samples, without nanoparticles, was also studied.

Aggregation was measured using a four-channel Chrono-log whole blood Lumi-Aggregometer linked to Aggro-Link data-reduction system¹⁴⁵⁻¹⁴⁷, and expressed relative to the control. The results were expressed as percentage of light transmission, where 100% transmission was taken as maximal aggregation, and were given as mean values of three or four replicates.

TRANSMISSION ELECTRON MICROSCOPY (TEM)

When HUVEC primary cells, growing in T-75 flasks, reached 80% confluence, they were washed twice with basal media and then incubated with 10-µg/ml 10SiNPs for an hour. HUVEC cells in the same media, but without nanoparticles (untreated cells), were also prepared. Afterwards, supernatants were removed and endothelial cells washed twice with basal media, and then collected in this media.

On the other hand, platelet aggregation was terminated at 30% maximal response in washed platelets exposed to 10-µg/ml 10SiNPs, as determined using an aggregometer. Untreated control (without nanoparticles) was also prepared.

Cell (in basal media) and platelet (in Tyrode's salt solution) suspensions were fixed by mixing them with an equal volume of **3%**

glutaraldehyde in 0.05M potassium phosphate buffer (pH 6.8)

for 1.5 hours at room temperature.

3% glutaraldehyde in 0.05M potassium phosphate buffer (pH 6.8)

1. *Preparation of 10 ml of 0.2M phosphate buffer (pH 6.8):* Mix 5.1 ml of 0.2M KH_2PO_4 in distilled water + 4.9 ml of 0.2M K_2HPO_4 in distilled water.
2. *Preparation of 24 ml of 3% glutaraldehyde in 0.05M potassium phosphate buffer (pH 6.8):* Mix 15 ml of distilled water, 6 ml of 0.2M phosphate buffer (pH 6.8), and 3 ml 25% glutaraldehyde.

After primary fixation, samples were centrifuged at 1500 x g for 10 minutes at room temperature; and then, pellets were washed 6 times with 0.05M potassium phosphate buffer (pH 6.8) to remove any un-reacted glutaraldehyde from the samples before post-fixation. Afterwards, pellets were post-fixed with **2% osmium tetroxide in 0.05M potassium phosphate buffer (pH 6.8)** for 30 minutes, while agitating samples on a rotator.

2% osmium tetroxide in 0.05M potassium phosphate buffer (pH 6.8)

1. Preparation of 4% osmium tetroxide in distilled water
2. Preparation of 2% osmium tetroxide in 0.05M potassium phosphate buffer (pH 6.8): Mix 2 ml of 4% osmium tetroxide in distilled water, 1 ml of 0.2M potassium phosphate buffer (pH 6.8), and 1 ml of distilled water.

Afterwards, pellets were dehydrated in series of graded ethanol solution at room temperature: 10% ethanol in distilled water for 10 minutes; 30%, 10 minutes; 50%, 10 minutes; 70%, 10 minutes; 95%, 10 minutes; 100%, 15 minutes; 100%, 15 minutes; and 100%, 30 minutes.

Afterwards, pellet samples were incubated in 100% propylene oxide (transitional fluid) for 15 minutes at room temperature, centrifugated and pellets incubated a further 30 minutes in fresh 100% propylene oxide.

This was followed by a three-hour incubation of the pellets in 50% propylene oxide / 50% agar 100 resin (10 ml resin + 10 ml propylene oxide) at room temperature; 100% agar 100 resin, 3 hours at room temperature; and 100% 24 hours in the oven at 60°C.

AGAR 100 RESIN

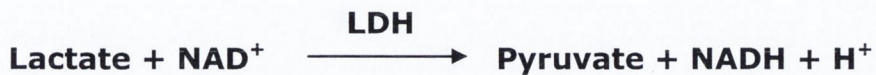
24.0g agar 100 Epoxy resin, 16.0g DDSA Hardener, 10g MNA Hardener, 1.5g BDMA accelerator

Afterwards, ultrathin sections were cut from the dried blocks with a diatome diamond knife on a LKB ULTRATOM III ultratome (LKB, Uppsala, Sweden). Samples were placed on grids and stained with 0.5% aqueous uranyl acetate (10 – 30 minutes depending on of the staining ability of the specimen) follow by Reynold's lead citrate (5-10 minutes), and examined by a JEM 2100 transmission electron microscope (JEOL Ltd, Herts, UK).

CYTOTOXICITY

Cytotoxicity of silica nanoparticles was assessed using a CytoTox96® Non-Radioactive Cytotoxicity Assay (Promega, Southampton, UK). The enzymatic activity of the stable cytosolic enzyme lactate dehydrogenase (LDH), which is released upon cell lysis, was measured. This is a simple- and quick-to-perform test, which assesses membrane damage, and therefore cell death. A coupled enzymatic reaction is used to measure LDH activity. Released LDH in cell culture supernatants catalyzes the oxidation of lactate to pyruvate, in a reaction that involved the reduction of the cofactor NAD^+ to $\text{NADH} + \text{H}^+$. Enzyme diaphorase (included in the assay)

catalyzes the oxidation of tetrazolium salt into formazan (red), in a reaction that involved the oxidation of NADH + H⁺ to NAD⁺. The amount of colour formed is proportional to the number of lysed cells. The general enzymatic reaction of the LDH assay is as followed:



Cytotoxicity analyses were performed following the supplier's recommendations. As HUVEC primary cells, growing in 96-well plates, reached 80% confluence, they were washed twice with basal media; and then, incubated with silica nanoparticles (various concentrations) (final volume 100 µl), in triplicate sets of wells (**LDHexp**) for 3, 7, 15, and 30 hours. Triplicate untreated control wells (without nanoparticles) were also prepared (**LDHcon**). After the treatment, 50 µl of the supernatants and 50 µl of LDH substrate (containing diaphorase) were mixed together into wells of a fresh 96-well plate; and then, incubated for 30 minutes protected from the light. Following the addition of a stop solution (50 µl), the LDH activity was measured spectrophotometrically at λ: 492 nm by a FLOUstar Optima spectrophotometer (BMG LABTECH GmbH, Offenburg, Germany). A set of triplicate wells, containing untreated controls, was lysed by addition of 10 µl of lysis solution to extract the maximum LDH activity

(**LDHmax**). A set of triplicate wells, containing medium with neither nanoparticles nor cells, was prepared (culture medium background, **CMB**). A set of triplicate wells was prepared to correct for volume changes caused by addition of lysis solution (volume correction control, **VCC**). The average of absorbance values of CMB was subtracted from the average of LDHcon and LDHexp. The average of absorbance values of VCC was subtracted from LDHmax. Afterwards, the percentage of cell viability was calculated according to the formula:

$$\% \text{ viability} = 100 - \left[\left(\frac{\text{LDHexp} - \text{LDHcon}}{\text{LDHmax} - \text{LDHcon}} \right) \times 100 \right]$$

An LDH positive control (bovine heart LDH) supplied with the assay was used to verify a correct performance of the assay.

It has been reported that the test material can interfere with the technique of measurement ¹⁴⁸. Further experiments were performed only with silica nanoparticles in deionised ultra-pure water to rule out the possibility of nanoparticle interference with the assay.

FREE RADICAL DETECTION

In order to detect free radicals generation, a fluorometric assay using intracellular oxidation of carboxy-H₂DFFDA was performed. Non-fluorescence carboxy-H₂DFFDA is converted by intracellular esterases to carboxy-H₂DFF, which is oxidized by free radicals to

carboxy-DFF, a high green fluorescence compound. Fluorescence formed is proportional to free radical production.

As HUVEC primary cells, growing in 6-well plates, reached 80% confluence, they were washed twice with basal media; and then, incubated with 10- $\mu\text{g/ml}$ 10SiNPs (final volume 1 ml) for 1 hour. Untreated control wells (without nanoparticles) were also prepared. After the treatment, cells were washed twice with basal media; and then, incubated with carboxy- H_2DFFDA (40 μM) contained in 1 ml of basal media for 30 minutes in a 37°C, 5% CO_2 humidified incubator. Afterwards, cells were washed twice with basal media; and then, examined in a Axiovert 200 M inverted fluorescence microscope (Carl Zeiss Ltd, Hertfordshire, UK) at $\lambda_{\text{ex}}/\lambda_{\text{em}}$: 485/530 nm.

NITRIC OXIDE (NO) AND PEROXYNITRITE (ONOO⁻) DETECTION BY NANOSENSORS

NANOSENSOR DESIGN: Biosensors were fabricated in order to measure NO and ONOO⁻ in the range of nanomol per litre (nmol/l) (nanosensors).

The basic element of a nanosensor for NO was constructed using a previously described technique¹⁴⁹. A capillary tube (100 mm diameter) was heated using a microburner, pulled to a diameter of 100-200 μm , and bent at an angle of 30° from straight. A carbon fibre was inserted into the capillary emerging from the smaller pulled tip. About 6.0 cm length of 18 AWG copper wires was sanded to

create a rough surface. Using mixed conductive silver epoxy, the copper wire was immersed in the epoxy and rolled into the carbon fibre filled capillary. Proto-electrodes were inserted into a vacuum oven and were heated under a vacuum, at 30-40 °C, for three hours. After removing and cooling these proto-electrodes, beeswax was liquefied and inserted into the pulled end of the electrode using capillary action. When the wax solidified, the tips of the proto-electrodes were sharpened using a micro burner. The electrode was inserted into the inner cone for ~1 second. This produced a final electrode diameter of ~400 nm. Finally, the electrodes were placed in 0.1M sodium hydroxide overnight to solubilize excess wax. Electrodes were removed from the 0.1M NaOH solution and cleaned using amperometry in 0.1 M NaOH, at 1.0 V and -1.0 V for three times at each voltage. The cleaned electrode was then stored in distilled H₂O until coating. The electrodes cleaned for this process were placed in a solution of monomeric porphyrin (Ni(II)-Tetra(3-methoxy-4-hydroxyphenyl) porphyrin, Ni(II)-TMHPP, in 0.1 M NaOH) and coated using cyclic voltammetry. After 15-30 cycles at a scan rate of 100 mV/s, between 0.0 V and 1.0 V, the electrodes were removed and rinsed with deionized water and immersed in 1% nafion in ethanol three times, for eight seconds. After drying the nafion coating, the electrodes were again placed in deionized water until calibration.

Electrodes were prepared for ONOO⁻ detection using the same uncoated electrode¹⁵⁰. The uncoated electrodes were removed

from the 0.1 M NaOH and cleaned using cyclic voltammetry in 0.5M H₂SO₄ between 1.0 V and -1.0 V over 5 cycles. The cleaned electrodes were stored in distilled H₂O before plating. The cleaned electrodes for this process were placed in a peroxydinitrite solution of monomeric manganese porphyrin (Mn-porphyrin in 5 mM DMSO) and coated using continuous cyclic voltammetry. After a maximum of 30 cycles at 100 mV/sec, between -0.5 mV and +1.0 V, the electrodes were removed and rinsed with acetone to remove uncoated porphyrin, followed by rinsing with distilled water. Following this, the electrodes were then immersed in 1% polyvinyl pyridine (PVP) in methanol for eight seconds three times each. After drying the PVP coating, the electrodes were again placed in double distilled H₂O and kept until measurement.

STUDIES IN CELLS: As HUVEC primary cells, growing in 12-well plates, reached confluence, they were washed twice with basal media; and then, exposed to silica nanoparticles (various concentrations) in cell culture media (basal media, supplemented with 2% FBS and 0.03-mg/ml endothelial cell growth supplement). Released NO and ONOO⁻ were measured by a tandem of NO and ONOO⁻ nanosensors placed 5 ± 2 μ m from the surface of a single HUVEC cell. Measurements of a single cell were simultaneously and continuously recorded after nanoparticle addition to cell culture.

STUDIES IN PLATELETS: Blood was obtained from healthy volunteers who had not taken any drugs, known to affect platelet function, for 2 weeks prior to the study. **Platelet-rich plasma (PRP)** was obtained as previously described¹⁴⁴. Briefly, blood was collected and anticoagulated using tri-sodium citrate (3.15% w/v; 9:1 v/v). The citrated blood was centrifuged at 250 x g for 20 minutes at room temperature. The samples of PRP were adjusted using Tyrode's salt solution to the final concentration of 2.5×10^8 platelets per millilitre. Released NO and ONOO⁻ were measured by a tandem of NO and ONOO⁻ placed in PRP. Measurements from platelets were simultaneously and continuously recorded after nanoparticle addition to PRP.

NUCLEAR FACTOR κB (NF- κB) ACTIVITY MEASUREMENT

NUCLEAR PROTEIN EXTRACTION: As HUVEC primary cells, growing in T-75 flasks, reached 80% confluence, they were washed twice with basal media; and then, incubated with silica nanoparticles (10- $\mu\text{g}/\text{ml}$ 10SiNPs for 1 hour; and 50- $\mu\text{g}/\text{ml}$ 50SiNPs, 150SiNPs, and 500SiNPs for 3 hours). Untreated control cells (without nanoparticles) were also prepared. Nuclear proteins were isolated using a Nuclear Extraction kit (Cayman Europe, Dublin, Ireland). The isolation was performed following the supplier's recommendations. Briefly, cells were washed once and then collected in a PBS/phosphatase inhibitor solution. Cells were centrifuged and pellets washed twice with the

same solution. Pellets were incubated in a hypotonic buffer (containing both phosphatase and protease inhibitors) to allow the cells to swell for 15 minutes. Followed the addition of nonidet P40 assay reagent, to disturb the plasma membrane, cells were centrifuged. Pellets were then incubated with a nuclear extraction buffer (containing both phosphatase and protease inhibitors) to disturb the nuclear membrane, and then centrifuged. Nuclear fractions, contained in the supernatants, were stored at -80°C. The samples and buffers were maintained in ice and/or at 4°C during the isolation process.

Protein concentration, in the nuclear extracts, was spectrophotometrically determined at λ : 595 nm by a FLOUstar Optima spectrophotometer using the Bradford's method and a calibration curved made with albumin.

MEASUREMENT OF NF- κ B (p65) DNA BINDING ACTIVITY:

The p65 subunit binding activity was assessed using a NF- κ B (p65) Transcription Factor Assay kit (Cayman Europe, Dublin, Ireland). The enzyme-linked immunoabsorbent assay (ELISA) was performed following the supplier's recommendations. Briefly, nuclear fractions, containing 30 μ g of proteins, were mixed with a binding buffer; and then loaded into duplicate set of wells of a 96-well plate. These wells held a specific double strand DNA, containing the NF- κ B response element (κ B site), immobilized onto the bottom. Following an

overnight incubation (4°C), samples were washed five times and then incubated, for an hour at room temperature, with an anti-p65 antibody. Samples were washed five times and then incubated, for one hour at room temperature, with a goat anti-rabbit horseradish peroxidase (HRP) conjugated antibody. Samples were then washed 5 times followed by addition of a developing solution. Samples were then incubated for 15 to 45 minutes at room temperature with gentle agitation and protected from light. Followed the addition of the stop solution, absorbance was read at λ : 450 nm by a FLOUstar Optima spectrophotometer.

Further experiments were performed only with silica nanoparticles in deionised ultra-pure water to rule out the possibility of nanoparticle interference with the assessment. A p65 positive control, supplied with the assay, was used to verify a correct performance of the assay.

REAL-TIME QUANTITATIVE PCR (qPCR)

As HUVEC primary cells, growing in T-25 flasks, reached 80% confluence, they were washed twice with basal media; and then, incubated with various concentrations of silica nanoparticles for 3, 7, and 15 hours. Untreated control flasks (without nanoparticles) were also prepared. Following incubation, cells were washed twice with phosphate buffer saline (PBS). DNA-free RNA was isolated by an Ambion RNAqueous®-4PCR kit (Applied Biosystems (AB),

Warrington, UK) according to the supplier's recommendations. Isolated RNA was aliquoted, to avoid freeze-thaw cycles, and stored at -70°C.

Isolated RNA, in each sample, was quantified by a NanoDrop® ND-1000 spectrophotometer (Fisher Scientific Ireland Ltd, Dublin, Ireland). An equal quantity of total RNA of each sample was reverse-transcribed to complementary DNA (cDNA) using a High Capacity cDNA Reverse Transcription kit (AB, Warrington, UK), according to the supplier's recommendations. Reverse transcription reactions were performed by a Realplex² Mastercycler (Eppendorf UK Ltd, Cambridge, UK) with the following conditions: step 1 (25°C, 10 minutes), step 2 (37°C, 120 minutes), step 4 (85°C, 5 minutes), and step 5 (4°C, ∞). Finally, cDNA was aliquoted, to avoid freeze-thaw cycles, and stored at -20°C.

An equal quantity of total cDNA of each sample was used to performed real-time qPCR according to the supplier's recommendations. Real-time qPCR was performed in duplicates, with pre-designed AB TaqMan® Gene Expression Assays (*ICAM1*, Hs00164932_m1; *VCAM1*, Hs00174239_m1; *SELE*, Hs00174057_m1; *MMP-9*, Hs00957562_m1; *PTGS2*, Hs00153133_m1; *F3*, Hs01076029_m1; *IL6*, Hs00174131_m1; *IL-8*, Hs00174103_m1) and AB TaqMan® Universal PCR Master Mix. 18S ribosomal ribonucleic acid (18S rRNA, Hs99999901_s1) was used as an internal control. Real-time qPCR reactions were performed by a Realplex² Mastercycler

with the following conditions: step 1 (95°C, 10 minutes (AmpliTaq Gold® DNA polymerase activation)), step 2 (95°C, 15 seconds (cDNA denature)) and step 3 (60°C, 60 seconds (cDNA annealing/extension)). The steps 2 and 3 were repeated for a total of 40 cycles.

Real-time qPCR data were analyzed by realplex 1.5 software. The expression of each gene, within each sample, was normalized against 18S rRNA expression (internal control) and expressed relative to the control sample using the formula $2^{-(\Delta\Delta Ct)}$, in which $\Delta\Delta Ct = (Ct \text{ mRNA} - Ct \text{ 18S rRNA}) \text{ sample} - (Ct \text{ mRNA} - Ct \text{ 18S rRNA}) \text{ control sample}$ ¹⁵¹.

Further experiments were performed only with silica nanoparticles in Ambion RT-PCR grade water (AB, Warrington, UK) to rule out the possibility of nanoparticle interference with the assay.

CYTOMETRIC BEAD ARRAY (CBA)

As HUVEC primary cells, growing in T-25 flasks, reached 80% confluence, they were washed twice with basal media; and then, incubated with various concentrations of silica nanoparticles for 15 hours. Untreated control flasks (without nanoparticles) were also prepared. Afterwards, a CBA Human Inflammatory Cytokine kit (BD, Oxford, UK) was used to detect IL-1 β , interleukin 10 (IL10), IL6, IL8, TNF- α , and interleukin 12p70 (IL-12p70) protein levels in culture supernatants. Experiments were performed by a FACSArray™

bioanalyzer (BD, Oxford, UK). The assays were performed following the supplier's recommendations. Briefly, protein concentration, within supernatant samples, was spectrometrically determined by the Bradford's method. Supernatant samples (50 μ l, 400 μ g/ml), captured beads (50 μ l) -coated with specific antibodies for the cytokines analyzed-, and PE detection reagent (50 μ l) were mixed together; and then, incubated at room temperature for 3 hours in the dark. Following a washing, sample data was acquired by a BD Analysis Software, and analyzed by FCAP Array™ Software. Cytokine levels were obtained using a calibration curve of human inflammation standards providing in the kit.

Further experiments were performed only with silica nanoparticles in deionised ultra-pure water to rule out the possibility of nanoparticle interference with the assay.

FLOW CYTOMETRY

The abundance of activated GPIIb/IIIa and SELP on the surface of platelets in the presence and absence of silica nanoparticles was measured by flow cytometry ^{121,152-155}. Flow cytometry was performed using a FACSAarray™ bioanalyzer. Flow cytometry was performed on single stained platelet samples as described previously ^{145,156}. The instrument was set up to measure the size (forward scatter), granularity (side scatter) and cell fluorescence.

SELECTIN P (SELP) ANALYSES: 10 μ l of either washed platelets or PRP, at 30% maximal aggregation response as determined using an aggregometer, were used to analyze platelet receptors. Resting platelets were used as control. To minimize the presence of aggregates in samples, 10 μ l of platelet suspensions and 10 μ l of fluorescent-labelled antibody suspension, containing 0.25 μ g of anti-P-selectin (BD, Oxford, UK), were diluted 10-fold using physiologic saline buffer and incubated afterward in the dark at room temperature for 5 minutes. Platelets were identified by forward and side scatter signals, and 10,000 platelet-specific events were analysed by the flow cytometer for fluorescence.

GPIIb/IIIa ANALYSES: 10 μ l of platelet suspension and 10 μ l of PAC-1 antibody (BD, Oxford, UK) suspension, containing 10 μ g of antibody, were incubated in the dark at room temperature for 15 minutes. PAC-1 specifically recognizes an epitope on the high-affinity GPIIb/IIIa complex of activated platelets at or near the platelet ¹⁵⁷. Afterwards, 10 μ l of a fluorescence-labelled antibody suspension, containing 2 μ g of anti-PAC-1 antibody, were added; Samples were then diluted 10 folds using physiologic saline buffer and incubated afterward in the dark at room temperature for farther 15 minutes. Platelets were identified by forward and side scatter signals, and 10,000 platelet-specific events were analysed by the cytometer for fluorescence.

Further experiments were performed to ensure that silica nanoparticles were not detected by the bioanalyser.

STATISTICAL ANALYSES

All data are presented as group of means \pm standard error of the mean (SEM) of $n \geq 3$. Statistical analysis of the mean difference between multiple groups was determined by one-way ANOVA followed by Tukey-Kramer multiple comparison post test; and between two groups by Student's *t* tests. A *P* value < 0.05 is considered to be statistically significant and calculated *P* values are given throughout. All statistical analyses were performed using GraphPad Prism version 5.00 for Windows (GraphPad Software, San Diego, California, USA).

RESULTS

CHARACTERIZATION OF AMORPHOUS SILICA NANOPARTICLES

The accurate and careful characterization of nanoparticles is of crucial importance for any nanotoxicology study ¹⁵⁸. **Table 1** summarizes physicochemical properties of the silica nanoparticles used in my studies. As specified by the supplier, commercially available negative surface charge 10-nm and 50-nm (colloidal); as well as, 150-nm and 500-nm silica nanoparticles were uniform amorphous solid (non-porous) pure silicon dioxide made via a precipitation process.

As significant deviations from nominal specifications are usual in commercially supplied samples ⁵⁹, I re-evaluated some nanoparticle properties. I measured hydrodynamic size and zeta potentials by a zetasizer (**Table 1**).

	10SiNPs	50SiNPs	150SiNPs	500SiNPs
Concentration (mg/ml) *	50	57	100	100
Size (nm) *	10.0	50.0	150.0	500.0
Size (nm) #	32.89 ± 0.13	89.54 ± 0.30	158.40 ± 0.38	533.20 ± 2.55
Particles per millilitre *	4.90 × 10 ¹⁶	3.92 × 10 ¹⁴	2.99 × 10 ¹³	7.42 × 10 ¹¹
Particles per gram *	9.55 × 10 ¹⁷	7.64 × 10 ¹⁵	2.83 × 10 ¹⁴	7.20 × 10 ¹²
Surface charge *	negative	negative	negative	negative
ZP (mV) #	-43.44 ± 1.75	-38.33 ± 0.20	-38.43 ± 0.30	-39.29 ± 0.12
Composition *	pure SiO ₂	pure SiO ₂	pure SiO ₂	pure SiO ₂
Synthesis *	precipitated	precipitated	precipitated	precipitated
Synthesis *	colloidal	colloidal	-	-
Porosity *	non-porous	non-porous	non-porous	non-porous

Table 1 | Silica nanoparticle characterization. Nanoparticle properties (stock suspension concentration, size, particle per millilitre, particle per gram, zeta potentials (ZP), composition, synthesis, and porosity) supplied by the manufacturer (*); as well as, re-evaluated (hydrodynamic size, zeta potential) in deionised ultra-pure H₂O by a zetasizer (#) are shown. 10-nm (10SiNPs), 50-nm (50SiNPs), 150-nm (150SiNPs) and 500-nm silica nanoparticles (500SiNPs).

Amorphous silica nanoparticles bore a strong negative surface charge (ζ -potentials were smaller than -38 mV), as specified by the supplier. Commercial and re-evaluated sizes differed greater for 10SiNPs and 50SiNPs than for 150SiNPs and 500SiNPs.

As nanoparticle size in the medium used in treatments (basal media + 2% FBS + 0.03-mg/ml endothelial cell growth supplement) is unknown, commercial nanoparticle size (10 nm, 50 nm, 150 nm, and 500 nm) will be used throughout my thesis.

I tested silica nanoparticles in HUVEC primary cells and human platelets. First, I began with endothelial cells.

AMORPHOUS SILICA NANOPARTICLES INDUCE MORPHOLOGY CHANGES IN HUVEC PRIMARY CELLS

To study the influence of amorphous silica nanoparticles on the endothelial cell morphology, I used phase-contrast microscopy. The **figure 23** shows the morphologic effects derived from the treatment of HUVEC primary cells with 10- $\mu\text{g}/\text{ml}$ 10SiNPs for 15 hours.

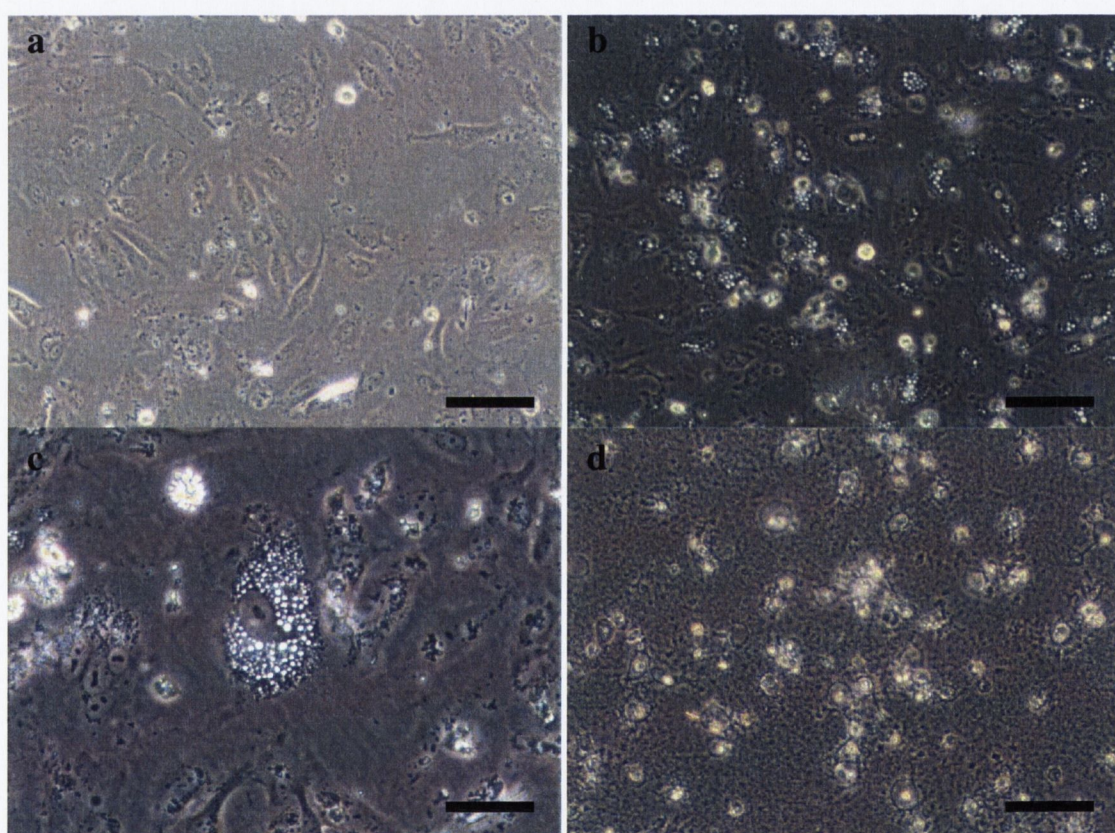


Figure 23 |Phase-contrast microscopy studies of HUVEC primary cells. Cells were treated with 10- $\mu\text{g}/\text{ml}$ (**b, c**) and 50- $\mu\text{g}/\text{ml}$ (**d**) 10SiNPs for 15 hours. Untreated control cells (without nanoparticles) were also prepared (**a**). Scale bars represent 100 μm (**a, b, d**) and 50 μm (**c**).

The exposure to 10- $\mu\text{g}/\text{ml}$ 10SiNPs led to vacuolization of some cells (**Figure 23b, 23c**) in 15 hours. However, vacuolization did not affect cellular nucleoplasm (**Figure 23c**). A concentration 5 times

bigger (50 $\mu\text{g/ml}$) was enough to severely damage all the cells (**Figure 23d**) indicating that silica nanoparticles are very toxic for cells. These findings also seem to indicate that 10SiNPs were able to penetrate into the cellular cytoplasm. Next, I used TEM in order to clearly demonstrate this point and study more in detail the silica nanoparticle-endothelial cell interaction.

UPTAKE OF AMORPHOUS SILICA NANOPARTICLES BY HUVEC PRIMARY CELLS

Silica nanoparticle internalization into cells was comprehensibly verified by TEM (**Figure 24**). An untreated Control (**Figure 24a**) and endothelial cells treated with 10- $\mu\text{g/ml}$ 10SiNPs for an hour (**Figure 24b – 24f**) were fixed and studied by TEM.

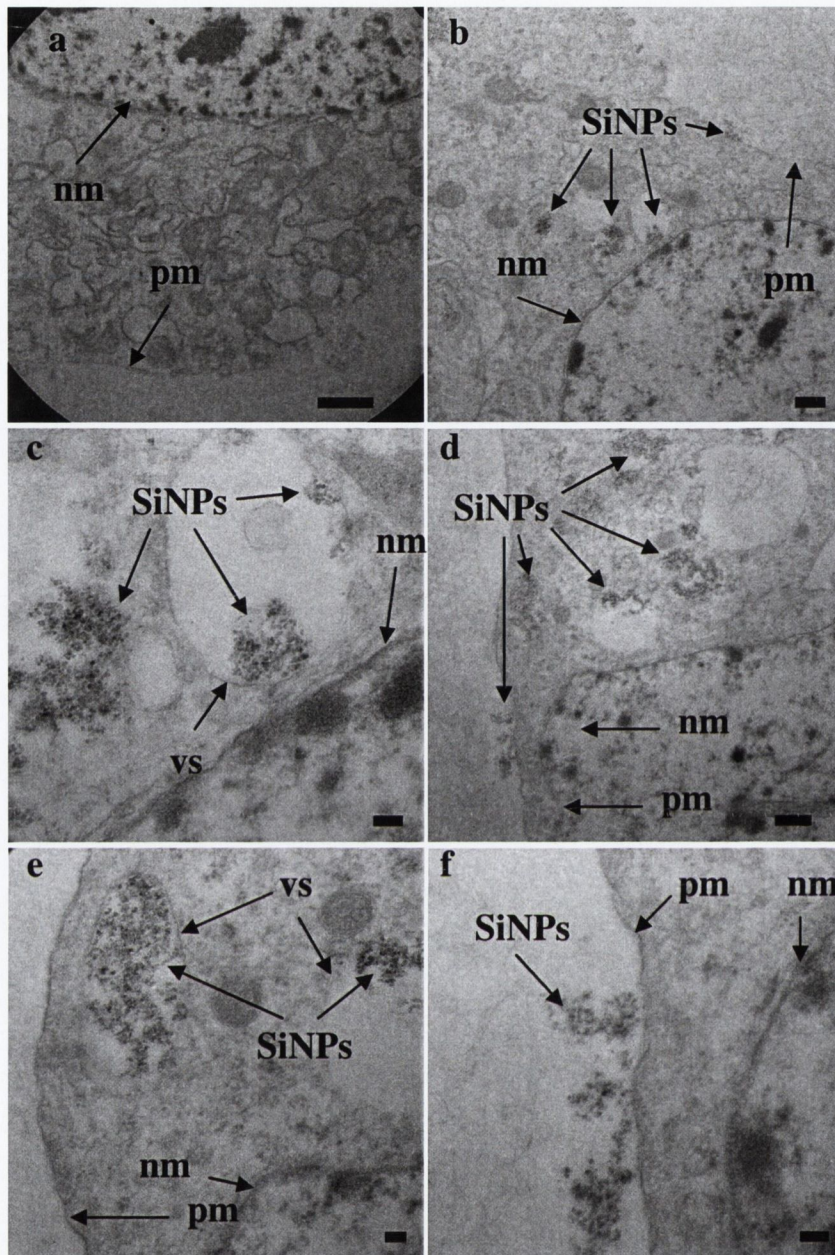


Figure 24 | Transmission electron microscopy studies of HUVEC primary cells. Cells were exposed to 10-µg/ml 10SiNPs for an hour, fixed for TEM and examined by a transmission electron microscope (**b – f**); untreated control cells (without nanoparticles) were also prepared (**a**). Scale bars represent 10 µm in micrograph **a**; 500 nm in **b** and **d**; and 100 nm in **c**, **e**, and **f**. Silica nanoparticles, SiNPs; endothelial plasma membrane, pm; endothelial nuclear membrane, nm; vesicle, vs.

Electron micrographs show how silica nanoparticles quickly interacted with the endothelial plasma membrane (**Figure 24b, 24d, 24f**), internalized and distributed into the cytoplasm of endothelial

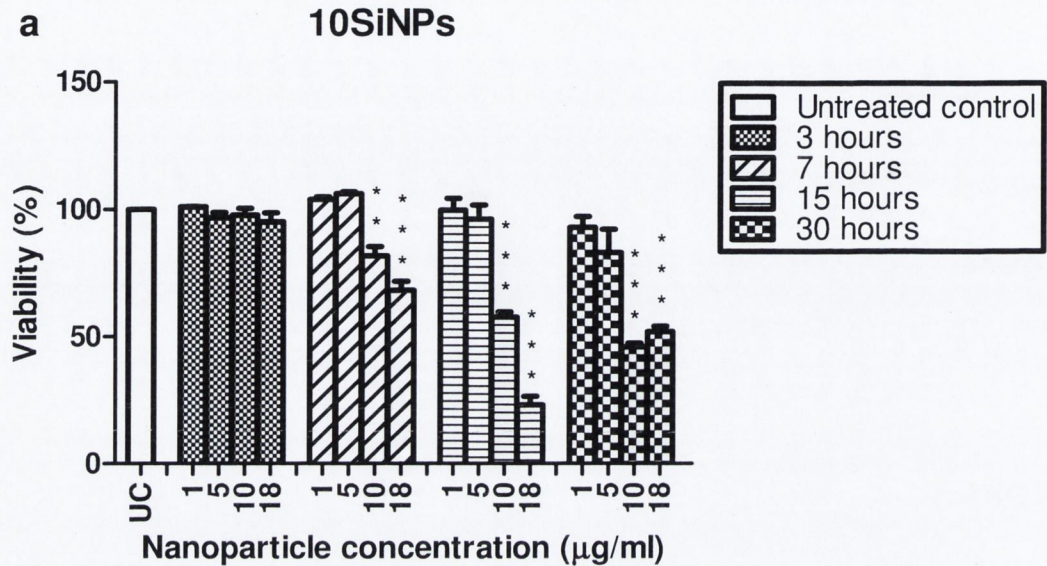
cells (**Figure 24b - 24f**). It appears that endocytosis was involved in nanoparticle uptake by cells, since they were found mainly encapsulated in vesicles; within these vesicles, they were found either floating or bound to the membrane (**Figure 24b - 24e**). However, non-encapsulated nanoparticles were also observed (**Figure 24c, 24d**). As expected, nanoparticles were mainly forming agglomerates (**Figure 24b - 24f**).

AMORPHOUS SILICA NANOPARTICLES INDUCE CYTOTOXICITY

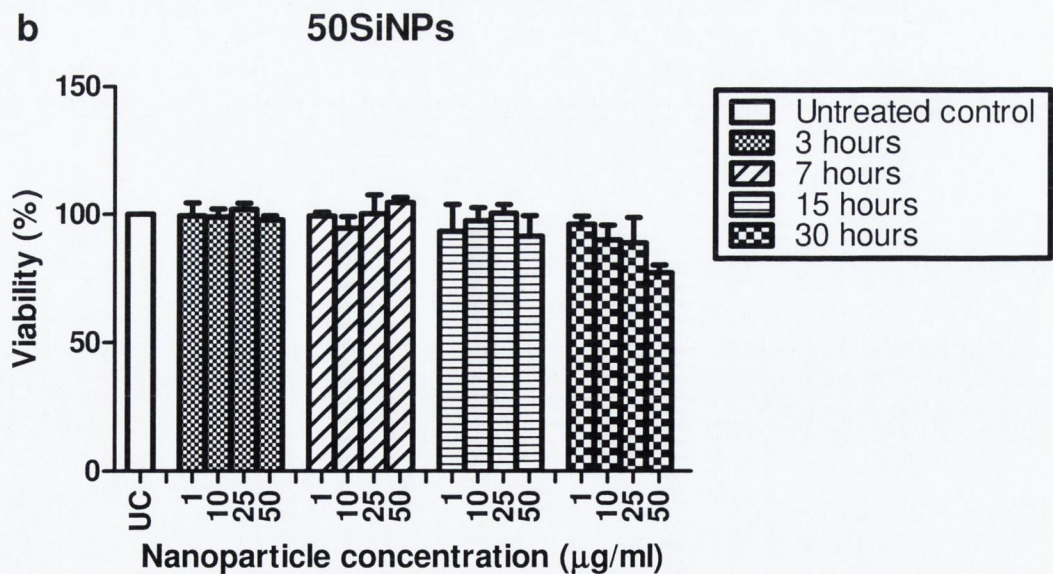
As silica nanoparticles seemed to be toxic for endothelial cells (**Figure 23**), I performed LDH assay to test silica nanoparticle-induced toxicity in HUVEC primary cells.

As it is possible that the test material interferes with the technique of measurement, I included extra controls to avoid potential bias and ensure that the cytotoxicity results shown are exclusively due to silica nanoparticle action. Absorbance readings of the reagents used to perform CytoTox96® Non-Radioactive Cytotoxicity Assay did not change with the addition of nanoparticles in deionised ultra-pure water, at any concentration used in my studies, indicating that silica nanoparticle did not interfere with this assay. Consequently, I performed my cytotoxicity studies. For this, endothelial cells were exposed to several concentrations of silica nanoparticles for 3, 7, 15, and 30 hours (**Figure 25**).

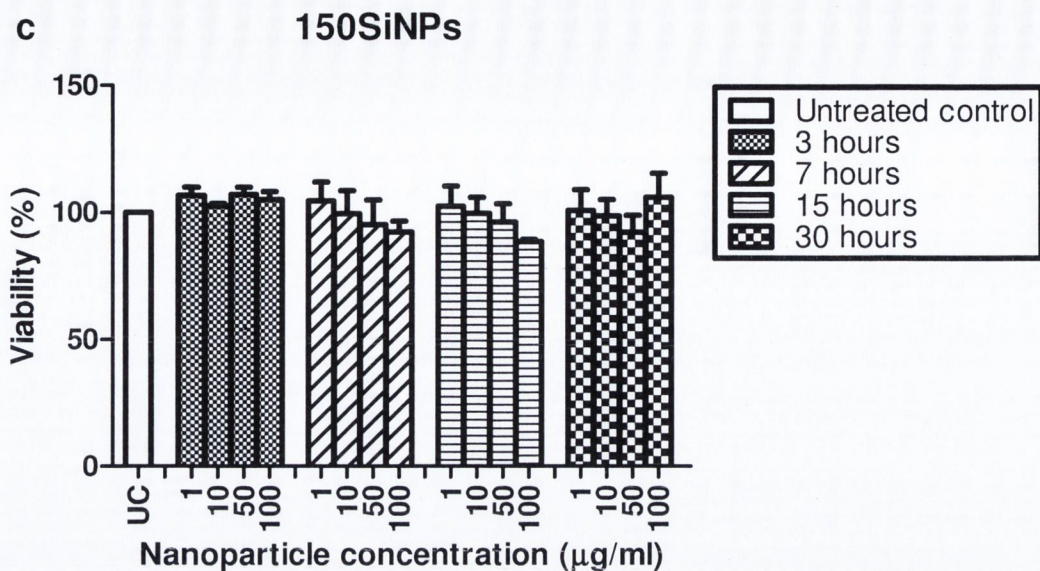
Figure 25 | Effects of amorphous silica nanoparticles in HUVEC primary cell viability.



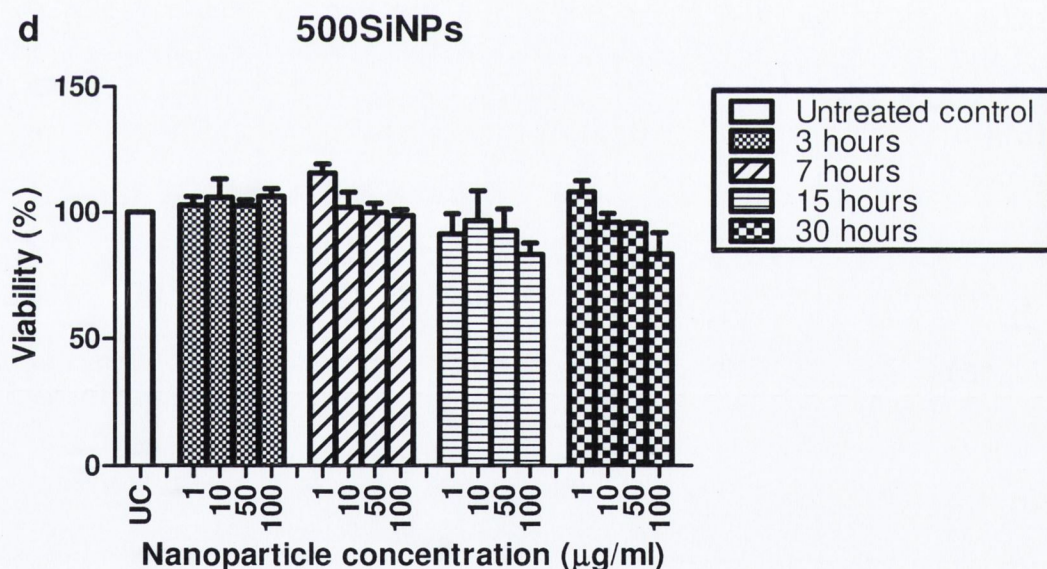
a. Cells were exposed to 10SiNPs for 3, 7, 15, and 30 hours. Cell viability was reduced in a concentration-dependent manner after a 7-, 15-, and 30-hour treatment. All values are mean \pm SEM of $n \geq 3$. One-way ANOVA: 3 hours ($P > 0.05$); 7 hours, 15 hours, 30 hours ($P < 0.0001$); Tukey-Kramer post test: ** $P < 0.01$, *** $P < 0.001$; untreated control (UC) vs treatments.



b. Cells were exposed to 50SiNPs for 3, 7, 15, and 30 hours. All values are mean \pm SEM of $n \geq 3$. One-way ANOVA: 3 hours, 7 hours, 15 hours, 30 hours ($P > 0.05$); untreated control (UC) vs treatments.



c. Cells were exposed to 150SiNPs for 3, 7, 15, and 30 hours. All values are mean \pm SEM of $n \geq 3$. One-way ANOVA: 3 hours, 7 hours, 15 hours, 30 hours ($P > 0.05$); untreated control (UC) vs treatments.



d. Cells were exposed to 500SiNPs for 3, 7, 15, and 30 hours. All values are mean \pm SEM of $n \geq 3$. One-way ANOVA: 3 hours, 7 hours, 15 hours, 30 hours ($P > 0.05$); untreated control (UC) vs treatments.

As compared with the untreated control, viability of HUVEC cells, exposed to 10- μ g/ml 10SiNPs (**Figure 25a**), was significantly reduced to 81.79 ± 3.62 % after a 7-hour, 57.63 ± 2.11 % after a

15-hour, and 45.88 ± 1.55 % after a 30-hour treatment. So did 18- $\mu\text{g}/\text{ml}$ 10SiNPs 68.25 ± 3.55 %, 23.23 ± 3.34 %, and 51.95 ± 2.06 % after a 7-, 15-, and 30-hour treatment respectively. However, equal nanoparticle concentrations did not statistically decrease cell viability after a 3-hour treatment. Larger particles (50SiNPs, 150SiNPs and 500SiNPs) did not statistically exacerbate cell death at any concentration tested (**Figure 25b – 25d**).

The approximate cell doubling time for HUVEC primary cells is 28.5 hours. This may explain why the cytotoxicity of 18- $\mu\text{g}/\text{ml}$ 10SiNPs is significantly lower after a 30- than a 15-hour treatment. For the same reason, after a 15-hour treatment, the speed of cell death also slowed down in the case of 10- $\mu\text{g}/\text{ml}$ 10SiNPs.

AMORPHOUS SILICA NANOPARTICLES INDUCE HUVEC PRIMARY CELLS TO PRODUCE FREE RADICALS

As oxidative stress and oxidant injury have been proposed as the most probable result of the cell-nanoparticle interactions ¹⁵⁹, I examined free radical generation resulting from endothelial cell-nanoparticle interaction.

First, a fluorometric assay served to assess cellular oxidative stress. The **figure 26** shows the effects of a 1-hour treatment of cells with 10- $\mu\text{g}/\text{ml}$ 10SiNPs regarding to free radical production. Green fluorescence, resulting from intracellular oxidation of the free radical-

sensitive probe carboxy-H₂DFFDA by ROS and RNS, was detected by fluorescence microscopy.

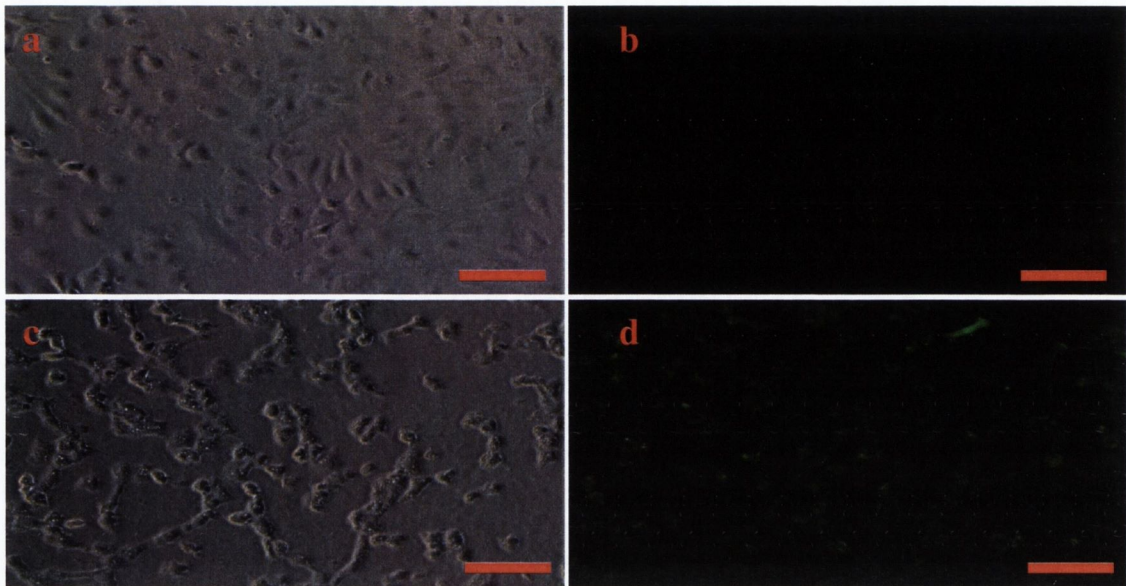


Figure 26 | Free radical production induced by amorphous silica nanoparticles in HUVEC primary cells. Cells were exposed to 10-μg/ml 10SiNPs and free radical production was observed by a fluorescence microscope (**d**); control cells (without nanoparticles) were also visualized (**b**). The corresponding phase-contrast micrographs of control (**a**) and treated (**c**) cells are also showed. Scale bars represent 100 μm.

As compared with the untreated control (**Figure 26b**), free radical production was induced in treated cells (**Figure 26d**). Consequently, it was demonstrated that silica nanoparticles induced free radical production what led to oxidative stress in HUVEC primary cells. Phase-contrast microscopy also showed a change in cellular morphology of treated cells (**Figure 26c**) when compared with untreated control (**Figure 26a**).

AMORPHOUS SILICA NANOPARTICLES STIMULATE HUVEC PRIMARY CELLS TO RELEASE NO AND ONOO⁻

As amorphous silica nanoparticles induced free radical production (**Figure 26**) from endothelial cells, the next step was to identify some of these elements. Due to their crucial role in cardiovascular physiology and pathophysiology, NO and ONOO⁻ released by endothelial cells following stimulation by silica nanoparticles were measured.

The **figure 27** shows a representative measurement of NO and ONOO⁻ released from a single endothelial cell following silica nanoparticle exposure.

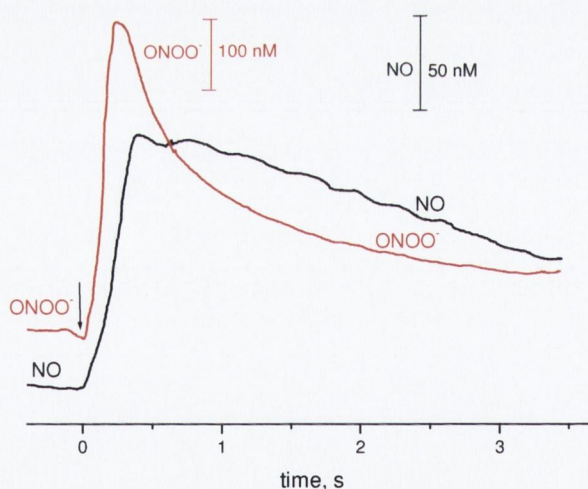


Figure 27 | Silica nanoparticles stimulate directly production of NO and ONOO⁻ from a HUVEC cell. Representative recordings of NO and ONOO⁻ after addition of 25- μ g/ml 10SiNPs to cell culture. The NO and ONOO⁻ were recorded with a tandem of NO/ONOO⁻ nanosensors placed 5 ± 2 μ m from the surface of a single cell. *Measurements performed in collaboration with Prof Tadeusz Malinski and Dr Adam Jacoby (Ohio University, Athens, Ohio, USA).*

Silica nanoparticles stimulated directly production of NO and ONOO⁻ from cells. After injection of 25- μ g/ml 10SiNPs, a rapid release of both NO and ONOO⁻ from a single HUVEC cell was observed. A maximum of 340 ± 25 nanomoles of ONOO⁻ per litre was recorded after 200 ± 20 ms. A maximum of 120 ± 10 nanomoles of NO per litre was observed after 400 ms. After that, both concentrations decreased to a level of about 100 nanomoles per litre for ONOO⁻ and to about 75 nanomoles per litre for NO. These concentrations decreased slowly to reach an undetectable level after 60 seconds.

The **figures 28** and **29** show maximum NO and ONOO⁻ release from a single endothelial cell resulting from direct stimulation by silica nanoparticles.

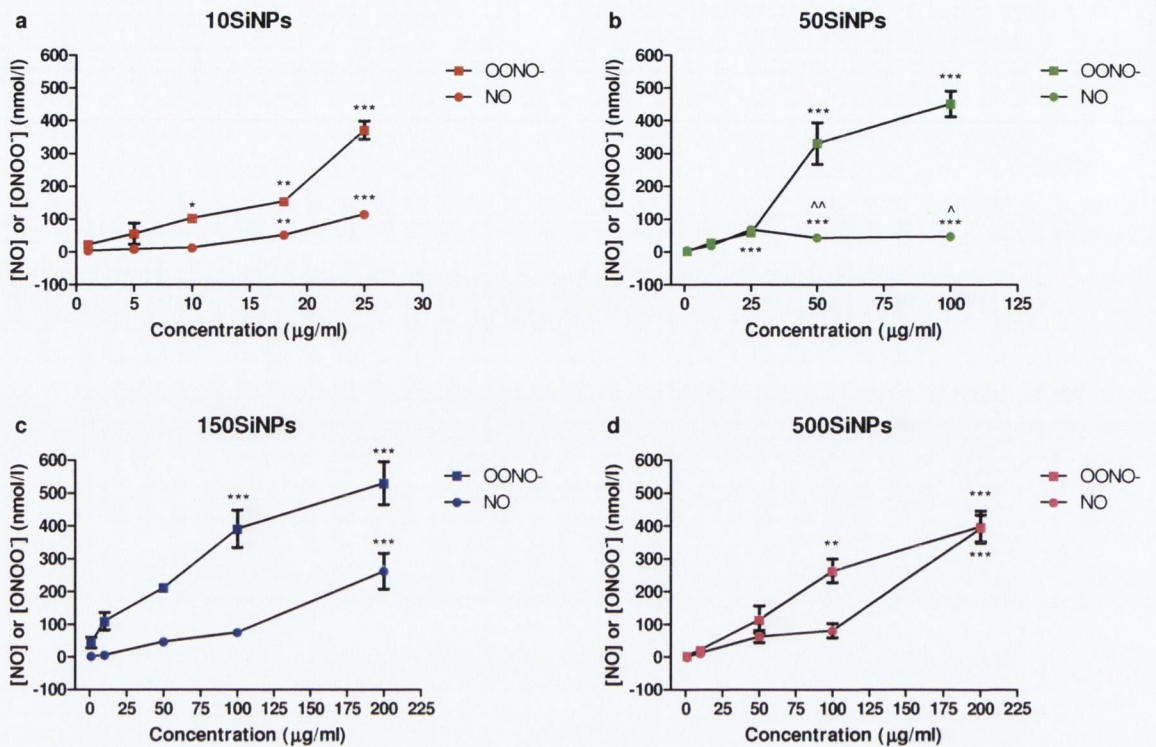


Figure 28 | Maximum ONOO⁻ and NO release from a single HUVEC cell stimulated by silica nanoparticles. Exposure of endothelial cells to 10SiNPs (**a**, red), 50SiNPs (**b**, green), 150SiNPs (**c**, blue), and 500SiNPs (**d**, pink) stimulated release of ONOO⁻ (squares) and NO (circles). All values are mean \pm SEM of $n \geq 3$. One-way ANOVA: a, b, c, d (NO, ONOO⁻; $P < 0.0001$); Tukey-Kramer post test: * $P < 0.05$, ** $P < 0.01$, *** $P < 0.001$; 1- $\mu\text{g/ml}$ vs treatments; ^ $P < 0.05$, ^^ $P < 0.01$; 25- $\mu\text{g/ml}$ 50SiNPs vs 50- $\mu\text{g/ml}$ 50SiNPs, 100- $\mu\text{g/ml}$ 50SiNPs (**b**). Measurements performed in collaboration with Prof Tadeusz Malinski and Dr Adam Jacoby (Ohio University, Athens, Ohio, USA).

The NO release, as a response to silica nanoparticle stimulation, represents the maximum NO concentration released from a single cell. The NO release from HUVEC cells exposed to 10SiNPs significantly increased at concentrations greater than 18 $\mu\text{g/ml}$. On the other hand, 50SiNP stimulation of cells demonstrated the greatest NO release at a concentration of 25 $\mu\text{g/ml}$. The use of 150SiNP and

500SiNP stimulation of cells also showed significant increases in NO but only with a nanoparticle concentration of 200 $\mu\text{g/ml}$ (**Figure 28**).

The ONOO^- release, as a response to silica nanoparticle stimulation, represents the ONOO^- concentration released from a single cell. The ONOO^- release from 10SiNP and 50SiNP stimulated cells increased significantly at concentrations greater than 10 $\mu\text{g/ml}$ and 50 $\mu\text{g/ml}$ respectively. The use of 150SiNP and 500SiNP stimulation of HUVEC cells showed increases in ONOO^- at concentrations higher than 100 $\mu\text{g/ml}$ (**Figure 28**).

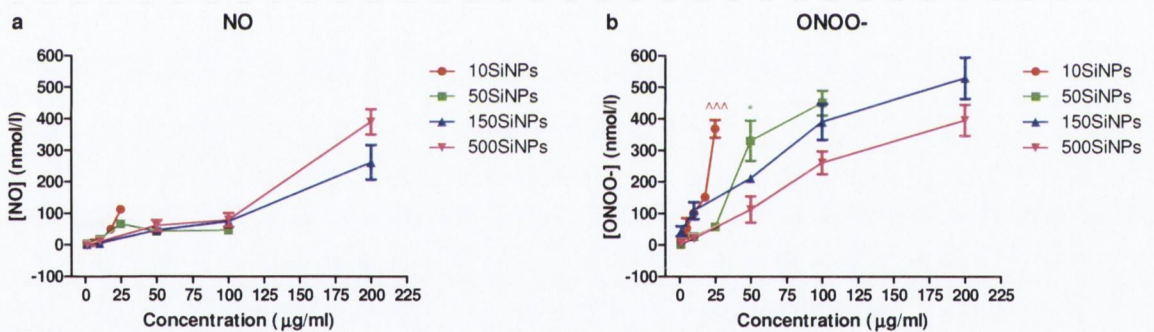


Figure 29 | Comparative maximum NO and ONOO^- release from a single cell stimulated by silica nanoparticles. For a clearer view, the maximum NO (**a**) and ONOO^- (**b**) release from endothelial cells exposed to 10SiNPs (**red**), 50SiNPs (**green**), 150SiNPs (**blue**), and 500SiNPs (**pink**) are plotted on the same graph. All values are mean \pm SEM of $n \geq 3$. One-way ANOVA: $P = 0.0212$; Tukey-Kramer post test: $*P < 0.05$; 50- $\mu\text{g/ml}$ 500SiNPs vs 50- $\mu\text{g/ml}$ 150SiNPs, 50- $\mu\text{g/ml}$ 50SiNPs (**b**). Two-tails unpaired Student's t-tests: $^{^^}P < 0.001$; 25- $\mu\text{g/ml}$ 50SiNPs vs 25- $\mu\text{g/ml}$ 10SiNPs. Measurements performed in collaboration with Prof Tadeusz Malinski and Dr Adam Jacoby (Ohio University, Athens, Ohio, USA).

25- $\mu\text{g/ml}$ 10SiNPs induced a significantly higher ONOO^- release from cells than that of 25- $\mu\text{g/ml}$ 50SiNPs. Cells stimulated by 50-

$\mu\text{g/ml}$ 50SiNPs significantly induced greater ONOO^- release than that induced by 50- $\mu\text{g/ml}$ 500SiNPs. 25- $\mu\text{g/ml}$ 10SiNPs induced a higher ONOO^- release from cells than those of 50- $\mu\text{g/ml}$ 50SiNPs, 150SiNPs, and 500SiNPs (**Figure 29**).

AMORPHOUS SILICA NANOPARTICLES INDUCE NF- κ B BINDING ACTIVITY IN HUVEC PRIMARY CELLS

In my transfer thesis studies ¹⁶⁰, I demonstrated that silica nanoparticles induced gene up-regulation of some inflammatory factors (ICAM1, VCAM1, SELE, MMP9) in an immortalized endothelial cell line. The transcription of these four genes into mRNA has been shown to be activated by transcription factor NF- κ B ⁸⁹. Moreover, nanoparticle exposure to cells has been demonstrated to result in NF- κ B binding activity activation ¹⁶¹. Furthermore, NF- κ B activity has been proved to be induced by oxidative stress in HUVEC cells ⁹⁰. Consequently, I tested if NF- κ B is involved in silica nanoparticle-induced noxious effects in HUVEC primary cells.

As it is possible that the test material interferes with the technique of measurement, I included extra controls to avoid potential bias and ensure that NF- κ B binding activity results shown are exclusively due to silica nanoparticle action. Absorbance readings of the reagents used to perform NF- κ B (p65) Transcription Factor Assay Kit did not change with the addition of nanoparticles in deionised ultra-pure water at any concentration used in my studies,

indicating that silica nanoparticle did not interfere with this assay. Then, I analysed the effects of silica nanoparticles on NF- κ B (p65) binding activity. Based on my cytotoxicity studies (**Figure 25**), I exposed HUVEC primary cells to 10- μ g/ml 10SiNPs for a hour as well as 50- μ g/ml 50SiNPs, 150SiNPs, and 500SiNPs for 3 hours (**Figure 30**).

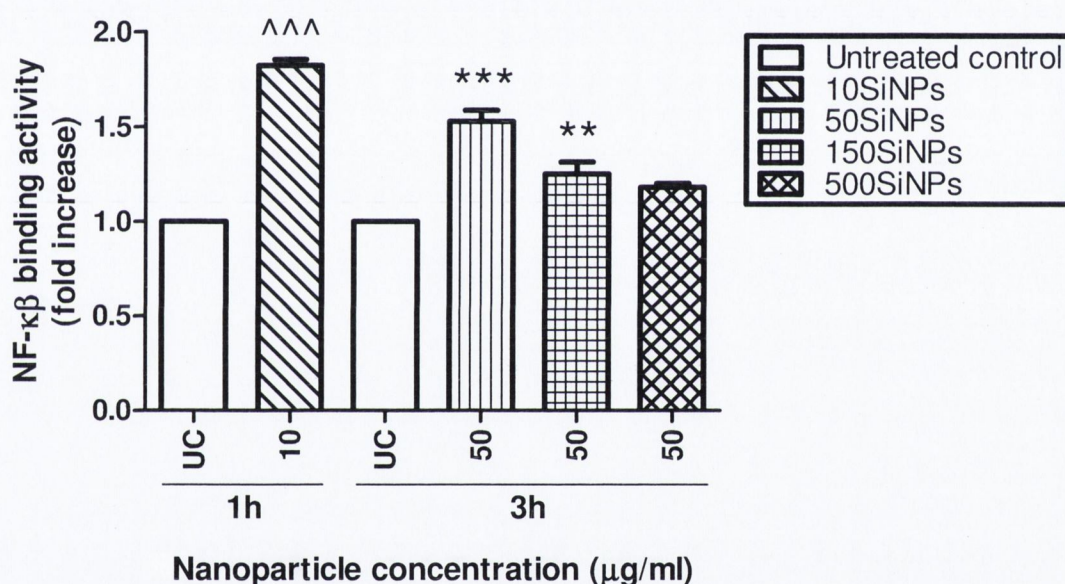


Figure 30 | Effects of amorphous silica nanoparticles on NF- κ B binding activity. Endothelial cells were exposed to 10- μ g/ml 10SiNPs, for 1 hour (1h); and 50- μ g/ml 50SiNPs, 150SiNPs and 500SiNPs, for 3 hours (3h). All values are mean \pm SEM of $n \geq 3$. Two-tails unpaired Student's t-test: $^{\wedge\wedge\wedge}P < 0.001$; untreated control (UC) vs treatment. One-way ANOVA: $P = 0.0007$; Tukey-Kramer post test: $^{**}P < 0.01$, $^{***}P < 0.001$; untreated control (UC) vs treatments.

Exposure of HUVEC cells to 10- μ g/ml 10SiNPs (fold change 1.82 ± 0.03 , as compared with the untreated control) for an hour and 50- μ g/ml 50SiNPs (1.5 ± 0.09), and 50- μ g/ml 150SiNPs (1.33 ± 0.05)

for 3 hours, caused a significant increase of the NF- κ B binding activity. In contrast, 50- μ g/ml 500SiNPs did not significantly increase NF- κ B activity in 3 hours.

AMORPHOUS SILICA NANOPARTICLES INDUCE GENE EXPRESSION OF ICAM1, VCAM1, SELE, MMP9, PTGS2, F3, IL6, and IL8

I have already demonstrated (transfer thesis studies) ¹⁶⁰ by real-time qPCR that a 15-hour treatment of immortalized HUVEC cells with 10- μ g/ml 10SiNPs significantly up-regulated expression of the genes *ICAM1* (3.27 ± 0.20 folds, as compared with the untreated control), *VCAM1* (5.43 ± 0.43), *SELE* (4.60 ± 0.52), and *MMP9* (4.14 ± 0.52). So did 100- μ g/ml 150SiNPs: *ICAM1* (17.61 ± 0.23), *VCAM1* (8.13 ± 0.27), *SELE* (30.03 ± 3.33), and *MMP9* (10.50 ± 0.59). Consequently, I performed real-time qPCR to evaluate whether silica nanoparticles influence gene expression of some key endothelial mediators in inflammation and coagulation. Once more, I analyzed gene expression of endothelial adhesion molecules (*ICAM1*, *VCAM1*, and *SELE*) and the proteinase, *MMP9*. Besides, I also examined gene expression of the synthase, *PTGS2*; the key initiator of coagulation, tissue factor (*F3*); and the cytokines, *IL6* and *IL8*.

The **figure 31** shows 3 representative real-time qPCR experiments which demonstrate that this technique did not interfere with the test material (silica nanoparticles) and *rRNA18S* could be

used as an internal control (housekeeping gene) to examine endothelial gene expression in the presence and absence of amorphous silica nanoparticles. In order to demonstrate non-interaction with nanoparticles, I performed real-time qPCR with RT-PCR grade water (**Figure 31a**) and 10- μ g/ml 10SiNPs (**Figure 31b**) and observed non-amplification of *rRNA18S*, *ICAM1*, *VCAM1*, *SELE*, *MMP9*, *PTGS2*, *IL6* and *IL8*. In contrast, logarithmic amplification of both *SELE* and *rRNA18S* genes was observed, when real-time qPCR was performed on cDNA, which was obtained by reverse transcription of RNA, in turn, isolated from cells treated with silica nanoparticles (1-, 5-, 10-, 18- μ g/ml 10SiNPs) and control cells (**Figure 31c**). Concentration-dependent up-regulation of *SELE* induced by nanoparticles, but not *rRNA18S*, is shown in **figure 31c**. In addition, C_t values of both genes are located between amplification cycle 5 and 35. Therefore, real-time qPCR is suitable to study gene expression in the presence of silica nanoparticles; and also, *rRNA18S* is suitable as internal control.

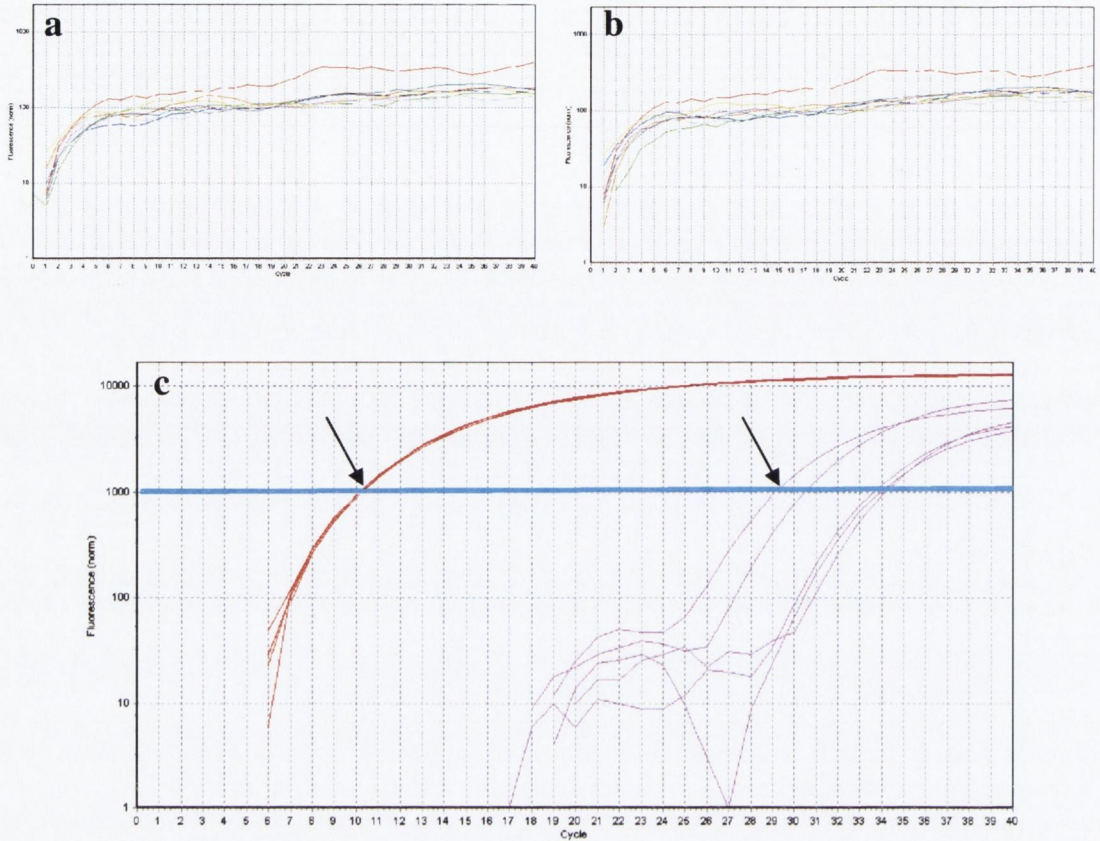
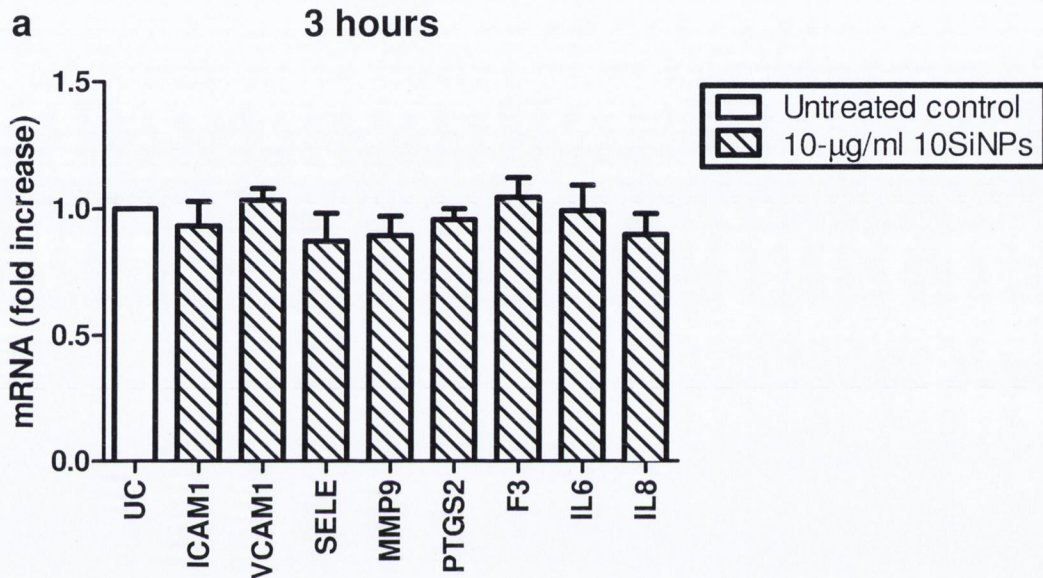


Figure 31 | Representative traces from real-time qPCR analyses. Real-time qPCR was performed with RT-PCR grade water (a) and 10 µg/ml 10SiNPs (b). Real-time qPCR was also used to analyse gene expression of *SELE* and *rRNA18S* in cells treated with silica nanoparticles and untreated control cells (c). The Y-axes represent fluorescence and the X-axes cycles of amplification of cDNA (40 in total). Red lines represent *rRNA18S*; yellow, *ICAM1*; dark blue, *VCAM1*; pink, *SELE*; grey, *MMP9*; orange, *PTGS2*; dark green, *IL6*; and bright green, *IL8*. The black arrows (c) point to the C_t value of *rRNA18S* and *SELE*. The thick straight navy blue line (c) represents the fluorescence level at which C_t values were compared. The five pink lines (c) represent from right to left control, 1-, 5-, 10-, and 18-µg/ml 10SiNPs; the five red lines (c) represent the same.

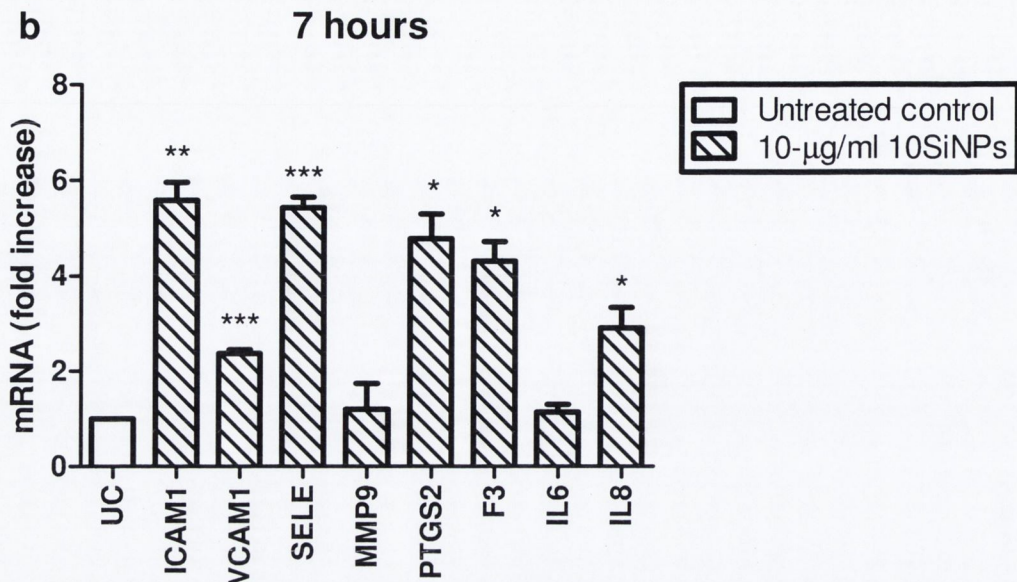
In order to examine silica nanoparticle-induced gene up-regulation in HUVEC primary cells, first I performed time-course real-time qPCR analyses. As 10-µg/ml 10SiNPs induced gene up-regulation in immortalized HUVEC cells, I treated HUVEC primary cells

with 10- μ g/ml 10SiNPs for 3 and 7 (**Figure 32**) as well as 15 hours (**Figure 33, 34**) base on my cytotoxicity studies (**Figure 25**).

Figure 32 | Effects of 10- μ g/ml 10SiNPs on gene expression of *ICAM1*, *VCAM1*, *SELE*, *MMP9*, *PTGS2*, *F3*, *IL6*, and *IL8* at 3 and 7 hours.



a. HUVEC primary cells were exposed to 10- μ g/ml 10SiNPs for 3 hours and gene expression of *ICAM1*, *VCAM1*, *SELE*, *MMP9*, *PTGS2*, *F3*, *IL6* and *IL8* was analyzed by real-time qPCR. All values are mean \pm SEM of $n \geq 3$. Two-tails unpaired Student's t-tests: $P > 0.05$; untreated control (UC) vs treatments.



b. HUVEC primary cells were exposed to 10-µg/ml 10SiNPs for 7 hours and gene expression of *ICAM1*, *VCAM1*, *SELE*, *MMP9*, *PTGS2*, *F3*, *IL6* and *IL8* was analyzed by real-time qPCR. All values are mean ± SEM of $n \geq 3$. Two-tails unpaired Student's t-tests: * $P < 0.05$, ** $P < 0.01$, *** $P < 0.001$; untreated control (UC) vs treatments.

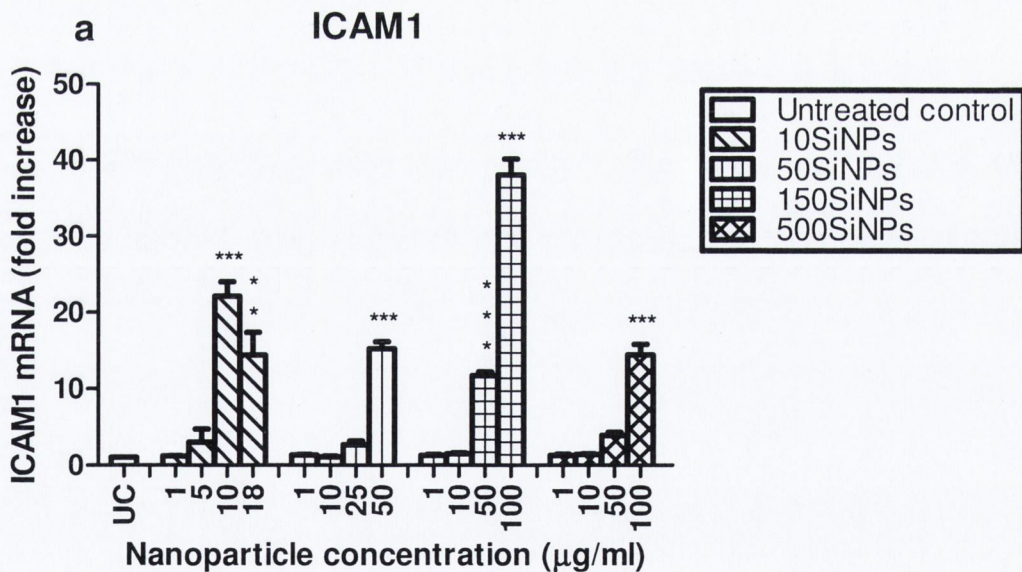
Gene expression of *ICAM1* (fold change 5.58 ± 0.38 , as compared with the untreated control), *SELE* (5.42 ± 0.23), *PTGS2* (4.77 ± 0.52), *F3* (4.31 ± 0.41), *IL8* (2.91 ± 0.43), and *VCAM1* (2.37 ± 0.08) were all significantly up-regulated after a 7-hour treatment. In contrast, *MMP9* and *IL6* were not. On the other hand, gene expression was not induced after 3 hours treatment. A 15-hour treatment of endothelial cells with 10-µg/ml 10SiNPs reported the highest gene up-regulation of all (**Figure 33, 34**).

Based on my time-course real-time qPCR analyses, I performed a concentration-course study at 15 hours to evaluate the influence of various concentrations of 10SiNPs on HUVEC primary cells. Furthermore, I also evaluated the influence of various concentrations

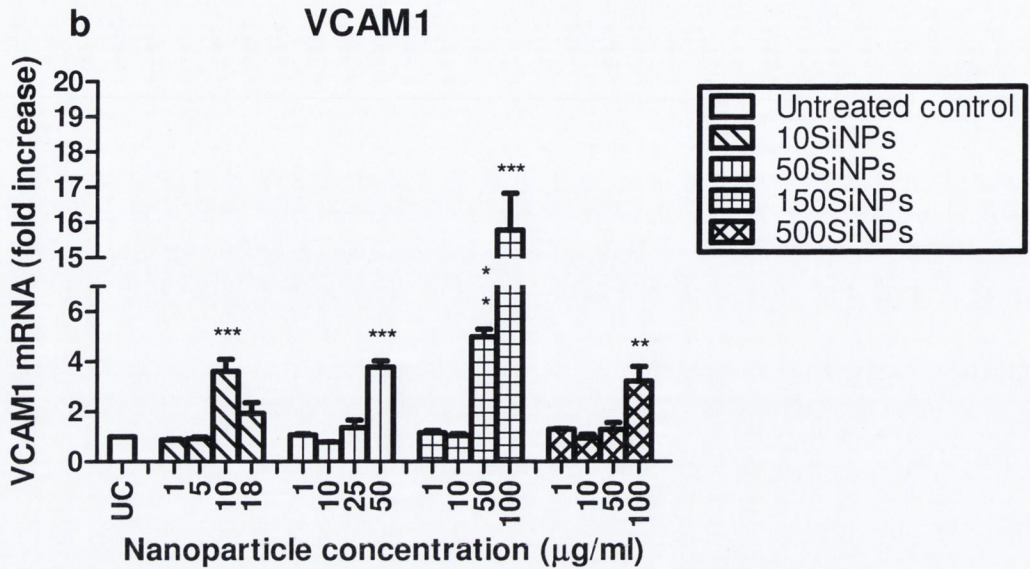
of 50SiNPs, 150SiNPs, and 500SiNPs at the same time point (**Figure 33, 34**).

The **figure 33** shows a concentration-course analysis (at 15 hours) by real-time qPCR on the expression of the genes *ICAM1*, *VCAM1*, *SELE*, and *MMP9* of treated HUVEC primary cells with 10SiNPs, 50SiNPs, 150SiNPs, and 500SiNPs. These genes were significantly up-regulated by 10- $\mu\text{g/ml}$ 10SiNPs and 100- $\mu\text{g/ml}$ 150SiNPs in immortalized HUVEC cells, as reported in my transfer thesis.

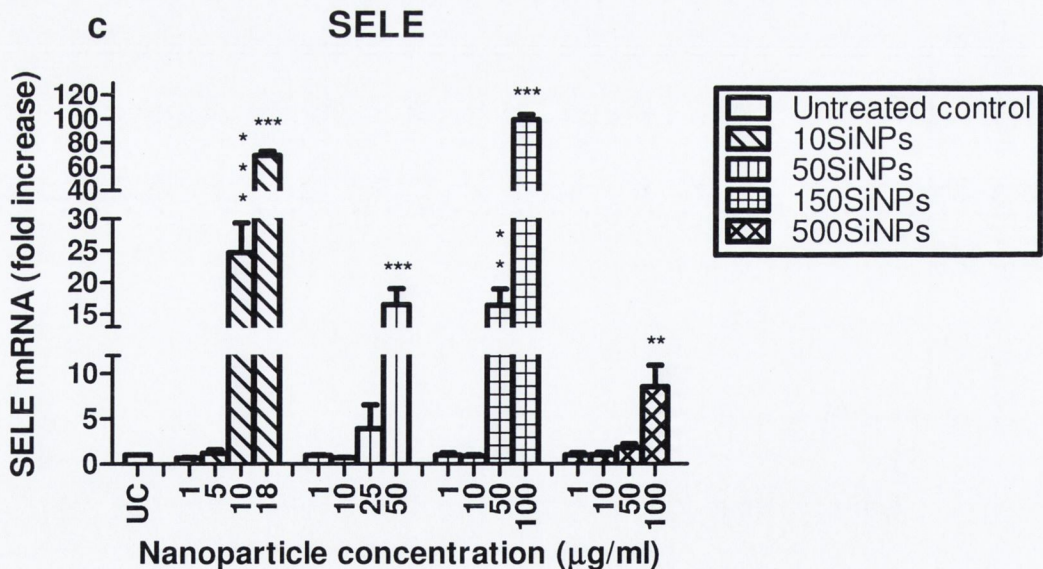
Figure 33 | Effects of silica nanoparticles on gene expression of *ICAM1*, *VCAM1*, *SELE*, and *MMP9* at 15 hours.



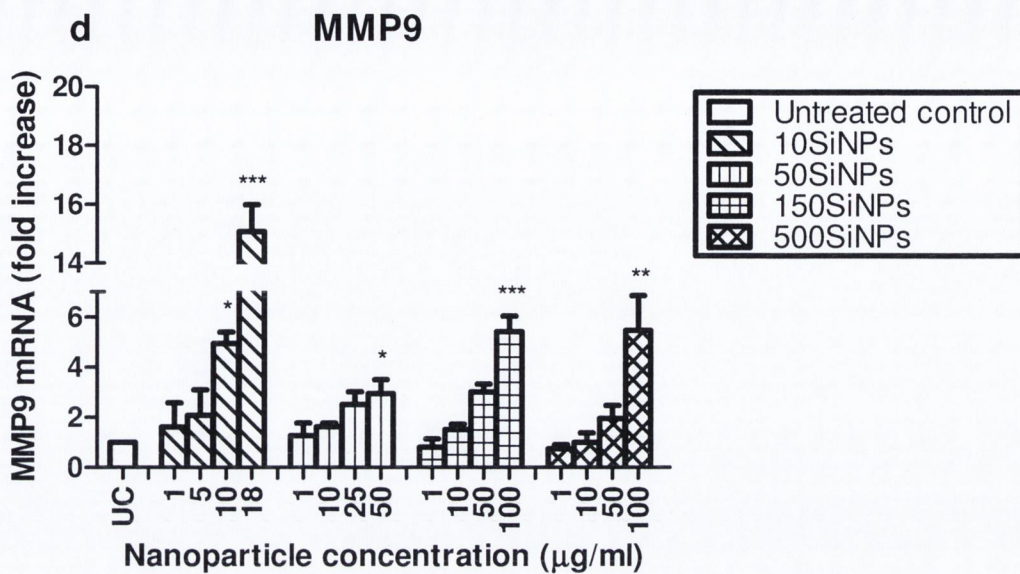
a. HUVEC primary cells were exposed to silica nanoparticles for 15 hours and *ICAM1* gene expression was quantified by real-time qPCR. All values are mean \pm SEM of $n \geq 3$. One-way ANOVA: 10SiNPs, 50SiNPs, 150SiNPs, 500SiNPs ($P < 0.0001$); Tukey-Kramer post test: ** $P < 0.01$, *** $P < 0.001$; untreated control (UC) vs treatments.



b. HUVEC cells were exposed to silica nanoparticles for 15 hours and *VCAM1* gene expression was quantified by real-time qPCR. All values are mean \pm SEM of $n \geq 3$. One-way ANOVA: 10SiNPs ($P = 0.0003$); 50SiNPs, 150SiNPs ($P < 0.0001$); 500SiNPs ($P = 0.0015$); Tukey-Kramer post test: ** $P < 0.01$, *** $P < 0.001$; untreated control (UC) vs treatments.



c. HUVEC cells were exposed to silica nanoparticles for 15 hours and *SELE* gene expression was quantified by real-time qPCR. All values are mean \pm SEM of $n \geq 3$. One-way ANOVA: 10SiNPs ($P < 0.0001$); 50SiNPs ($P = 0.0002$); 150SiNPs ($P < 0.0001$); 500SiNPs ($P = 0.0022$); Tukey-Kramer post test: ** $P < 0.01$, *** $P < 0.001$; untreated control (UC) vs treatments.

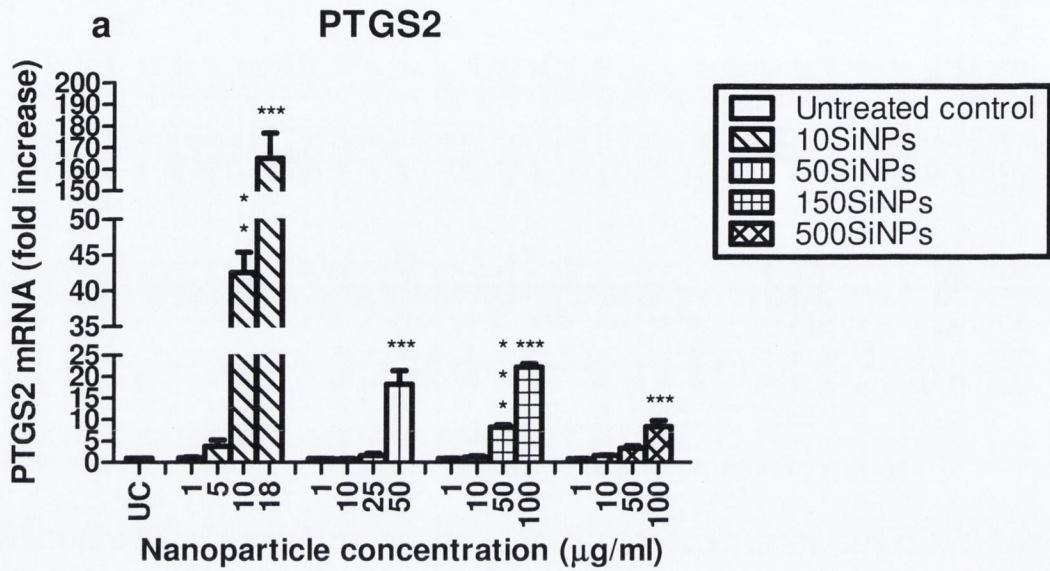


d. HUVEC cells were exposed to silica nanoparticles for 15 hours and *MMP9* gene expression was quantified by real-time qPCR. All values are mean \pm SEM of $n \geq 3$. One-way ANOVA: 10SiNPs ($P < 0.0001$); 50SiNPs ($P = 0.0344$); 150SiNPs ($P < 0.0001$); 500SiNPs ($P = 0.0031$); Tukey-Kramer post test: * $P < 0.05$, ** $P < 0.01$, *** $P < 0.001$; untreated control (UC) vs treatments.

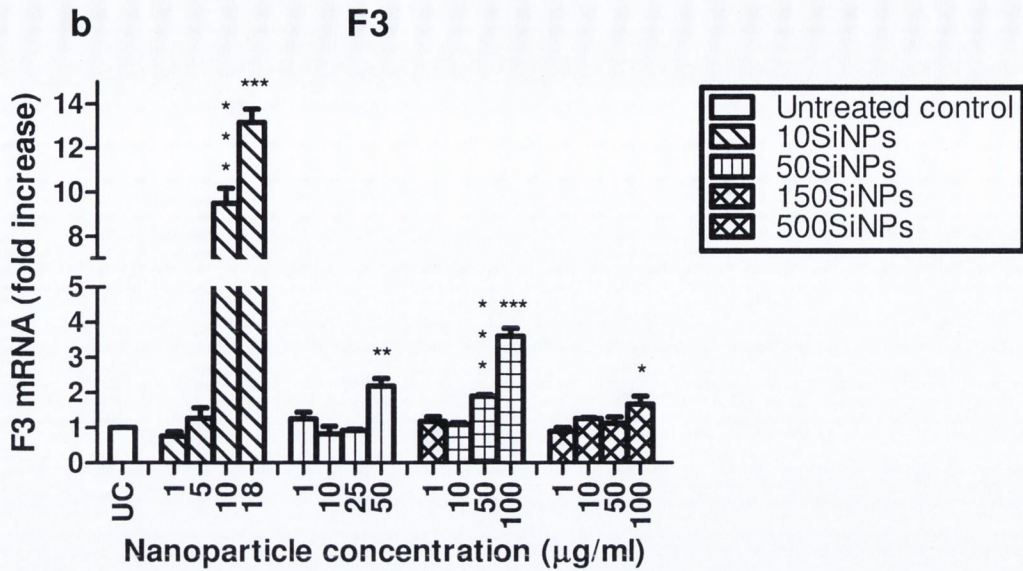
Statistically significant gene expression up-regulation (fold increase) resulting from exposure of HUVEC primary cells to silica nanoparticles are shown in **table 2**.

The **figure 34** shows the concentration-course analysis (at 15 hours) by real-time qPCR on the expression of the genes *PTGS2*, *F3*, *IL6*, and *IL8* of treated HUVEC primary cells with 10SiNPs, 50SiNPs, 150SiNPs, and 500SiNPs.

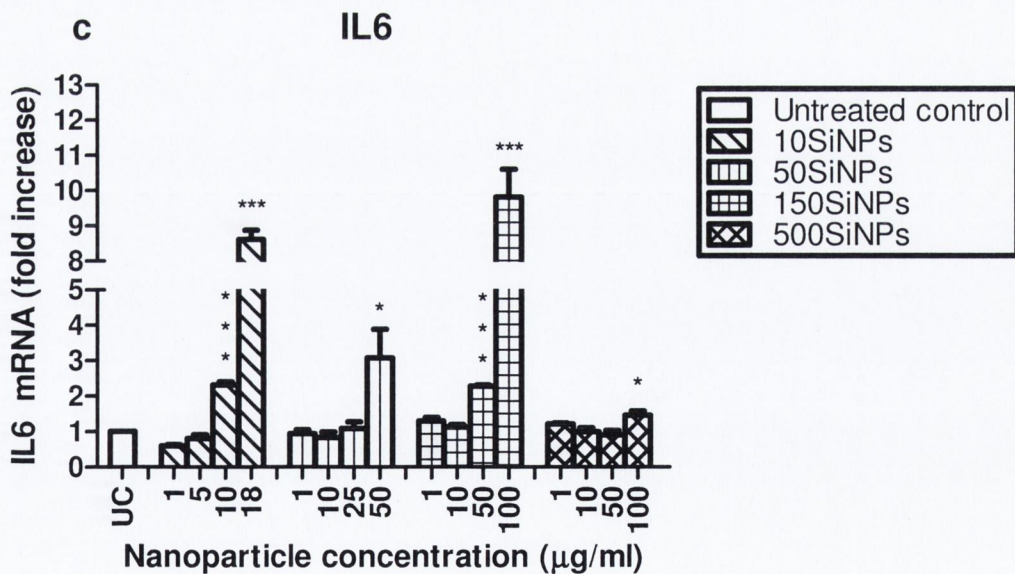
Figure 34 | Effects of silica nanoparticles on gene expression of *PTGS2*, *F3*, *IL6*, and *IL8* at 15 hours.



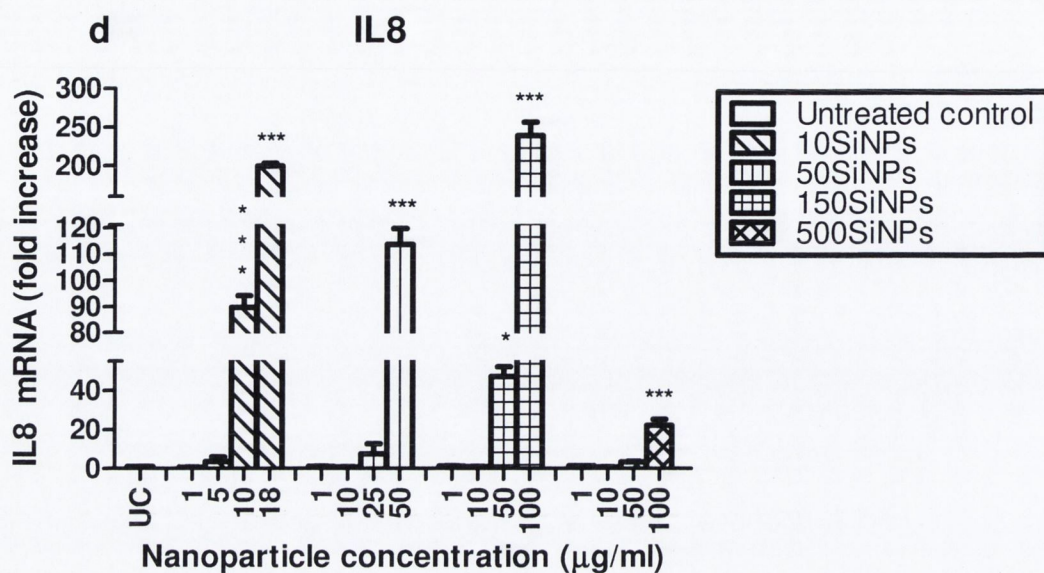
a. HUVEC cells were exposed to silica nanoparticles for 15 hours and *PTGS2* gene expression was quantified by real-time qPCR. All values are mean \pm SEM of $n \geq 3$. One-way ANOVA: 10SiNPs, 50SiNPs, 150SiNPs, 500SiNPs ($P < 0.0001$); Tukey-Kramer post test: ** $P < 0.01$, *** $P < 0.001$; untreated control (UC) vs treatments.



b. HUVEC cells were exposed to silica nanoparticles for 15 hours and *F3* gene expression was quantified by real-time qPCR. All values are mean \pm SEM of $n \geq 3$. One-way ANOVA: 10SiNPs ($P < 0.0001$); 50SiNPs ($P = 0.0009$); 150SiNPs ($P < 0.0001$); 500SiNPs ($P = 0.0168$); Tukey-Kramer post test: * $P < 0.05$, ** $P < 0.01$, *** $P < 0.001$; untreated control (UC) vs treatments.



c. HUVEC cells were exposed to silica nanoparticles for 15 hours and *IL6* gene expression was quantified by real-time qPCR. All values are mean \pm SEM of $n \geq 3$. One-way ANOVA: 10SiNPs ($P < 0.0001$); 50SiNPs ($P = 0.0086$); 150SiNPs ($P < 0.0001$); 500SiNPs ($P = 0.0092$); Tukey-Kramer post test: * $P < 0.05$, *** $P < 0.001$; untreated control (UC) vs treatments.



d. HUVEC cells were exposed to silica nanoparticles for 15 hours and *IL8* gene expression was quantified by real-time qPCR. All values are mean \pm SEM of $n \geq 3$. One-way ANOVA: 10SiNPs, 50SiNPs, 150SiNPs, 500SiNPs ($P < 0.0001$); Tukey-Kramer post test: * $P < 0.05$, *** $P < 0.001$; untreated control vs treatments.

As compared with the untreated control, statistically significant gene expression up-regulation (fold increase) of *ICAM1*, *VCAM1*, *SELE*, *MMP9*, *PTGS2*, *F3*, *IL6*, and *IL8* resulting from exposure of HUVEC cells to silica nanoparticles are shown in **table 2**.

	10- 10SiNPs	18- 10SiNPs	50- 50SiNPs	50- 150SiNPs	100- 150SiNPs	100- 500SiNPs
ICAM1	22.12±1.90	14.40±2.95	15.21±0.93	11.67±0.50	38.03±2.12	14.46±1.35
VCAM1	3.61±0.49	ns	3.76±0.27	4.98±0.30	15.78±1.05	3.21±0.72
SELE	24.66±4.70	69.29±3.53	16.47±2.49	16.35±2.59	99.14±4.17	8.54±2.37
MMP9	4.94±0.44	15.08±0.92	2.94±0.56	3.01±0.32	5.41±0.62	5.47±1.37
PTGS2	42.57±2.84	165.1±11.56	18.20±3.16	8.20±0.58	22.19±0.83	8.35±1.40
F3	9.50±0.69	13.17±0.60	2.19±0.22	1.90±0.04	3.60±0.23	1.66±0.24
IL6	2.31±0.09	8.62±0.26	3.07±0.80	2.27±0.04	9.02±0.30	1.46±0.11
IL8	89.62±4.40	199.40±3.62	113.6±6.04	47.05±5.12	239.00±17.21	22.06±3.16

Table 2 | Real-time qPCR analyses of HUVEC cells exposed to silica nanoparticles. Endothelial cells were treated with silica nanoparticles (various concentrations) for 15 hours and gene expression analyzed by real-time qPCR. As compared with untreated control, statistically significant gene fold increases are shown in this table. All values are mean ± SEM. 10-10SiNPs, 10-µg/ml 10SiNPs; 18-10SiNPs, 18-µg/ml 10SiNPs; 50-50SiNPs, 50-µg/ml 50SiNPs; 50-150SiNPs, 50-µg/ml 150SiNPs; 100-150SiNPs, 100-µg/ml 150SiNPs; 100-500SiNPs, 100-µg/ml 500SiNPs.

AMORPHOUS SILICA NANOPARTICLE INDUCE RELEASE OF THE CYTOKINES IL6 AND IL8

I have already demonstrated (transfer thesis studies) ¹⁶⁰ that IL8 release into cell culture media significantly increased (2.38 ± 0.13 folds) when immortalized HUVEC cells were exposed for 15 hours to 100-µg/ml 150SiNPs as shown by CBA analyses. Furthermore, silica nanoparticles induced the up-regulation of *IL6* and *IL8* gene expression in HUVEC primary cells (**Figure 32, 34**). Consequently, I performed CBA on HUVEC primary cells treated with nanoparticles for 15 hours to demonstrate that cytokines up-regulation is also observed at protein level.

Although, I also analyzed the release of IL1β, IL10, TNFα, and IL12p70 into the culture media, the level of these molecules remained below the detection limit of the technique (20 pg/ml); and therefore, they were not taken into account.

The **figure 35** shows traces of two representative CBA studies that demonstrate that this technique did not interfere with the test material (silica nanoparticles) and therefore could be used to analyse protein release in the presence and absence of silica nanoparticles. Analysis by CBA with deionised ultra-pure water (**Figure 35a**) and 10- $\mu\text{g/ml}$ 10SiNPs in deionised ultra-pure water (**Figure 35b**) did not show differences proving no interference.

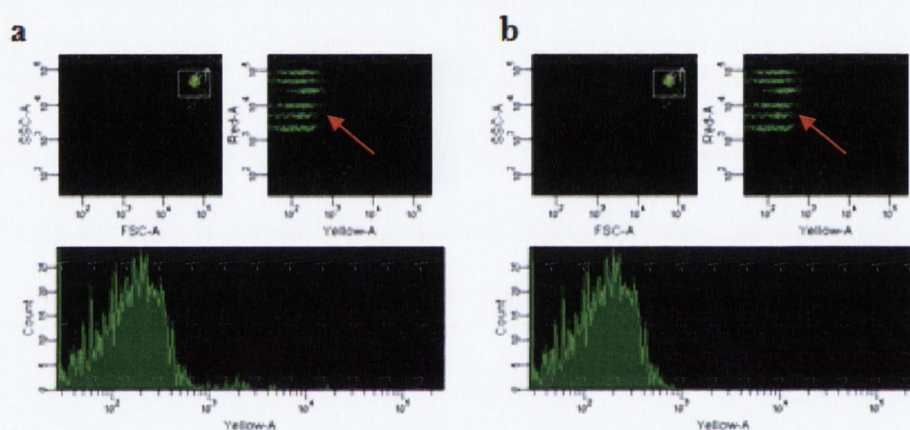
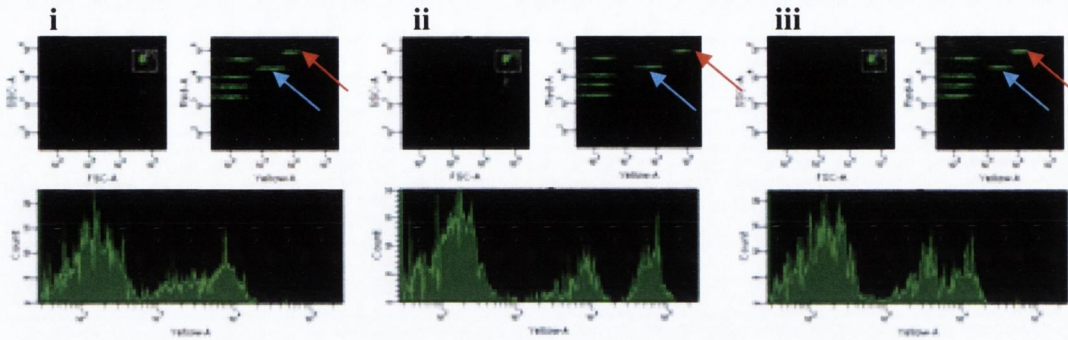


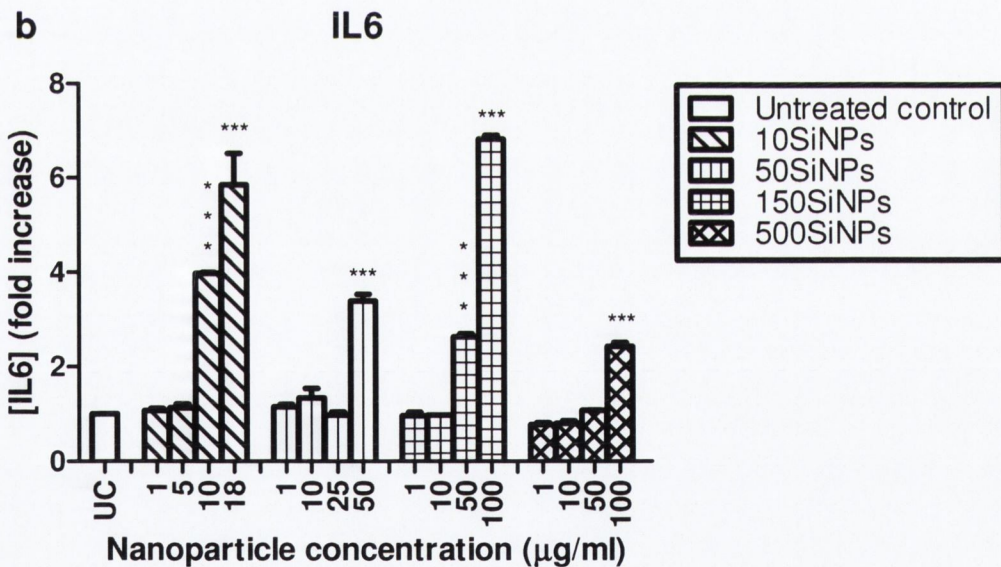
Figure 35 | Representative traces from CBA analyses. Deionised ultra-pure water (**a**) and 10- $\mu\text{g/ml}$ 10SiNPs in deionised ultra-pure water (**b**) are represented. Bars pointed by the red arrows represent the cytokines detected by the Human Inflammatory Cytokine kit. From top to bottom: IL8, IL1 β , IL6, IL10, TNF α , and IL12p70. A shift of a particular bar from left to right in the X-axis indicates an increased concentration of this cytokine.

As nanoparticles did not interfere with CBA analyses, I analyzed the released of the cytokines IL6 and IL8 into the culture supernatant of control cells and cells treated with 10SiNPs, 50SiNPs, 150SiNPs, and 500SiNPs for 15 hours (**Figure 36**).

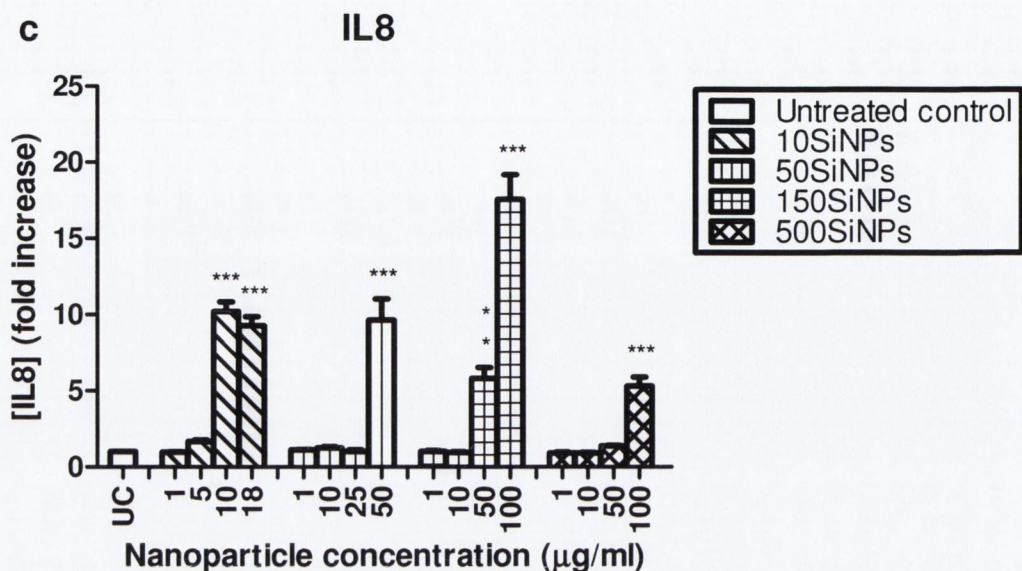
Figure 36 | Effects of silica nanoparticles on the release of the cytokines IL6 and IL8 at 15 hours.



a. Representative traces from CBA analyses (**i**, control; **ii**, 10- μ g/ml 10SiNPs; **iii**, 10- μ g/ml 500SiNPs) showing detection of IL6 and IL8. As compared with the untreated control (**i**), a shift of the green bars representing IL8 (red arrow) and IL6 (blue arrow) from left to right in the X-axis indicate an increase in cytokine release when cells were exposed to 10- μ g/ml 10SiNPs (**ii**). In contrast, 10- μ g/ml 500SiNPs did not produce an increase in cytokine release (**iii**).



b. HUVEC cells were exposed to silica nanoparticles for 15 hours and released IL6 was analyzed by CBA. All values are mean \pm SEM of $n \geq 3$. One-way ANOVA: 10SiNPs, 50SiNPs, 150SiNPs, 500SiNPs ($P < 0.0001$); Tukey-Kramer post test: *** $P < 0.001$; untreated control (UC) vs treatments.



c. HUVEC cells were exposed to silica nanoparticles for 15 hours and released IL8 was analyzed by CBA. All values are mean \pm SEM of $n \geq 3$. One-way ANOVA: 10SiNPs, 50SiNPs, 150SiNPs, 500SiNPs ($P < 0.0001$); Tukey-Kramer post test: ** $P < 0.01$, *** $P < 0.001$; untreated control (UC) vs treatments.

As compared with the untreated control, statistically significant increased release of the cytokines IL6 and IL8 into the cell culture media (fold increase) resulting from exposure of HUVEC cells to silica nanoparticles are shown in **table 3**.

	10- 10SiNPs	18- 10SiNPs	50- 50SiNPs	50- 150SiNPs	100- 150SiNPs	100- 500SiNPs
IL6	3.97±0.03	5.85±0.67	3.39±0.15	2.63±0.07	6.82±0.08	2.43±0.08
IL8	10.19±0.64	9.28±0.58	9.63±1.38	5.80±0.73	17.56±1.59	5.31±0.58

Table 3 | CBA time-course analysis of HUVEC cells exposed to silica nanoparticles. Endothelial cells were treated with silica nanoparticle for 15 hours and IL6 and IL8 released into the cell culture analyzed by CBA. As compared with untreated control, statistically significant gene fold increases are shown in this table. All values are mean ± SEM. 10-10SiNPs, 10-µg/ml 10SiNPs; 18-10SiNPs, 18-µg/ml 10SiNPs; 50-50SiNPs, 50-µg/ml 50SiNPs; 50-150SiNPs, 50-µg/ml 150SiNPs; 100-150SiNPs, 100-µg/ml 150SiNPs; 100-500SiNPs, 100-µg/ml 500SiNPs.

UPTAKE OF AMORPHOUS SILICA NANOPARTICLES BY HUMAN PLATELETS

It has been demonstrated that platelet function is influenced by exposure to nanoparticles ¹⁴³. Consequently, I tested if silica nanoparticles also affected platelet function.

First, I studied silica nanoparticle-platelet interactions by TEM (**Figure 37**). For this, washed platelets were exposed to 10-µg/ml 10SiNPs in an aggregometer, platelet aggregation was terminated at 30% maximal response, and then platelets were fixed for TEM and micrographs taken (**Figure 37b - 37d**). Untreated platelets (without nanoparticles) were also prepared (**Figure 37a**).

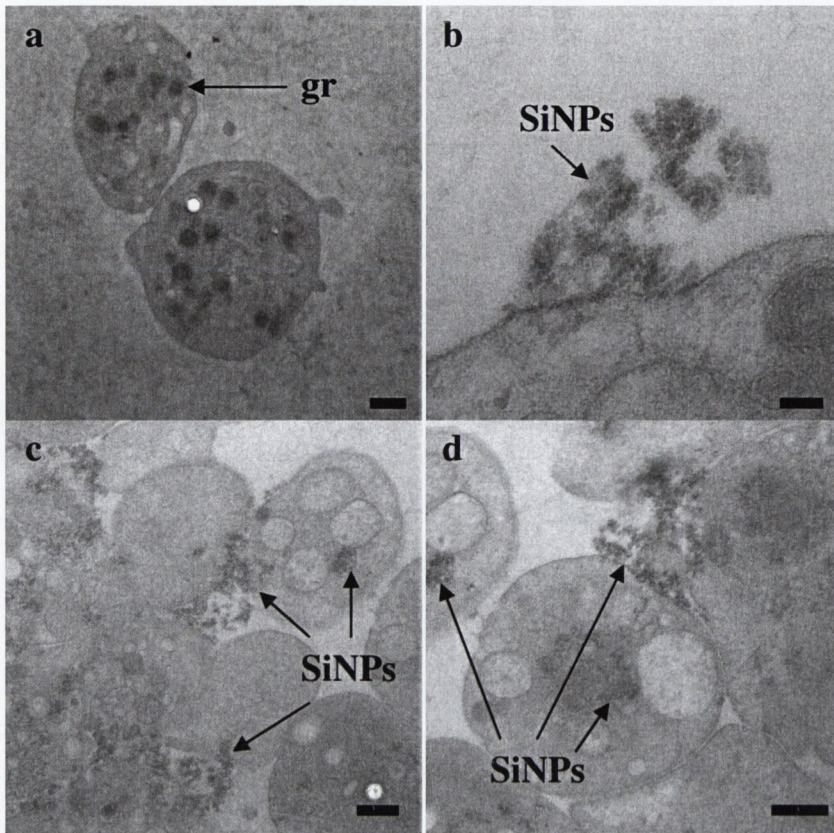


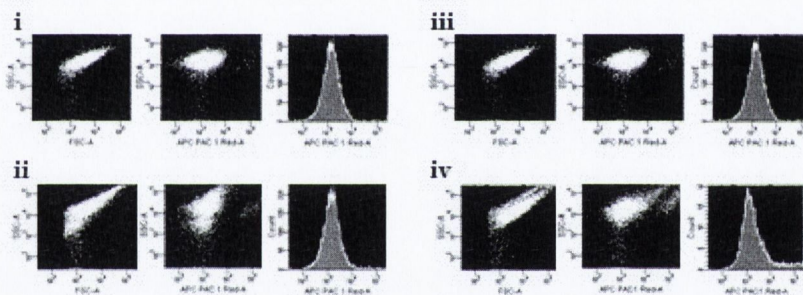
Figure 37 | Silica nanoparticles interact with human platelets. Platelet aggregation was terminated at 30% maximal response, as determined using an aggregometer, fixed for TEM and examined by a transmission electron microscope (**b - d**); resting platelets (control, without nanoparticles) were also prepared (**a**). Scale bars represent 500 nm in **a**, **c**, and **d**; and 100 nm in **b**. Silica nanoparticles, SiNPs; platelet granule, gr.

As exposed to platelets, silica nanoparticles quickly interacted with the membrane (**Figure 37b**) and internalized (**Figure 37c, 37d**). In contrast with the case of endothelial cells (**Figure 24**), nanoparticles encapsulated into vesicles were not observed into platelets. Platelets without granules (**Figure 37c**), indicating platelet activation, were found. As in the case of endothelial cells (**Figure 24**), nanoparticles were found forming agglomerates.

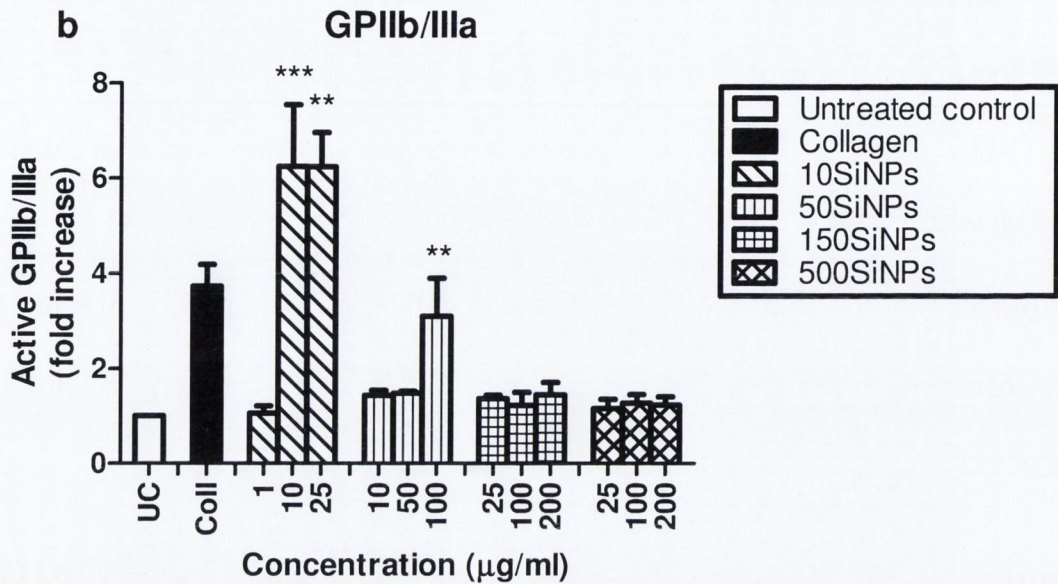
AMORPHOUS SILICA NANOPARTICLES INDUCE GPIIb/IIIa ACTIVATION IN WASHED PLATELETS

The **figure 38** shows silica nanoparticle effects on GPIIb/IIIa activation on the platelet surface membrane in washed platelet preparations as measured by flow cytometry. The test material did not interfere with this technique. The FACSArray™ analyzer did not detect the silica nanoparticles used in my studies.

Figure 38 | Effects of silica nanoparticles on GPIIb/IIIa activation.



a. Representative traces from flow cytometry analyses: **i**, resting platelets (untreated control); **ii**, collagen-induced GPIIb/IIIa activation (positive control); **iii**, 50- $\mu\text{g}/\text{ml}$ 50SiNPs did not induce GPIIb/IIIa activation; **iv**, 100- $\mu\text{g}/\text{ml}$ 50SiNPs induced GPIIb/IIIa activation.

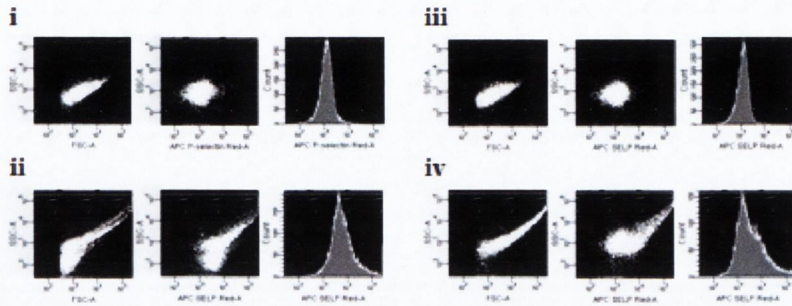


b. Washed platelet preparations were exposed to silica nanoparticle and GPIIb/IIIa activation was analyzed by flow cytometry. All values are mean \pm SEM of $n \geq 3$. One-way ANOVA: 10SiNPs ($P < 0.0001$); 50SiNPs ($P = 0.0081$); 150SiNPs, 500SiNPs ($P > 0.05$); Tukey-Kramer post test, $**P < 0.01$, $***P < 0.001$; untreated control (UC) vs treatments.

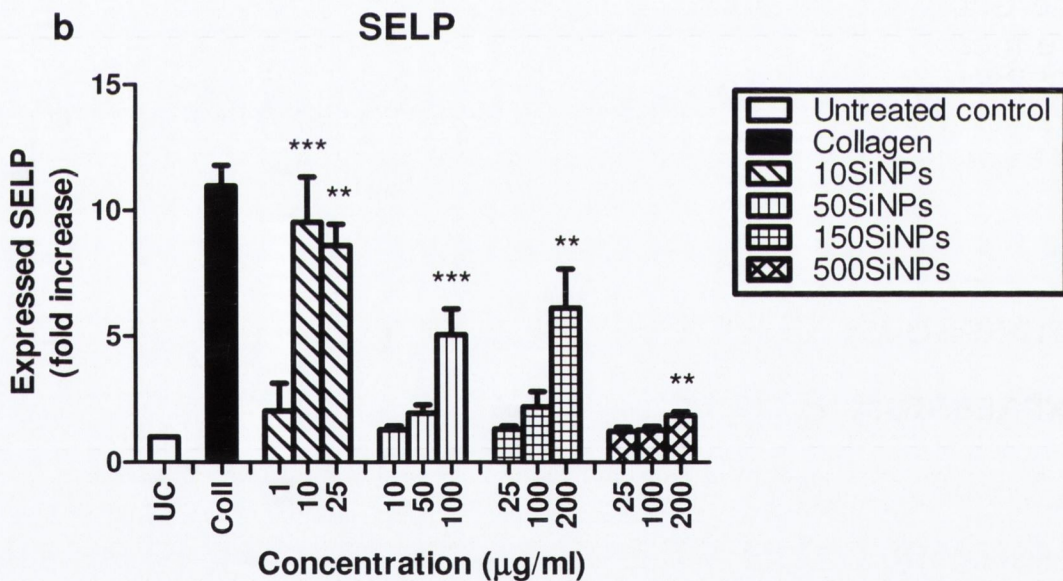
AMORPHOUS SILICA NANOPARTICLES INDUCE SELP EXPRESSION IN WASHED PLATELETS

The **figure 39** shows silica nanoparticle effects on SELP expression on the platelet surface membrane in washed platelet preparations.

Figure 39 | Effects of silica nanoparticles on SELP expression.



a. Representative traces from flow cytometry analyses: **i**, resting platelets (untreated control); **ii**, collagen-induced SELP expression (positive control); **iii**, 10- μ g/ml 50SiNPs did not induce SELP expression; **iv**, 10- μ g/ml 10SiNPs induced SELP expression.



b. Washed platelet preparations were exposed to silica nanoparticle and SELP expression was analyzed by flow cytometry. All values are mean \pm SEM of $n \geq 3$. One-way ANOVA: 10SiNPs ($P < 0.0001$); 50SiNPs ($P = 0.0007$); 150SiNPs ($P = 0.0035$); 500SiNPs ($P = 0.0067$); Tukey-Kramer post test, ** $P < 0.01$, *** $P < 0.001$; untreated control (UC) vs treatments.

AMORPHOUS SILICA NANOPARTICLES INDUCE PLATELET AGGREGATION IN WASHED PLATELETS

The **figure 40** shows silica nanoparticle effects on platelet aggregation in washed platelet preparations.

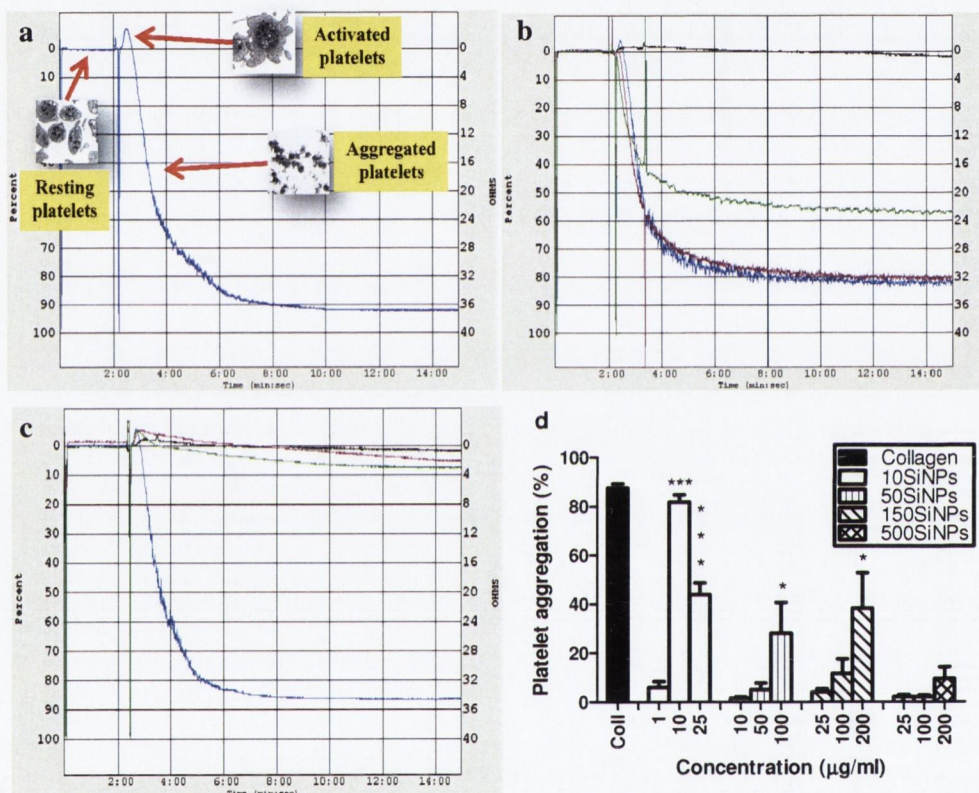


Figure 40 | Effects of silica nanoparticles on platelet aggregation. Representative traces from aggregometry analyses: **a**, collagen-induced platelet aggregation, TEM micrographs indicate platelet state (resting, activated, aggregated) in each section of the graph; **b**, blue, collagen (positive control); red, 10-µg/ml 10SiNPs; green, 25-µg/ml 10SiNPs; and black, 1-µg/ml 10SiNPs; **c**, blue, collagen; red, 100-µg/ml 500SiNPs; green, 200-µg/ml 500SiNPs; and black, 25-µg/ml 500SiNPs. **d**, Washed platelet preparations were exposed to silica nanoparticles and platelet aggregation was analyzed by aggregometry. All values are mean ± SEM of $n \geq 3$. One-way ANOVA: 10SiNPs ($P < 0.0001$); 50SiNPs ($P = 0.0329$); 150SiNPs ($P = 0.0219$); 500SiNPs ($P > 0.05$); Tukey-Kramer post test, * $P < 0.05$, *** $P < 0.001$, untreated control (0 % aggregation) vs treatments.

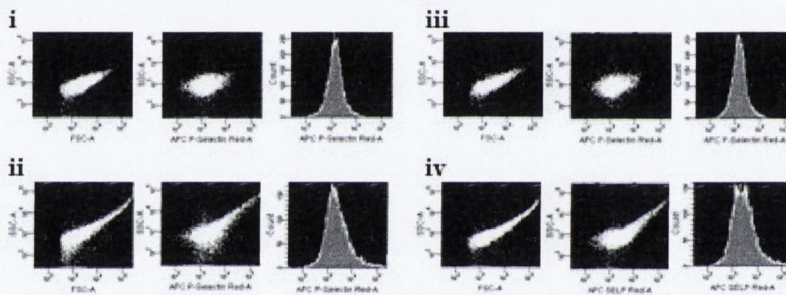
As compared with the untreated control (without nanoparticles), 10- $\mu\text{g/ml}$ 10SiNPs induced a significant increase in GPIIb/IIIa activation (6.25 ± 1.29 folds) (**Figure 38b**) and SELP expression (9.52 ± 1.81 folds) (**Figure 39b**) on the platelet surface membrane as measure by flow cytometry. Equal nanoparticle and concentration also induced an 81.79 ± 2.30 % of platelet aggregation (**Figure 40d**), as measured by aggregometry. In contrast, 10- $\mu\text{g/ml}$ 50SiNPs did not significantly induce GPIIb/IIIa activation (**Figure 38b**), SELP expression (**Figure 39b**) or platelet aggregation (**Figure 40d**). As compared with the untreated control 25- $\mu\text{g/ml}$ 10SiNPs significantly induced GPIIb/IIIa activation (**Figure 38b**), SELP expression (**Figure 39b**), and platelet aggregation (**Figure 40d**). However, effect of 25- $\mu\text{g/ml}$ 10SiNPs on GPIIb/IIIa activation, SELP expression, and platelet aggregation was not significantly higher than that of 10- $\mu\text{g/ml}$ 10SiNPs; being even significantly smaller in the case of platelet aggregation (**Figure 40d**). As compared with the untreated control, platelets exposed to a high concentration of 50SiNPs (100 $\mu\text{g/ml}$) significantly induced GPIIb/IIIa activation (**Figure 38b**), SELP expression (**Figure 39b**), and platelet aggregation (**Figure 40d**). 200- $\mu\text{g/ml}$ 150SiNPs did significantly induced SELP expression (**Figure 39b**) and platelet aggregation (**Figure 40d**), but not GPIIb/IIIa activation (**Figure 38b**). 200- $\mu\text{g/ml}$ 500SiNPs did significantly induce SELP expression (**Figure 39b**), but

did not GPIIb/IIIa activation (**Figure 38b**) and platelet activation (**Figure 40d**).

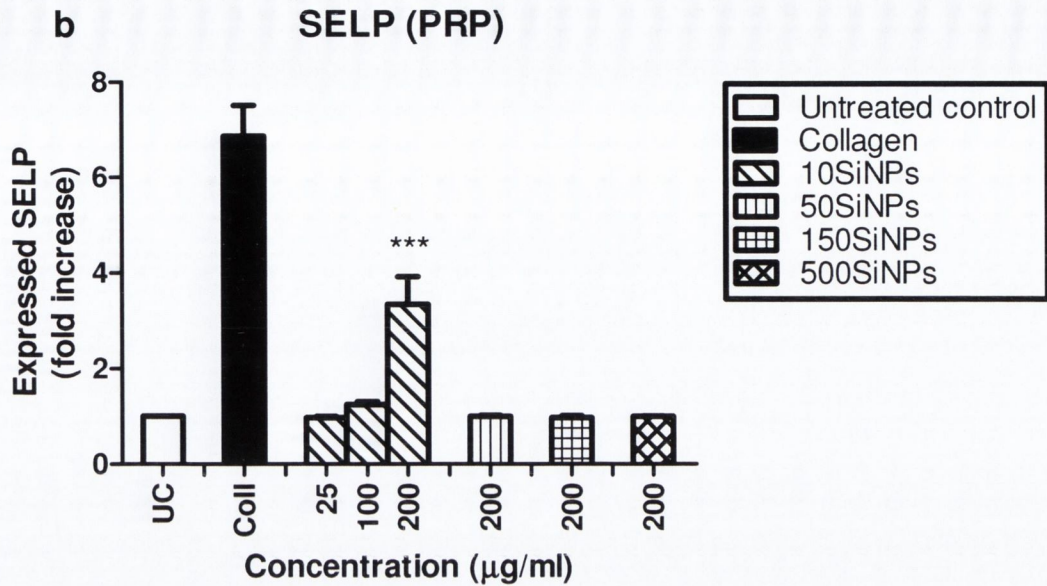
EFFECTS OF AMORPHOUS SILICA NANOPARTICLES ON SELP IN PRP

The **figure 41** shows silica nanoparticle effects on SELP expression by silica nanoparticles in PRP.

Figure 41 | Silica nanoparticles induce SELP expression on the platelet surface membrane when added to PRP.



a. Representative traces from flow cytometry analyses: **i**, resting platelets (untreated control); **ii**, collagen-induced SELP expression (positive control); **iii**, 200-µg/ml 150SiNPs did not induce SELP expression; **iv**, 200-µg/ml 10SiNPs induced SELP expression.



b. Platelet-rich plasma was exposed to silica nanoparticles and SELP expression was analyzed by flow cytometry. All values are mean \pm SEM of $n \geq 3$. One-way ANOVA: 10SiNPs ($P = 0.0002$); Tukey-Kramer post test, $***P < 0.001$; untreated control (UC) vs treatments. Two-tail unpaired Student's t-tests: $P > 0.05$; untreated control vs 200- $\mu\text{g/ml}$ 50SiNPs, 200- $\mu\text{g/ml}$ 150SiNPs, 200- $\mu\text{g/ml}$ 500SiNPs.

EFFECTS OF AMORPHOUS SILICA NANOPARTICLES ON PLATELET AGGREGATION IN PRP

The **figure 42** shows silica nanoparticle effects on platelet aggregation by nanoparticles in PRP.

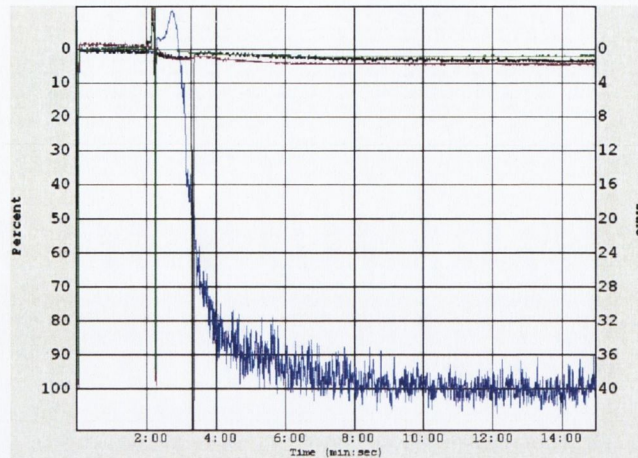


Figure 42 | Representative traces from aggregometry studies in PRP. Collagen (blue) was used as a positive control. 10SiNPs (red), 50SiNPs (black), and 150SiNPs (green) did not induce platelet aggregation when added to PRP at a concentration of 200 $\mu\text{g}/\text{ml}$. Lower concentration did not either induce platelet aggregation.

As compared with the untreated control, 200- $\mu\text{g}/\text{ml}$ 10SiNPs induced a statistically significant SELP expression on platelet surface membrane (3.34 ± 0.58 folds) when added to PRP (**Figure 41b**). In contrast, 10SiNPs at concentrations lower than 200- $\mu\text{g}/\text{ml}$ as well as 200- $\mu\text{g}/\text{ml}$ 50SiNPs, 150SiNPs, and 500SiNPs did not induce significant SELP expression (**Figure 41b**), as measure by flow cytometry. Interestingly, silica nanoparticles even at 200- $\mu\text{g}/\text{ml}$ were not able to induce platelet aggregation as measured by aggregometry (**Figure 42**).

AMORPHOUS SILICA NANOPARTICLES STIMULATE HUMAN PLATELETS TO RELEASE NO AND ONOO⁻ IN PRP

Nitric oxide and peroxynitrite released from human platelets were measured as silica nanoparticles were added to PRP. The

figures 43 and 44 show the maximum release of NO and ONOO⁻ from human platelets as a direct response to silica nanoparticle stimulation.

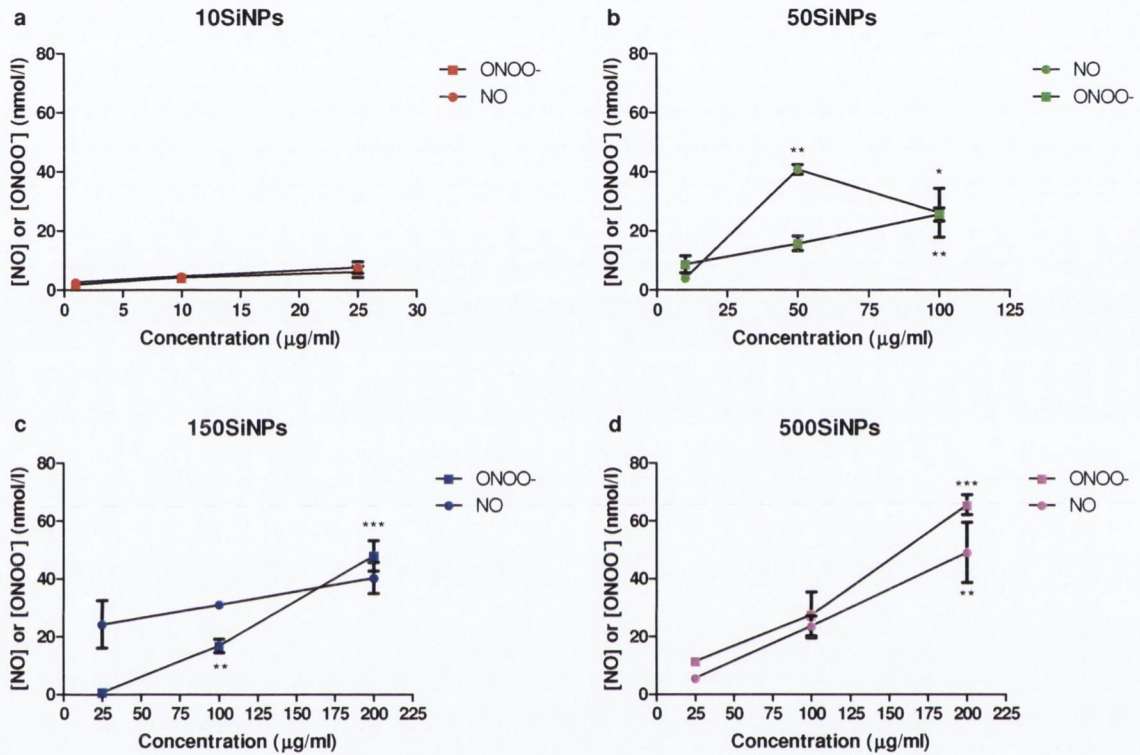


Figure 43 | Maximum ONOO⁻ and NO release from platelets as silica nanoparticles were added to PRP. Addition of 10SiNPs (**a**, red), 50SiNPs (**b**, green), 150SiNPs (**c**, blue), and 500SiNPs (**d**, pink) induced production and release of ONOO⁻ (squares) and NO (circles). All values are mean ± SEM of n ≥ 3. One-way ANOVA: **a** (NO, ONOO⁻, P > 0.05); **b** (NO, P = 0.0053; ONOO⁻, P = 0.0094); **c** (NO, P > 0.05; ONOO⁻, P = 0.0002); **d** (NO, P = 0.0081; ONOO⁻, P = 0.0007); Tukey-Kramer post test: *P < 0.05, **P < 0.01, ***P < 0.001, when compared with human platelets exposed to nanoparticles at a concentration of 1-µg/ml (**a**), 10-µg/ml (**b**), and 25-µg/ml (**c**, **d**). Measurements performed in collaboration with Prof Tadeusz Malinski and Dr Adam Jacoby (Ohio University, Athens, Ohio, USA).

Nitric oxide release, as a response to silica nanoparticle stimulation, represented the maximum NO concentration raised from

PRP. Stimulated NO released from platelets directly stimulated by 10SiNPs did not significantly increase at any concentration tested. 50-nm silica nanoparticles induced a maximum NO release at a concentration of 50 $\mu\text{g/ml}$. 150-nm silica nanoparticles did not significantly increase NO release from cells at any concentration tested while 500-nm did at a concentration of 200- $\mu\text{g/ml}$ (**Figure 43**).

Peroxynitrite release, as a response to silica nanoparticle stimulation, represented the ONOO^- concentration released from PRP. Again, 10SiNPs did not significantly stimulate ONOO^- release from platelets at any concentration tested. The exposure to 50SiNPs and 150SiNPs significantly stimulated platelets to release ONOO^- at a concentration higher than 100 $\mu\text{g/ml}$. 500-nm silica nanoparticles did so at a concentration of 200 $\mu\text{g/ml}$ (**Figure 43**).

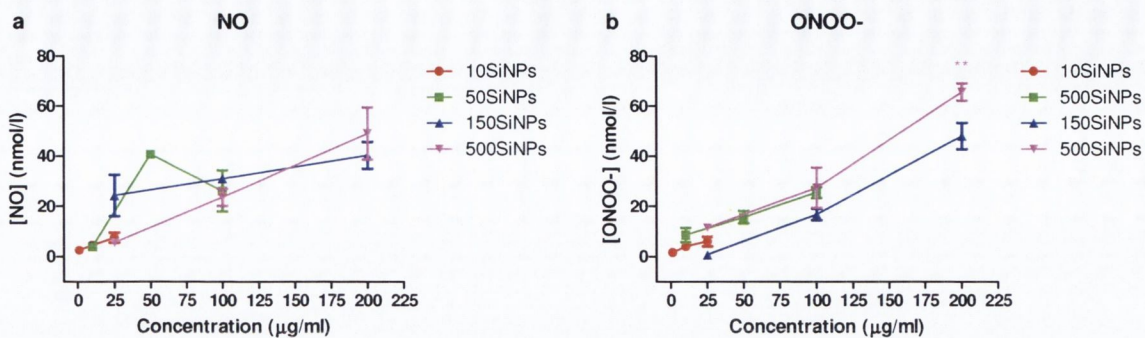


Figure 44 | Comparative maximum ONOO⁻ and NO release from platelets as silica nanoparticles were added to PRP. For a clearer view, the maximum NO (a) and ONOO⁻ (b) release from human platelets as 10SiNPs (red), 50SiNPs (green), 150SiNPs (blue), and 500SiNPs (pink) when added to PRP are plotted on the same graph. All values are mean ± SEM of n ≥ 3. Two-tails unpaired Student's t-test: **P < 0.01; 200-µg/ml 150SiNPs vs 200-µg/ml 500SiNPs. Measurements performed in collaboration with Prof Tadeusz Malinski and Dr Adam Jacoby (Ohio University, Athens, Ohio, USA).

Interestingly, stimulation of platelets by 200-µg/ml 500SiNPs was significantly higher than that of 150SiNPs. This tendency was also observed when these nanoparticles were used at 25 and 100 µg/ml (Figure 44).

DISCUSSION

There is increasing evidence that the exposure of humans to FPs, especially UFPs, adversely affects the cardiorespiratory system. Indeed, apart from causing respiratory diseases ¹⁶², airborne PM_{2.5} is able to deposit deep in the lungs ²⁵ and reach extra-pulmonary tissues. Moreover, it is increasingly recognized that elements of the cardiovascular system are targeted by FPs, especially UFPs; and the smaller the particle is in size, the easier it reaches its target ¹⁸. Furthermore, Miller, K. A. *et al.* (2007) ³² published a cohort study on long-term exposure of women to ambient FPs in 36 U.S. metropolitan areas (1994 – 1998), showing that each increase of 10 µg of FPs per cubic metre of air was associated with a 24% increase in the risk of a cardiovascular event, a 76% increase in the risk of death from cardiovascular disease, and a 35% increase in the risk of cerebrovascular events.

The human population is progressively exposed to a higher amount and variety of nanoparticles, as nanotechnology is used in a fast-growing number of applications and industries (e.g. computing, electronic, and high-tech manufacturing). Also, the release of high amounts of nanoparticles in an enclosed environment may be of grand concern for workers (e.g. airline crews and hardware engineering) ²².

Although no official data on ambient airborne concentrations of amorphous silica nanoparticles is available ⁶⁰, human population

might be exposed to these nanoparticles via inhalation, in all their varieties: nano-objects as well as incidental and engineered nanoparticles. Silica nanoparticles can arise from volcanic eruptions (e.g. Eyjafjallajökull volcanic system) and others natural sources; as well as, industrial and farming emissions. Engineered amorphous silica nanoparticles are produced and applied in a large scale ⁴⁰. They are used in food and feed industries ³⁹, and also added to cosmetics. Consequently, exposure of humans to these nanoparticles, via ingestion and skin application, is also a real issue. Furthermore, amorphous silica nanoparticles are being tested to be used in nanomedicine (e.g. drug delivery systems, imaging) and other areas of nanotechnology. As a result, the number of applications of these nanoparticles, along with their exposure to human population, will grow further in a near future. Therefore, it is necessary to undoubtedly ensure that synthetic amorphous silica nanoparticles are safe for humans.

In my transfer thesis as part fulfilment of the degree of Doctorate of Philosophy (defended on September 4th, 2009) ¹⁶⁰, I demonstrated the ability of silica nanoparticles to induce inflammatory responses in immortalized HUVEC cells in vitro. Gene expression of *ICAM1*, *VCAM1*, *SELE*, and *MMP9* was up-regulated by 10-nm (10- μ g/ml in cell culture media) and 150-nm (100- μ g/ml) silica nanoparticles; the latter also increased IL8 release into the cell culture media. Silica nanoparticle-cell interaction was also

demonstrated by using fluorescence silica particles. These results demonstrated that amorphous silica nanoparticles were noxious for endothelial cells; however, they left many unanswered questions: do silica nanoparticles internalize or remain on the plasma membrane? If they get into the cell, how do they internalize and where do they locate? How are these nanoparticles able to up-regulate *ICAM1*, *VCAM1*, *SELE*, and *MMP9* gene expression? Do silica nanoparticles induce up-regulation of other endothelial genes? Are free radicals involved? Do noxious effects depend on particle size? Are silica nanoparticles toxic for other blood elements?

To address these important questions in my thesis studies, I explored in depth silica nanoparticle-induced toxicity in human endothelial cells to find an explanation underpinning silica nanoparticle noxious effects. As in my transfer thesis studies, I tested 10- and 150-nm silica nanoparticles. In addition, I included two more commercially available amorphous silica nanoparticle sizes (50 nm and 500 nm). Moreover, in order to confirm the data obtained using the immortalized HUVEC cells, I have now used a HUVEC primary cell line. Once more, I used HUVEC cells because this cell line has been used as a reference for in vitro studies of endothelial cell function, since Jafee, E. A. *et al.* (1973)¹⁶³ developed a procedure to isolate them from the umbilical cord by collagenase digestion. As platelets, along with endothelial cells, play a crucial role in physiology and

pathophysiology of the cardiovascular system, I also studied the effects of silica nanoparticles on human platelets.

As significant deviations from commercial specifications on various nanoparticles have been reported ⁵⁹, prior to my studies on the effects of nanoparticles on HUVEC primary cells and human platelets, I re-evaluated two key nanoparticle characteristics (size and zeta potential) in deionised ultra-pure water. The four nanoparticles, which I used in my studies, met the criterion of charge for which they were purchased. Silica nanoparticles bore a strong negative surface charge (ζ -potentials were smaller than -38 mV). On the other hand, hydrodynamic particle sizes measured by a zetasizer were larger than those provided by the manufacturer. All particles suspended in water bear a hydration layer on their surface; and a zetasizer measures hydrodynamic size (i.e. particle size + hydration layer) rather than absolute size (i.e. particle size). Differences between zetasizer and commercial measurements were greater for 10SiNPs and 50SiNPs than for 150SiNPs and 500SiNPs. This may be explained because of nanoparticle aggregation, different conditions of measurement and/or different technique of measurement.

One of the most remarkable characteristics of silica nanoparticles is their extremely high stability. They are able to break even the ultra-microtome diamond knife used to cut sections of samples for TEM studies. In my studies, nanoparticle hydrodynamic

size and zeta potentials remain unchanged for up to one year and a half.

Furthermore, all silica nanoparticles used in my studies had the same manufacturing batch number, indicated that they were synthesized exactly in the same conditions. This point is crucial to compare experimental results.

EFFECTS OF AMORPHOUS SILICA NANOPARTICLES IN HUMAN ENDOTHELIAL CELLS

During my studies leading to my transfer examination ¹⁶⁰, I found using fluorescence microscopy that silica nanoparticles remained associated with HUVEC cells following nanoparticle-cell incubations. I have now used TEM to investigate in detail nanoparticle-cell interactions. As nanoparticles tend to aggregate, protein corona ⁵⁹, fluid characteristics, hydrophobicity, and zeta potentials can all influence the tendency of nanoparticles to agglomerate ¹⁶⁴. This is consistent with my TEM studies that showed silica nanoparticles forming agglomerates. Synthetic amorphous silica nanoparticles pose a high surface-area-to-volume ratio, which increases in the opposite direction to size. This property allows adsorption of organic molecules and macromolecules such as proteins, lipids, and nucleic acids on their surfaces, what may interfere with normal cell physiology. Thus, this high ratio, which makes nanoparticles very useful in industry, also turns them very

reactive in the cellular environment. Adsorption of proteins at nanoparticle surfaces spontaneously occurs as soon as particles are placed in a protein solution. It has been shown that protein corona, thus formed, may have fundamental significance for bionanointeractions⁵⁹. The common forms of amorphous silica, except for fused silica glass, consist of extremely small particles, the surface of which are hydrated as silanol groups⁵⁶. Therefore, hydrophilic interactions tend to dominate the energy balance, but electrostatics interactions can also play an important role. Proteins that first adsorb, due to high concentration in solution, are replaced by others with higher affinity (Vroman effect). The importance of protein adsorption to nanoparticle surfaces (i.e. protein corona) in mediating binding to the cell surface, irrespective of the identity of these proteins, has been reported¹⁶⁵.

Literature shows that nanoparticle uptake may typically occur through nonspecific diffusion and/or endocytosis¹⁶⁶. Two mechanisms of endocytosis have been described in mammalian cells: phagocytosis and pinocytosis (also known as fluid-phase uptake)¹⁶⁷. Moreover, several mechanisms of pinocytosis have been described: macropinocytosis, clathrin-mediated endocytosis, caveolin-mediated endocytosis, and clathrin- and caveolin-independent endocytosis¹⁶⁷. It is increasingly recognized that nanoparticles of very different materials can enter into cells easily by endocytosis and accumulate in the lysosomes. A study by He, Q. *et al.* (2009)¹⁶⁸, in human breast-

cancer (MDA-MB-468) cells, indicated that mesoporous silica ¹⁶⁹ (a form of porous silica) nanoparticles were internalized by endocytosis; being the smaller particles (190 nm) easier and quicker to endocytose than larger. Inside the cells, they mainly located either within the lysosomes or around the nuclei (in 4 hours). This data is consistent with my own findings showing that 10SiNPs quickly (less than an hour) interacted with the endothelial plasma membrane, internalized and distributed into the cytoplasm. They were mainly encapsulated into vesicles and some of them located very close to the nucleus. These vesicles are likely to be part of the cellular endosomal-lysosomal system. However, more studies are necessary to clarify if non-porous silica nanoparticles accumulate in lysosomes. Interestingly, I have also found non-encapsulated particles in the endothelial cytoplasm. This indicates that nanoparticles could have been gained internalized into cells by other mechanisms rather than endocytosis or that the content of vesicle/lysosome was released into the cytosol following its rupture.

It has been reported that silanol groups, on the surface of silica nanoparticles, might be a prerequisite for silica nanoparticle attachment to the cell membrane. This is supported by a study showing that these groups form hydrogen bond with some sites on the cell membrane ¹⁷⁰. Synthesis-based form precipitated amorphous silica nanoparticles pose completely hydroxylated surfaces, while other forms (e.g. fumed silica) pose lower amount of silanol surface

groups; although, this number increase with the time after their synthesis ⁵⁸. Furthermore, it is known that the smaller the particle is the greater noxious effects produces; and smaller particles pose a greater number of surface silanol groups per surface area than larger particles, due to their higher surface-area-to-volume ratio. The relation between silica surface properties and increased uptake of nanoparticles by cells as well as higher cytotoxic effects, have not been demonstrated yet.

The TEM micrographs from my experiments did not showed evidence of silica nanoparticle-nuclear membrane interaction, and intranuclear nanoparticles were not observed. Perhaps, longer incubation times, use of smaller nanoparticles, or used of nanoparticles which aggregate less, might allow silica nanoparticles to reach the nucleoplasm, and interact with DNA. The association of silanol groups, on silica nanoparticle surfaces, with the phosphate groups of DNA by a specific binding has been shown ¹⁷¹. It has been also demonstrated that short-lived radicals from the active sites of silica surface may damage DNA due to their proximity after binding ¹⁷².

A study by Nan, A. *et al.* (2008) ¹⁷³ showed that fluid phase endocytosis was involved in silica nanotube uptake by an epithelial cancer cell line (MDA-MB-231) and HUVEC primary cells, and internalized nanotubes accumulated within lysosomes. In addition, they also tested silica nanotube cytotoxicity by 3-(4,5-

dimethylthiazol-2-yl)-2,5-diphenyltetrazolium bromide (MTT) assay, showing that both 200-nm and 500-nm positively charged nanotubes (functionalized with aminopropyltrimethoxysilane) and also non-functionalized nanotubes (negatively charge) decreased cell viability in both cell lines. I have also demonstrated that silica nanoparticles decreased viability of HUVEC primary cells in a size-dependent manner. Interestingly, 10SiNPs induced significant cytotoxicity, while larger nanoparticles did not. My findings are also consistent with a study by Napierska, D. *et al* (2009) ¹⁷⁴ in EAHY926 cells (a hybrid of HUVEC and A549 cells, a lung cancer cell line ¹⁷⁵), where they showed size-dependent cytotoxicity of Stöber amorphous silica nanoparticles ¹⁷⁶ by LDH and MTT assays. Although, the failure of MTT as a toxicity testing agent for mesoporous silica particles has been reported ¹⁷⁷; this test appears to work perfectly with non-porous silica nanoparticles ¹⁷⁴.

Though made by the same material (silicon dioxide), mesoporous and non-porous (solid) silica nanoparticles appear to differ in the noxious effects they induced. Cytotoxicity of mesoporous and solid silica nanoparticles has been compared in vitro by Lin, Y.S. *et al.* (2010) ¹⁷⁸ in human erythrocytes. They systematically compared cytotoxicity of Stöber non-porous (24, 37, 142, and 263 nm) and mesoporous (25, 42, 93, 155, and 225 nm) silica nanoparticles on red cells haemolysis. Their study showed a size-dependent increase in the haemolytic activity of both types of silica

nanoparticles. However, higher haemolysis was produced by solid silica as compared to similar sized mesoporous counterparts. An important issue on cytotoxicity studies of mesoporous silica particles is their degradation (dissolution), into silicic acid, and subsequent collapse of pores. In a study by Lin, Y.S. *et al.* (2010)¹⁷⁸, this led to a greatly increase of haemolytic activity. The authors suggested that increased haemolytic activity observed must have been a consequence of a change in the nanoparticle itself, because some of their results combined demonstrated that the dissolved silicic acid species were not the source. Mesoporous and non-porous silica particle-induced haemolysis have been also reported by Slowing, I.I. *et al.* (2009)¹⁷⁹ in rabbit red cells. This study also suggests that silica haemolytic properties were related to the number of surface silanol groups accessible to erythrocyte cell membrane. It has been also suggested in a study on mesoporous silica by He, Q. *et al.* (2009)¹⁶⁸ that oxidative and/or hydrolaxytive harm of lysosomes underpins endothelial damage. More studies are necessary to confirm if the same explanation is valid for solid silica nanoparticles.

As shown by my cytotoxicity studies, HUVEC primary cells died soon after being exposed to silica nanoparticles. My data also suggest that oxidative stress was most likely involved in silica nanoparticle-induced toxicity in endothelial cells. This observation agrees with the proposition by Li, N. *et al.* (2008)¹⁵⁹ that interactions between nanoparticles and cells lead to the generation of oxidative stress and

oxidant injury. My work indicates that the balance between NO and ONOO⁻ may be involved in mediating the cytotoxic effects of silica nanoparticles on endothelial cells. Indeed, our studies demonstrate that amorphous silica nanoparticles directly stimulated HUVEC cells to release both NO and ONOO⁻. The use of nanosensors to precisely measure NO and ONOO⁻ released from cells with nanomol-per-litre (nmol/l) sensitivity is a powerful tool which helped understand effects of silica nanoparticles in endothelial cells. Direct measurements by these nanosensors have been successfully performed in cell culture¹⁴⁹, platelets^{143,180} and live tissue^{143,181}. We observed that silica nanoparticles triggered massive production of ONOO⁻ by endothelial cells indicating that nanoparticle-induced dysfunction of nitric-oxide synthase 3 (eNOS), the major form in endothelial cells, was extremely high. Nitric-oxide synthase 3 catalyzes NO synthesis from Arg^{65,82}. Nitric oxide can also be produced by the mitochondrial respiratory chain under hypoxic conditions¹³². On the other hand, ONOO⁻ is produced from the reaction of superoxide anion (O₂^{•-}) with NO that leads to a deprivation of NO⁸². It is also possible that dysfunctional eNOS may directly produce O₂^{•-} which will react with NO to produce ONOO⁻. The concentration of NO measured in our experiments was low. Therefore, the very high ratio of ONOO⁻ to NO observed was indicative of extremely high nitrosative stress especially for 10-nm and 50-nm silica nanoparticles. Nitrosative stress affects the nitrosation or nitration of cellular targets, including

proteins and glutathione as well as produces oxidation of proteins and nucleic acids. Collectively, excessive accumulation of free radicals and the uncontrolled oxidation of cellular components are referred to as oxidative stress. Nitrosative and oxidative stress accompany aging and several diseases, including hypertension, atherosclerosis, Alzheimer's disease and a variety of dementias ¹²⁹.

My studies indicate that free radicals induced by exposure of HUVEC cells to silica nanoparticles led to cellular oxidative stress. This exposure might have severely damaged the most sensitive cells quickly and activate transcription factors to initiate defence mechanisms in the survival cells. Oxidative stress leads to transcription factor NF- κ B activation. A study by Tumur, Z. *et al.* (2010) ⁹⁰ concluded that indoxyl sulphate (a uremic toxin, which is considered a risk factor for cardiovascular disease in chronic kidney disease) up-regulated the expression of ICAM1 and MCP1 by oxidative stress-induced NF- κ B activation in HUVEC cells. Moreover, a study by Shono, T. *et al.* (1996) ¹⁸², in human microvascular endothelial cells, isolated from surgically removed omental tissue, demonstrated increased NF- κ B activity induced by H₂O₂. However, a study by Bowie, A. G. *et al.* (1997) ¹⁸³ showed that H₂O₂ failed to activate NF- κ B in primary HUVEC cells; but interestingly, induced NF- κ B activation in immortalized human endothelial (ECV304) cells. This phenomenon, which could not be explained by the authors, serves to

highlight important differences between immortalized and primary cell lines.

My data suggest NF- κ B involvement in silica nanoparticle toxic effects in endothelial cells. I demonstrated size-dependent NF- κ B activation in HUVEC primary cells exposed to silica nanoparticles. The smallest nanoparticles (10- μ g/ml 10SiNPs) induced NF- κ B activation within a hour, while a 5 times more concentrated 50SiNPs and 150SiNPs induced a lower NF- κ B activation in 3 hours; 500SiNPs did not up-regulated NF- κ B binding activity. Interestingly, other nanoparticles have been also shown to induce NF- κ B activation. A study by Mroz, R.M. *et al.* (2007)¹⁶¹ demonstrated that nanoparticulate carbon black (NPCB) (14 nm) increased 2.3 fold NF- κ B binding activity and 1.5 AP-1, in an hour, in A595 cell line. They also evidenced that N-acetylcysteine (NAC) blocked nanoparticle driven NF- κ B and AP-1 DNA binding, what indicated that oxidative stress was involved in activation of these two pro-inflammatory transcription factors. Finally, this study showed by a single gel electrophoresis assay (also known as comet assay) that NPCB induced DNA damage after 3-hour exposure. This assay detected unrepaired DNA strand breaks and alkali-labile sites. In contrast, in a study carried out in two different laboratories, Barnes, C.A. *et al.* (2008)¹⁸⁴ demonstrated also by comet assay performed in a mouse embryonic fibroblast-adipose like cell line (3T3-L1), non-genotoxicity of amorphous silica nanoparticles (various concentrations) in the size

range from 20 nm to below 400 nm, with both positive and negative surface characteristics.

Oxidative stress is also involved in crystalline silica-induced noxious effects in cells. As shown in a study by Chen, F. *et al.* (1995)¹⁸⁵, crystalline silica (2 - 7 μm) induced in vitro a stronger than or comparable with lipopolysaccharide-induced NF- κB (p50/p50, p65/p50, p65/p52) activation at 30 minutes and 2 hours in a mouse macrophage cell line RAW 264.7. Antioxidant NAC blocked NF- κB activation but not completely (especially clear in p50/p50 homodimer), which demonstrated that oxidative stress is involved, along with other factors, in NF- κB activation leading to increases in mRNA expression of COX2, iNOS, TNF- α , and IL-1 α . My data also showed that exposure of endothelial cells to amorphous silica nanoparticles leads to gene up-regulation. I demonstrated that silica nanoparticles induced gene up-regulation of some key endothelial factors (ICAM1, VCAM1, SELE, MMP9, PTGS2, F3, IL6, and IL8), involved in inflammation and coagulation, in a size-dependent manner. The smallest particles (10SiNPs) induced the most dramatic gene up-regulation after a treatment of 15 hours. These nanoparticles influenced gene expression also after 7 hours, but not 3 hours. This data is consistent with the results I obtained with transformed HUVEC cells in the set of experiments leading to my transfer thesis¹⁶⁰. A 15-hour incubation of immortalized HUVEC cells with 10- $\mu\text{g}/\text{ml}$ 10SiNPs induced gene up-regulation. Genes *ICAM1*

and *SELE* were profoundly, and MMP9 slightly, more up-regulated in primary than transformed cells; but curiously, *VCAM1* was less. These findings highlight the differences between both cell lines. Metal oxide nanoparticles have been shown to up-regulate gene expression in vitro. A study by Gojova, A. *et al.* (2007)¹⁸⁶ in immortalized human aortic endothelial (HAEC) cells showed that a 4-hour incubation of cells with 10- μ g/ml Y_2O_3 nanoparticles (C-type cubic structure with primary particle size in the range of 20-60 nm) induced gene expression of *ICAM1*. So did ZnO (zincite crystal structure and rod-shaped, with lengths of 100–200 nm and diameters of 20–70 nm). Also, 50- μ g/ml Y_2O_3 induced *ICAM1*, *IL8*, and *MCP-1*; and ZnO, *ICAM* and *IL8*.

My data show that incubation of HUVEC primary cells with silica nanoparticles resulted in release of IL6 and IL8 in a size-dependent manner. Interestingly, silica nanoparticle-induced gene expression up-regulation of cytokine IL8, as measured by real-time qPCR, was always much higher than that of protein release, as measured by CBA. These differences may be explained by the fact that IL8 can be stored in Weibel-Palade bodies in the cytoplasm of endothelial cells¹⁸⁷. In contrast, gene up-regulation of IL6 and protein release (fold to fold comparison) corresponded well to each other.

I showed that 10SiNPs, 50SiNPs, and 150SiNPs statistically induced a concrete NF- κ B binding activity as compared with untreated controls. In contrast, my real-time qPCR studies showed

that exposure of cells to silica nanoparticles did not up-regulate the expression of each of the genes analyzed by the same fold increase. This might indicate that activation of other transcription factors may also underpin silica nanoparticle effects in endothelial cells. However, more studies are necessary to clarify this point.

As shown by the LDH assay, 50SiNPs and 150SiNPs did not significantly decrease cell viability, but they significantly up-regulated the expression of all the inflammatory mediators analyzed in 15 hours, except for MMP9 by 150SiNPs. This is a very important finding since commonly safety of nanoparticles is simply evaluated on the basis of cytotoxicity assays (e.g. LDH and MTT).

Amorphous silica nanoparticles have been shown to induce inflammation *in vivo*. The literature suggests that these nanoparticles induce transient inflammatory effects *in vivo*. Cho, M. *et al.* (2009)¹⁸⁸ studied silica nanoparticle distribution in five-week-old male BALB/c mice, which received a single intravenous injection of a total of 100 μ l of 50-, 100-, and 200-nm RITC-labelled fluorescence silica nanoparticle suspension at a dose of 50 mg/kg via a tail vein. By histopathology, they reported a clear size-dependent inflammatory response in the liver at 12 hours; 100-nm and 200-nm, but not 50-nm, nanoparticles induced acute inflammation. This relation vanished and inflammation was slighter in longer treatments. A size-dependent silica nanoparticle clearance (quicker and in higher concentration), via urine and bile, was also reported. They also observed that all three

nanoparticles remained aggregated in the liver and spleen after a 4-week treatment, and nanoparticle aggregate distribution appeared to be associated with macrophages. The aggregation state of nanoparticles is an important factor for distribution and excretion.

Park, E.J. *et al.* (2009)¹⁸⁹ injected intraperitoneally (50 mg/kg) silica nanoparticles (12 nm in average) in ICR mice and took blood samples and isolated peritoneal macrophages at different times (0, 12, 24, 48, and 72 hours). They reported an increase in IL-1 β and TNF- α level in blood, which reached a peak at 12 – 24 hours, and decreased gradually in a time dependent manner to 72 hours. They also showed increased gene expression of IL-1 β , TNF- α , IL6, iNOS, and COX2 in macrophages in a time-dependent manner.

Literature also shows a size-dependent silica nanoparticle-induced damage in vivo. A study by Kaewamatawong, T. *et al.* (2005)⁶² showed a size-dependent acute pulmonary inflammation and severe tissue injury of female ICR mice (10 – 12 week of age) after intratracheal installation of 50 μ l aqueous suspension of 3 mg of amorphous silica (primary particle diameter of 14 nm or 213 nm). Exposure times: 30 minutes, 2h, 6h, 12h, 24h. In only 30 minutes exposure, severe degeneration and necrosis of bronchiolar epithelial cells were observed.

Other study by Kaewamatawong, T. *et al.* (2006)⁶³ showed a transient (30 days) moderate inflammation and tissue damage of the lungs of male ICR mice (7 – 8 weeks of age) after intratracheal

installation of 50 μ l aqueous suspension of up to 100 μ g of amorphous silica (primary particle diameter of 14 nm).

In summary, my studies using precipitated amorphous silica nanoparticles suggest that nanoparticle-induced noxious effects on HUVEC primary cells are most likely driven by free radical generation. Nanoparticles stimulate endothelial cells to produce and release ONOO⁻ in very high quantities indicating that eNOS dysfunction is very high. Contrary, the production of free NO was low. The nitrosative and oxidative stress, thus produced, most likely induced cell death and NF- κ B activation. This activation in turn, induced gene expression of mediators involved in inflammation and coagulation.

EFFECTS OF AMORPHOUS SILICA NANOPARTICLES IN HUMAN PLATELETS

The endothelial injury and dysfunction are associated with platelet aggregation. Human platelets and endothelial cells are involved together in several physiological and pathophysiological functions, such as inflammation, haemostasis, and thrombosis. Taking advantage of my group's expertises, based on over 30 years experience working on platelet function, I studied silica nanoparticle-induced noxious effects in human platelets.

First, I demonstrated nanoparticle-human platelet association and uptake by TEM. As in the case of endothelial cells, nanoparticle agglomerates quickly interacted with platelet surface membranes and

internalized. However, evidences of nanoparticles encapsulated in vesicles were not found. More studies are necessary to understand the differences in nanoparticle uptake between platelets and endothelial cells. Interestingly, nanoparticles were also observed within platelet aggregates dispersed among platelets, and interacting with platelet membranes. These observations are consistent with a study by my group (2005) ¹⁴³ in human platelets. They showed that an urban PM standard reference material (SMR1648; average size 1.4 μm), purified fullerenes (C60CS), and a mixture of amorphous carbon with approximately 7% C60CS (MCN), at a concentration of 200 $\mu\text{g}/\text{ml}$, located within platelet aggregates dispersed among platelets; however, particle uptake by platelets was not reported. In this study, they also demonstrated that exposure of washed platelets to 200- $\mu\text{g}/\text{ml}$ MCN, SRM1648, carbon single-walled (SWNT) and multi-walled (MWNT) nanotubes resulted in the activation of GPIIb/IIIa; but only, MCN (200- $\mu\text{g}/\text{ml}$) led to the translocation of P-selectin to platelet surface membranes. In my studies, I have showed that exposure of platelets to silica nanoparticles induced SELP expression on the platelet surface membrane in a size-dependent manner. However, only 10SiNPs and 50SiNPs had the ability to activate GPIIb/IIIa. In their study, Radomski, A. *et al.* (2005) ¹⁴³ also showed that MCN, SMR1648, SWNT and MWNT, but not C60CS, at a concentration of 200 $\mu\text{g}/\text{ml}$, had the ability to induce aggregation of human platelets, as measured by aggregometry in washed platelets. I have also

demonstrated that silica nanoparticles induced platelet aggregation in a size dependent manner. The ability of SWNT (100 µg/ml) (outer diameter: < 2 nm, length: 1-5 µm) to induce platelet aggregation in PRP has been reported in a study by Bihari, P. *et al* (2010) ¹⁹⁰. They also showed that the same nanoparticle concentration induced translocation of SELP to the platelet surface membrane after incubation of human whole blood. All these findings demonstrate the ability of nanoparticles to influence the cell function in vitro.

The noxious effects of nanoparticles in human platelets have been also demonstrated in vivo. Both studies by Radomski, A. *et al* (2005) ¹⁴³ and by Bihari, P. *et al* (2010) ¹⁹⁰ reported the ability of SWNT to induce vascular thrombosis in vivo.

My group has also shown that the use of biodegradable nanoparticles, such as poly(D,L-lactide-co-glycolide) (PLGA), chitosan and PLGA-chitosan nanoparticles does not modify neither platelet aggregation nor platelet activation in vitro ¹⁹¹. Therefore, the use of biodegradable nanoparticles as drug delivery system and in other applications in nanomedicine seems to be the solution to the toxicity induced by some non-biodegradable nanoparticles in biological systems.

Although, my data showed that silica nanoparticles induced very strong noxious affects in washed platelets; most likely, the presence of proteins in PRP slowed down the damage. Only 10SiNPs (200 µg/ml) significantly induced SELP expression on the platelet

surface membrane as measured by flow cytometry in PRP. In addition, concentrations up to 200- $\mu\text{g}/\text{ml}$ 10SiNPs did not induce platelet aggregation. Furthermore, larger particle induced neither platelet aggregation nor SELP expression. These observations may have two important consequences: first, plasma proteins seem to induce some kind of protection, which delays nanoparticle noxious effects in platelets suggesting that protein corona ⁵⁹ might be involved. A second consequence is that aggregometry might not be accurate enough to detect small platelet aggregates, and therefore report false negatives.

Our studies using nanosensors have demonstrated that amorphous silica nanoparticles directly stimulated human platelets to release both NO and ONOO⁻, as nanoparticles were added to PRP. The amount of released NO and ONOO⁻ induced by amorphous silica nanoparticles in platelets was much lower than that in endothelial cells. None of the silica nanoparticles tested, except 10-nm, were able to either induce SELP expression or platelet aggregation as they were added to PRP. However, 50SiNPs, 150SiNPs, and 500SiNPs significantly stimulated platelets to release ONOO⁻ at a high concentration (100 and 200 $\mu\text{g}/\text{ml}$). Peroxynitrite is rapidly converted to NO donors in the present of plasma proteins; and therefore, platelet activation and aggregation detectable in washed platelet suspensions is avoided ¹⁹². Nitric oxide released from these NO

donors could also protect platelets against amorphous silica nanoparticles-induced damage.

In summary, my studies of amorphous silica nanoparticle-induced noxious effects in human platelets revealed that silica nanoparticles are able to activate platelets by inducing expression of SELP and GPIIb/IIIa activation on the platelet surface membrane. These events lead to platelet aggregation. The platelet aggregating effects of silica nanoparticles are most likely delayed and attenuated by the presence of plasma proteins. Finally, amorphous silica nanoparticles stimulate platelets to release NO and ONOO⁻ which modulate platelet function.

PHYSIOLOGICAL SIGNIFICANCE: A HYPOTHESIS

The potential physiological significance of the noxious effects induced by amorphous silica nanoparticles in human endothelial cells and platelets, which I have reported in my thesis studies, are shown in **Figure 45** and **46**.

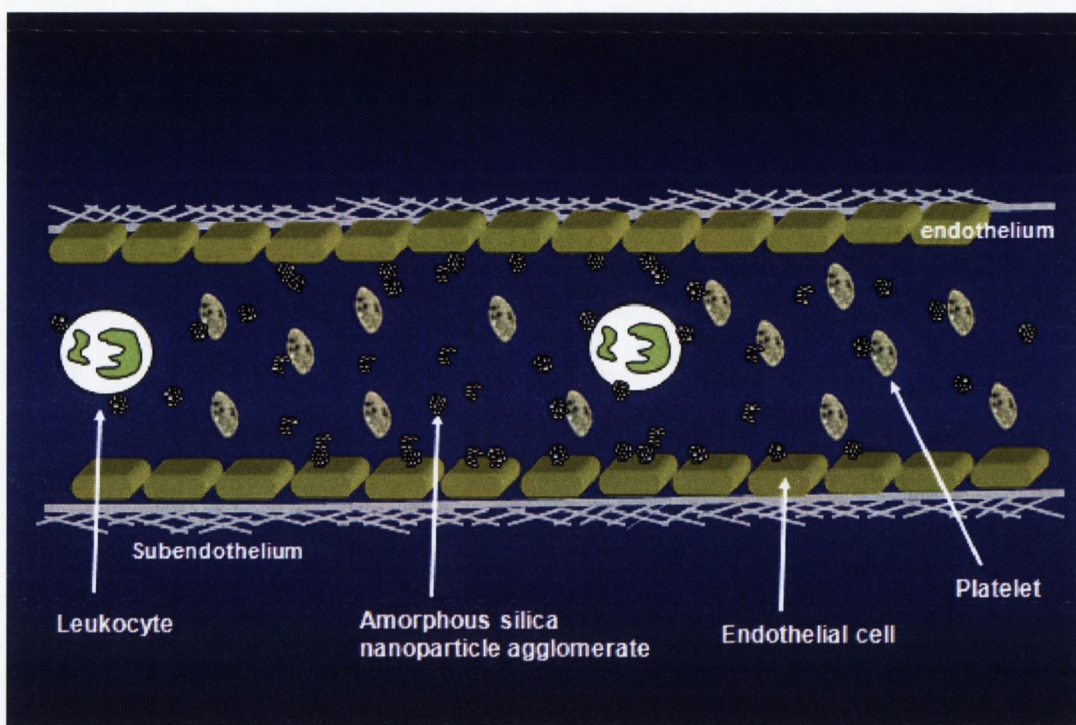


Figure 45 | Amorphous silica nanoparticle aggregates in a standard vein or artery. This figure shows normal blood elements (leukocytes, mainly neutrophils; resting platelets) travelling through a standard artery or vein in absence of infection and/or vascular damage. Erythrocytes and plasma proteins are not represented. Amorphous silica nanoparticles are shown as agglomerates. The elements of this figure are not in scale.

The presence of amorphous silica nanoparticles in the cardiovascular system may interfere with the normal physiology. Compared with monodisperse nanoparticles, nanoparticle agglomerates stay longer time in blood; and therefore, the time available to interact with vascular elements is greater. Nanoparticle agglomerates make nanoparticles more difficult to eliminate by the kidney than monodisperse nanoparticles. Nanoparticles may interact with and internalize in platelets, endothelial cells, and other vascular elements.

Uptake of silica nanoparticles by endothelial cells will lead to inflammation in the absence of infection or damage.

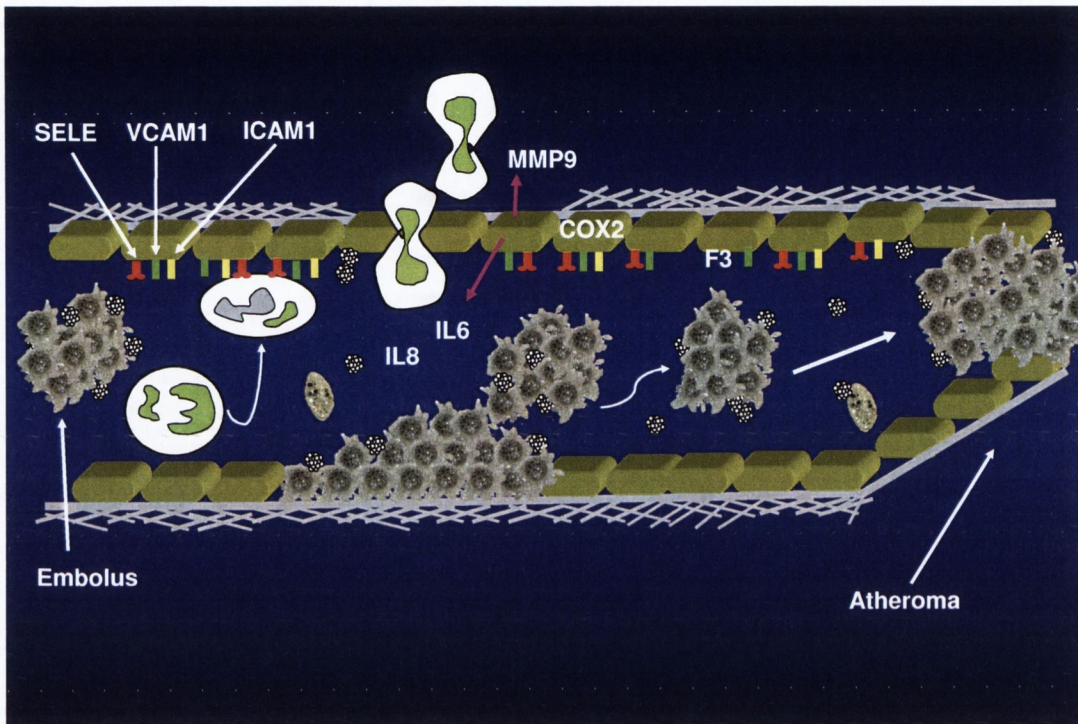


Figure 46 | Potential pathological consequences of the presence of amorphous silica nanoparticles in blood. This figure shows an inflamed and damaged artery or vein by the action of silica nanoparticles. Inflamed endothelial cells recruit leukocytes from the blood into the tissue, with the possibility of atheroma formation, especially in patients with high LDL level. Silica nanoparticles may also produce damage of the endothelium. Silica nanoparticles themselves and endothelium damage may induce platelet activation and aggregation. This may lead finally to embolus formation; since, it is not possible to eliminate the stimulus, which triggered the inflammatory response (i.e. nanoparticles). Embolus formation may lead to important health issues, especially in patients who have already atherosclerotic disease. Inflammatory response may occur in both veins and arteries, but atherosclerotic lesion is related with arteries.

Amorphous silica nanoparticles will induce endothelial cells to rapidly produce an excess of free radicals, such as ONOO^- . Oxidative stress thus produced will severely damage the most sensitive cells and induce transcription factor activation (e.g. $\text{NF-}\kappa\text{B}$) in the rest.

Free radicals can also oxidize LDLs trapped in the tunica intima of the vessel wall leading to atherosclerotic lesion. Activated transcription factors will activate transcription of mediators involved in inflammation (e.g. ICAM1, VCAM1, SELE, MMP9, PTGS2, IL6, and IL8) and coagulation (F3) to mRNA. The expression of the adhesion molecules (ICAM1, VCAM1, and SELE) on the endothelial surface membrane will recruit white cells. Leukocytes will tether, roll and extravasate into tissues. Release of MMP9 from endothelial cells into the subendothelium will digest components of the extracellular matrix to accommodate leukocytes. Release of IL8 to the bloodstream will attract more leukocytes to this site. IL6 will be also involved in the recruitment. The action of COX2 will produce vasorelaxation by prostacyclin synthesis.

On the other hand, endothelial cell death will lead to exposure of subendothelial components to the flowing blood that in turn will produce platelet activation. This along with the activation of the coagulation cascade by tissue factor will lead to blood thrombus formation. In physiological conditions, the fibrinolytic system will disaggregate the clot; however, persistent activation of thrombotic responses by nanoparticles may eventually exhaust the fibrinolytic system capacity. Also acute endothelial inflammation will evolve to chronic. This may conduct to stable clot formation (embolus), with dramatic consequences especially for patients with atherosclerotic disease.

Of course, the pathological and "doomsday" scenario that I have drawn based on the results of my in vitro experiments is likely to be attenuated in vivo. Therefore, more studies are needed to evaluate the significance of my findings to human vascular diseases.

CONCLUSIONS

- 1. Synthetic amorphous silica nanoparticles are internalized into HUVEC primary cells and stored mainly in vesicles in vitro.** Nanoparticles (10 nm) were found forming agglomerates. They were most likely up-taken by endocytosis. Non-encapsulated particle agglomerates free in the cytosol were also present.
- 2. Synthetic amorphous silica nanoparticles induce nitrosative stress in HUVEC primary cells in vitro.** Silica nanoparticles triggered a massive production of ONOO^- by endothelial cells. This means that the dysfunction of eNOS is extremely high. Contrary, the concentration of free NO is low. Therefore, the ratio of ONOO^- to NO is very high, which indicates extremely high nitrosative stress especially for 10-nm and 50-nm silica nanoparticles.
- 3. Synthetic amorphous silica nanoparticles induce cytotoxicity in HUVEC primary cells in vitro.** Increased of free radical production by endothelial cells exposed to silica nanoparticles, most likely induced cell death by oxidation of cellular components. Nanoparticles (10 nm) were cytotoxic.

4. **Synthetic amorphous silica nanoparticles induce transcription factor NF- κ B binding activity in HUVEC primary cells in vitro.** In the surviving cells, most likely oxidative stress induced free radical-sensitive NF- κ B activation. Nanoparticles (10 nm (1 hour), 50 nm (3 hours), and 150 nm (3 hours)) induced NF- κ B binding activity.

5. **Synthetic amorphous silica nanoparticles induce up-regulation of the genes *ICAM1*, *VCAM1*, *SELE*, *MMP9*, *PTGS2*, *F3*, *IL6*, and *IL8* in HUVEC primary cells in vitro.** Activated NF- κ B most likely underpins the activation of the transcription of these eight genes codifying key factors involved in the inflammatory response and coagulation cascade. It was 10SiNPs which induced the strongest effect at 15 hours. However, 50SiNPs, 150SiNPs, and 500SiNPs also induced gene expression up-regulation at 15 hours. The smallest nanoparticles also induced gene up-regulation at 7 hours.

6. **Synthetic amorphous silica nanoparticles induce cytokines, IL6 and IL8, release from HUVEC primary cells in vitro.** Increased IL6 and IL8 were released to cell culture medium, as a result of the exposure of endothelial cells to silica nanoparticles. It was 10SiNPs which induced the strongest

effect at 15 hours. However, 50SiNPs, 150SiNPs, and 500SiNPs also induced protein release.

7. Synthetic amorphous silica nanoparticles are internalized into platelets and remained non-encapsulated in vitro.

Nanoparticles (10 nm) were found forming agglomerates. Encapsulated particle agglomerates were not present into platelets.

8. Synthetic amorphous silica nanoparticles induce GPIIb/IIIa activation and SELP expression on the platelet surface membrane in vitro.

Nanoparticles influenced GPIIb/IIIa activation (10 nm and 50 nm) and SELP expression (10 nm, 50 nm, 150 nm, and 500 nm).

9. Synthetic amorphous silica nanoparticles induce platelet aggregation in vitro.

Activation of GPIIb/IIIa and expression of SELP on the platelet surface membrane led to platelet aggregation. Nanoparticles (10 nm, 50 nm, 150 nm) induced platelet aggregation.

10. Platelet activation and aggregation induced by exposure of platelets to synthetic amorphous silica nanoparticles was attenuated by the presence of plasma proteins. I

hypothesize protein corona formed as a consequence of the introduction of nanoparticle in a protein-rich solution, such as PRP, might be involved in these observations.

11. Synthetic amorphous silica nanoparticles induce nitrosative stress in human platelets. The addition of silica

nanoparticles to PRP stimulated platelets to release ONOO⁻. The level of NO remained low.

FUTURE DIRECTIONS

1. To find the exact mechanism/s involved by silica nanoparticles to reach the cytoplasm of endothelial cells and to study the relation between silica particle size and uptake by TEM. To find in which organelles nanoparticles accumulate in the cytoplasm and why they are free in the cytosol.
2. To study whether or not silica nanoparticles are able to activate other transcription factors (e.g. AP-1).
3. To clearly study the influence of silica nanoparticle-induced NF- κ B activation, and other potentially involved transcription factors, in the gene expression up-regulation derived from the exposure of nanoparticles to endothelial cells by the use of selective inhibitors for the transcription factors.
4. To study if the silica nanoparticle-induced gene up-regulation leads to up-regulation of the corresponding proteins.
5. To study in greater depth more nanoparticle-induced free radical released by nanosensors detecting radicals such H_2O_2 , $\text{O}_2^{\bullet-}$, and OH^{\bullet} .

6. To study the influence of protein corona in the synthetic amorphous silica nanoparticle-induced effects in endothelial cells.
7. To study the molecular mechanism underpinning the effect derived from the exposure of silica nanoparticles to platelets.
8. To understand why the protein corona attenuates the effects of silica nanoparticles in platelets; as well as, to know the degree of implication of the different plasma proteins in these effects.
9. To use flow systems to study the effects of silica and other nanoparticles on platelets, leukocytes, and endothelial cells.
10. To study the influence of the silica nanoparticle surface on the effects derived from their exposure to biological systems.
11. To study the effects of other types of nanoparticles.
12. To perform in vivo studies to corroborate my in vitro findings.

REFERENCES

1. National Nanotechnology Initiative (USA): <http://www.nano.gov/> (accessed August 2010).
2. Nanotechnology (EU): <http://cordis.europa.eu/nanotechnology/> (accessed August 2010).
3. Feynman, R.P. There's Plenty of Room at the Bottom. *Eng Sci.* **23**, 22 - 36 (1960).
4. Joachim, C. & Plevart, L. *Nanosciences: The Invisible Revolution*. World Scientific, London (2009).
5. Moore, G.E. Cramming more components onto integrated circuits. *Electronics Magazine*, Vol. 38. McGraw-Hill and Penton Publishing, USA (1965).
6. Intel Corporation: <http://www.intel.com> (accessed August 2010).
7. Taniguchi, N. On the Basic Concept of 'Nano-Technology'. *Proc ICPE Tokio* **2**, 18-23 (1974).
8. Binnig, G., Quate, C.F. & Gerber, C. Atomic force microscope. *Phys Rev Lett* **56**, 930-933 (1986).
9. Binnig, G., Rohrer, H., Gerber, C. & Weibel, E. Surface Studies by Scanning Tunneling Microscopy. *Phys Rev Lett* **49**, 57-61 (1982).
10. Drexler, K.E. *Engines of Creation: The Coming Era of Nanotechnology*. Anchor Books, New York (1986).

11. Drexler, K.E. *Nanosystems: Molecular Machinery, Manufacturing, and Computation*. Wiley-Interscience, New York (1992).
12. FP7 (EU): http://cordis.europa.eu/fp7/home_en.html (accessed August 2010).
13. Nel, A., Xia, T., Madler, L. & Li, N. Toxic potential of materials at the nanolevel. *Science* **311**, 622-627 (2006).
14. European Technology Platform on Nanomedicine (EU). *Nanomedicine: Nanotechnology for Health* (2006).
15. Jain, K.K. The role of nanobiotechnology in drug discovery. *Drug Discovery Today* **10**, 1435-1442 (2005).
16. Jain, K.K. Role of nanobiotechnology in developing personalized medicine for cancer. *Technol Cancer Res Treat.* **4**, 645-650 (2005).
17. Jain, K.K. Personalized medicine. *Current Opinion in Molecular Therapeutics* **4**, 548-558 (2002).
18. Medina, C., Santos-Martinez, M.J., Radomski, A., Corrigan, O.I. & Radomski, M.W. Nanoparticles: pharmacological and toxicological significance. *Br J Pharmacol* **150**, 552-558 (2007).
19. Seaton, A. & Donaldson, K. Nanoscience, nanotoxicology, and the need to think small. *Lancet* **365**, 923-924 (2005).
20. Kipen, H.M. & Laskin, D.L. Smaller is not always better: nanotechnology yields nanotoxicology. *Am J Physiol Lung Cell Mol Physiol* **289**, L696-697 (2005).

21. Chen, Z., *et al.* Age-related differences in pulmonary and cardiovascular responses to SiO₂ nanoparticle inhalation: nanotoxicity has susceptible population. *Environ Sci Technol* **42**, 8985-8992 (2008).
22. Lam, C.W., James, J.T., McCluskey, R. & Hunter, R.L. Pulmonary toxicity of single-wall carbon nanotubes in mice 7 and 90 days after intratracheal instillation. *Toxicol Sci* **77**, 126-134 (2004).
23. Tiede, K., *et al.* Detection and characterization of engineered nanoparticles in food and the environment. *Food Addit Contam Part A Chem Anal Control Expo Risk Assess* **25**, 795-821 (2008).
24. Faraji, A.H. & Wipf, P. Nanoparticles in cellular drug delivery. *Bioorg Med Chem* **17**, 2950-2962 (2009).
25. Brook, R.D., *et al.* Air pollution and cardiovascular disease: a statement for healthcare professionals from the Expert Panel on Population and Prevention Science of the American Heart Association. *Circulation* **109**, 2655-2671 (2004).
26. Nemery, B., Hoet, P.H. & Nemmar, A. The Meuse Valley fog of 1930: an air pollution disaster. *Lancet* **357**, 704-708 (2001).
27. Helfand, W.H., Lazarus, J. & Theerman, P. Donora, Pennsylvania: an environmental disaster of the 20th century. *Am J Public Health* **91**, 553 (2001).

28. Logan, W.P. Mortality in the London fog incident, 1952. *Lancet* **1**, 336-338 (1953).
29. Samet, J.M., Geyh, A.S. & Utell, M.J. The legacy of World Trade Center dust. *N Engl J Med* **356**, 2233-2236 (2007).
30. Nel, A. Atmosphere. Air pollution-related illness: effects of particles. *Science* **308**, 804-806 (2005).
31. Peters, A., *et al.* Exposure to traffic and the onset of myocardial infarction. *N Engl J Med* **351**, 1721-1730 (2004).
32. Miller, K.A., *et al.* Long-term exposure to air pollution and incidence of cardiovascular events in women. *N Engl J Med* **356**, 447-458 (2007).
33. Pope, C.A., 3rd. The expanding role of air pollution in cardiovascular disease: does air pollution contribute to risk of deep vein thrombosis? *Circulation* **119**, 3050-3052 (2009).
34. Mills, N.L., *et al.* Ischemic and thrombotic effects of dilute diesel-exhaust inhalation in men with coronary heart disease. *N Engl J Med* **357**, 1075-1082 (2007).
35. Pope, C.A., 3rd, Ezzati, M. & Dockery, D.W. Fine-particulate air pollution and life expectancy in the United States. *N Engl J Med* **360**, 376-386 (2009).
36. Brunekreef, B. Air pollution and life expectancy: is there a relation? *Occup Environ Med* **54**, 781-784 (1997).

37. Nevalainen, J. & Pekkanen, J. The effect of particulate air pollution on life expectancy. *Sci Total Environ* **217**, 137-141 (1998).
38. Coyle, D., *et al.* Impact of particulate air pollution on quality-adjusted life expectancy in Canada. *J Toxicol Environ Health A* **66**, 1847-1863 (2003).
39. Food Safety Authority of Ireland. The Relevance for Food Safety of Application of Nanotechnology in the Food and Feed Industries (2008).
40. Dutch National Institute for public Health and the Environment. Nanotechnology in Perspective: Risks to Man and the Environment (2009).
41. Hofheinz, R.D., Gnad-Vogt, S.U., Beyer, U. & Hochhaus, A. Liposomal encapsulated anti-cancer drugs. *Anticancer Drugs* **16**, 691-707 (2005).
42. Moghimi, S.M. & Szebeni, J. Stealth liposomes and long circulating nanoparticles: critical issues in pharmacokinetics, opsonization and protein-binding properties. *Progress in Lipid Research* **42**, 463-478 (2003).
43. Sarker, D.K. Engineering of nanoemulsions for drug delivery. *Curr Drug Deliv* **2**, 297-310 (2005).
44. Agnihotri, S.A., Mallikarjuna, N.N. & Aminabhavi, T.M. Recent advances on chitosan-based micro- and nanoparticles in drug delivery. *Journal of Controlled Release* **100**, 5-28 (2004).

45. Lee, L.J. Polymer nano-engineering for biomedical applications. *Ann Biomed Eng* **34**, 75-88 (2006).
46. Cherian, A.K., Rana, A.C. & Jain, S.K. Self-assembled carbohydrate-stabilized ceramic nanoparticles for the parenteral delivery of insulin. *Drug Dev Ind Pharm* **26**, 459-463 (2000).
47. Gupta, A.K. & Gupta, M. Synthesis and surface engineering of iron oxide nanoparticles for biomedical applications. *Biomaterials* **26**, 3995-4021 (2005).
48. Hirsch, L.R., *et al.* Metal nanoshells. *Ann Biomed Eng* **34**, 15-22 (2006).
49. Bosi, S., Da Ros, T., Spalluto, G. & Prato, M. Fullerene derivatives: an attractive tool for biological applications. *European Journal of Medicinal Chemistry* **38**, 913-923 (2003).
50. Pagona, G. & Tagmatarchis, N. Carbon nanotubes: materials for medicinal chemistry and biotechnological applications. *Current Medicinal Chemistry* **13**, 1789-1798 (2006).
51. Weng, J. & Ren, J. Luminescent quantum dots: a very attractive and promising tool in biomedicine. *Curr Med Chem* **13**, 897-909 (2006).
52. Reilly, R.M. Carbon nanotubes: potential benefits and risks of nanotechnology in nuclear medicine. *J Nucl Med* **48**, 1039-1042 (2007).
53. Jin, Y. & Gao, X. Plasmonic fluorescent quantum dots. *Nat Nanotechnol* **4**, 571-576 (2009).

54. Elwell, D., Rao, G.M. Electrolytic Production of Silicon. *Journal of Applied Electrochemistry* **18**, 15 - 22 (1988).
55. *The SGTE Casebook: Thermodynamics at Work (2nd ed)*. Woodhead Pub. Ltd, Cambridge (2008).
56. Iler, R.K. *The Chemistry of Silica: Solubility, Polymerization, Colloid and Surface Properties, and Biochemistry*. Wiley-International Publication, New York (1979).
57. Binks, B.P. & Horozov, T.S. Colloidal Particles at Liquid Interfaces: An Introduction. In *Colloidal particles at Liquid Interfaces*, 1-69. University press Cambridge, Cambridge (2006).
58. Bogdan, A., Kulmala, M. Pyrogenic Silica and Alumina. in *Encyclopedia of Surface and Colloid Science*, Vol. 4, 4396-4410. Marcel Dekker, Inc., New York (2002).
59. Lundqvist, M., *et al*. Nanoparticle size and surface properties determine the protein corona with possible implications for biological impacts. *Proc Natl Acad Sci U S A* **105**, 14265-14270 (2008).
60. Environmental Protection Agency (USA). Ambient Level and Noncancer and Health Effects of Inhaled Crystalline and Amorphous Silica: Health Issue Assessment (1996).
61. Merget, R., *et al*. Health hazards due to the inhalation of amorphous silica. *Arch Toxicol* **75**, 625-634 (2002).

62. Kaewamatawong, T., *et al.* Acute pulmonary toxicity caused by exposure to colloidal silica: particle size dependent pathological changes in mice. *Toxicol Pathol* **33**, 743-749 (2005).
63. Kaewamatawong, T., *et al.* Acute and subacute pulmonary toxicity of low dose of ultrafine colloidal silica particles in mice after intratracheal instillation. *Toxicol Pathol* **34**, 958-965 (2006).
64. Cines, D.B., *et al.* Endothelial cells in physiology and in the pathophysiology of vascular disorders. *Blood* **91**, 3527-3561 (1998).
65. Pober, J.S. & Sessa, W.C. Evolving functions of endothelial cells in inflammation. *Nat Rev Immunol* **7**, 803-815 (2007).
66. Rosmarin, A.G., Yang, Z. & Resendes, K.K. Transcriptional regulation in myelopoiesis: Hematopoietic fate choice, myeloid differentiation, and leukemogenesis. *Exp Hematol* **33**, 131-143 (2005).
67. Janeway, C.A., Jr. Approaching the asymptote? Evolution and revolution in immunology. *Cold Spring Harb Symp Quant Biol* **54 Pt 1**, 1-13 (1989).
68. Medzhitov, R. Toll-like receptors and innate immunity. *Nat Rev Immunol* **1**, 135-145 (2001).
69. Rock, F.L., Hardiman, G., Timans, J.C., Kastelein, R.A. & Bazan, J.F. A family of human receptors structurally related to *Drosophila* Toll. *Proc Natl Acad Sci U S A* **95**, 588-593 (1998).

70. Medzhitov, R., Preston-Hurlburt, P. & Janeway, C.A., Jr. A human homologue of the *Drosophila* Toll protein signals activation of adaptive immunity. *Nature* **388**, 394-397 (1997).
71. Medzhitov, R. Recognition of microorganisms and activation of the immune response. *Nature* **449**, 819-826 (2007).
72. Rifkin, I.R., Leadbetter, E.A., Busconi, L., Viglianti, G. & Marshak-Rothstein, A. Toll-like receptors, endogenous ligands, and systemic autoimmune disease. *Immunol Rev* **204**, 27-42 (2005).
73. Schatz, D.G., Oettinger, M.A. & Schlissel, M.S. V(D)J recombination: molecular biology and regulation. *Annu Rev Immunol* **10**, 359-383 (1992).
74. Klein, L., Hinterberger, M., Wirnsberger, G. & Kyewski, B. Antigen presentation in the thymus for positive selection and central tolerance induction. *Nat Rev Immunol* **9**, 833-844 (2009).
75. Hansen, T.H. & Bouvier, M. MHC class I antigen presentation: learning from viral evasion strategies. *Nat Rev Immunol* **9**, 503-513 (2009).
76. Batista, F.D. & Harwood, N.E. The who, how and where of antigen presentation to B cells. *Nat Rev Immunol* **9**, 15-27 (2009).
77. Gros, P., Milder, F.J. & Janssen, B.J. Complement driven by conformational changes. *Nat Rev Immunol* **8**, 48-58 (2008).

78. Sprague, A.H. & Khalil, R.A. Inflammatory cytokines in vascular dysfunction and vascular disease. *Biochem Pharmacol* **78**, 539-552 (2009).
79. Marshall, J.S. Mast-cell responses to pathogens. *Nat Rev Immunol* **4**, 787-799 (2004).
80. Gordon, S. & Taylor, P.R. Monocyte and macrophage heterogeneity. *Nat Rev Immunol* **5**, 953-964 (2005).
81. Weibel, E.R. & Palade, G.E. New Cytoplasmic Components in Arterial Endothelia. *J Cell Biol* **23**, 101-112 (1964).
82. Alonso, D. & Radomski, M.W. Nitric oxide, platelet function, myocardial infarction and reperfusion therapies. *Heart Fail Rev* **8**, 47-54 (2003).
83. Lorant, D.E., *et al.* Coexpression of GMP-140 and PAF by endothelium stimulated by histamine or thrombin: a juxtacrine system for adhesion and activation of neutrophils. *J Cell Biol* **115**, 223-234 (1991).
84. Romano, M., *et al.* Role of IL-6 and its soluble receptor in induction of chemokines and leukocyte recruitment. *Immunity* **6**, 315-325 (1997).
85. Gainetdinov, R.R., Premont, R.T., Bohn, L.M., Lefkowitz, R.J. & Caron, M.G. Desensitization of G protein-coupled receptors and neuronal functions. *Annu Rev Neurosci* **27**, 107-144 (2004).
86. Gilmore, T.D. The Rel/NF-kappaB signal transduction pathway: introduction. *Oncogene* **18**, 6842-6844 (1999).

87. Chen, F.E. & Ghosh, G. Regulation of DNA binding by Rel/NF-kappaB transcription factors: structural views. *Oncogene* **18**, 6845-6852 (1999).
88. Karin, M. How NF-kappaB is activated: the role of the IkappaB kinase (IKK) complex. *Oncogene* **18**, 6867-6874 (1999).
89. Pahl, H.L. Activators and target genes of Rel/NF-kappaB transcription factors. *Oncogene* **18**, 6853-6866 (1999).
90. Tumor, Z., Shimizu, H., Enomoto, A., Miyazaki, H. & Niwa, T. Indoxyl sulfate upregulates expression of ICAM-1 and MCP-1 by oxidative stress-induced NF-kappaB activation. *Am J Nephrol* **31**, 435-441 (2010).
91. Nelson, D.L. & Cox, M.M. *Lehninger Principles of Biochemistry*. W. H. Freeman and Company, New York (2008).
92. Barclay, A.N. Membrane proteins with immunoglobulin-like domains--a master superfamily of interaction molecules. *Semin Immunol* **15**, 215-223 (2003).
93. Williams, A.F. & Barclay, A.N. The immunoglobulin superfamily--domains for cell surface recognition. *Annu Rev Immunol* **6**, 381-405 (1988).
94. van de Stolpe, A. & van der Saag, P.T. Intercellular adhesion molecule-1. *J Mol Med* **74**, 13-33 (1996).
95. Lawson, C. & Wolf, S. ICAM-1 signaling in endothelial cells. *Pharmacol Rep* **61**, 22-32 (2009).

96. Pepinsky, B., *et al.* Structure/function studies on vascular cell adhesion molecule-1. *J Biol Chem* **267**, 17820-17826 (1992).
97. Hession, C., *et al.* Cloning of an alternate form of vascular cell adhesion molecule-1 (VCAM1). *J Biol Chem* **266**, 6682-6685 (1991).
98. Polte, T., Newman, W. & Gopal, T.V. Full length vascular cell adhesion molecule 1 (VCAM-1). *Nucleic Acids Res* **18**, 5901 (1990).
99. Graves, B.J., *et al.* Insight into E-selectin/ligand interaction from the crystal structure and mutagenesis of the lec/EGF domains. *Nature* **367**, 532-538 (1994).
100. Sternlicht, M.D. & Werb, Z. How matrix metalloproteinases regulate cell behavior. *Annu Rev Cell Dev Biol* **17**, 463-516 (2001).
101. Visse, R. & Nagase, H. Matrix metalloproteinases and tissue inhibitors of metalloproteinases: structure, function, and biochemistry. *Circ Res* **92**, 827-839 (2003).
102. Mitchell, J.A. & Warner, T.D. COX isoforms in the cardiovascular system: understanding the activities of non-steroidal anti-inflammatory drugs. *Nat Rev Drug Discov* **5**, 75-86 (2006).
103. Steffel, J., Luscher, T.F. & Tanner, F.C. Tissue factor in cardiovascular diseases: molecular mechanisms and clinical implications. *Circulation* **113**, 722-731 (2006).

104. Bevilacqua, M.P., *et al.* Recombinant tumor necrosis factor induces procoagulant activity in cultured human vascular endothelium: characterization and comparison with the actions of interleukin 1. *Proc Natl Acad Sci U S A* **83**, 4533-4537 (1986).
105. Furie, B. & Furie, B.C. Mechanisms of thrombus formation. *N Engl J Med* **359**, 938-949 (2008).
106. Bogdanov, V.Y., *et al.* Alternatively spliced human tissue factor: a circulating, soluble, thrombogenic protein. *Nat Med* **9**, 458-462 (2003).
107. Censarek, P., Bobbe, A., Grandoch, M., Schror, K. & Weber, A.A. Alternatively spliced human tissue factor (asHTF) is not pro-coagulant. *Thromb Haemost* **97**, 11-14 (2007).
108. Mackman, N., Morrissey, J.H., Fowler, B. & Edgington, T.S. Complete sequence of the human tissue factor gene, a highly regulated cellular receptor that initiates the coagulation protease cascade. *Biochemistry* **28**, 1755-1762 (1989).
109. Mackman, N. & Taubman, M. Tissue factor: past, present, and future. *Arterioscler Thromb Vasc Biol* **29**, 1986-1988 (2009).
110. Furie, B. & Furie, B.C. The molecular basis of blood coagulation. *Cell* **53**, 505-518 (1988).
111. Hirano, T., *et al.* Complementary DNA for a novel human interleukin (BSF-2) that induces B lymphocytes to produce immunoglobulin. *Nature* **324**, 73-76 (1986).

112. Hou, T., *et al.* Roles of IL-6-gp130 Signaling in Vascular Inflammation. *Curr Cardiol Rev* **4**, 179-192 (2008).
113. Baggiolini, M., Walz, A. & Kunkel, S.L. Neutrophil-activating peptide-1/interleukin 8, a novel cytokine that activates neutrophils. *J Clin Invest* **84**, 1045-1049 (1989).
114. Baldwin, E.T., *et al.* Crystal structure of interleukin 8: symbiosis of NMR and crystallography. *Proc Natl Acad Sci U S A* **88**, 502-506 (1991).
115. Baggiolini, M., Moser, B. & Clark-Lewis, I. Interleukin-8 and related chemotactic cytokines. The Giles Filley Lecture. *Chest* **105**, 95S-98S (1994).
116. Hoffmann, E., Dittrich-Breiholz, O., Holtmann, H. & Kracht, M. Multiple control of interleukin-8 gene expression. *J Leukoc Biol* **72**, 847-855 (2002).
117. Michelson, A.D. How platelets work: platelet function and dysfunction. *J Thromb Thrombolysis* **16**, 7-12 (2003).
118. Ruggeri, Z.M. Platelets in atherothrombosis. *Nature Medicine* **8**, 1227 (2002).
119. Jurasz, P., Alonso-Escolano, D. & Radomski, M.W. Platelet-cancer interactions: mechanisms and pharmacology of tumour cell-induced platelet aggregation. **143**, 819-826 (2004).
120. Jurasz, P., Santos-Martinez, M.J., Radomska, A. & Radomski, M.W. Generation of platelet angiostatin mediated by urokinase

- plasminogen activator: effects on angiogenesis. *Journal of Thrombosis and Haemostasis* **4**, 1095-1106 (2006).
121. Medina, C., *et al.* Platelet Aggregation-Induced by Caco-2 Cells: Regulation by Matrix Metalloproteinase-2 and Adenosine Diphosphate. *J Pharmacol Exp Ther* **317**, 739-745 (2006).
122. Chen, J. & Lopez, J.A. Interactions of platelets with subendothelium and endothelium. *Microcirculation* **12**, 235-246 (2005).
123. Coller, B.S. Blockade of platelet GPIIb/IIIa receptors as an antithrombotic strategy. *Circulation* **92**, 2373-2380 (1995).
124. Cramer, E.M., *et al.* Alpha-granule pool of glycoprotein IIb-IIIa in normal and pathologic platelets and megakaryocytes. *Blood* **75**, 1220-1227 (1990).
125. Radomski, M.W. & Radomski, A.S. Regulation of Blood Cell Function by the Endothelial cells. In *Vascular Endothelium in Human Physiology and Pathophysiology*, 95-106. Harwood Academic Publishers, London (2000).
126. Sawicki, G., Salas, E., Murat, J., Miszta-Lane, H. & Radomski, M.W. Release of gelatinase A during platelet activation mediates aggregation. *Nature* **386**, 616-619 (1997).
127. Needleman, P., *et al.* Identification of an enzyme in platelet microsomes which generates thromboxane A₂ from prostaglandin endoperoxides. *Nature* **261**, 558-560 (1976).

128. Born, G.V. Effects of adenosine diphosphate (ADP) and related substances on the adhesiveness of platelets in vitro and in vivo. *British Journal of Haematology* **12**, 37-38 (1966).
129. Poyton, R.O., Ball, K.A. & Castello, P.R. Mitochondrial generation of free radicals and hypoxic signaling. *Trends Endocrinol Metab* **20**, 332-340 (2009).
130. Griending, K.K., Sorescu, D., Lassegue, B. & Ushio-Fukai, M. Modulation of protein kinase activity and gene expression by reactive oxygen species and their role in vascular physiology and pathophysiology. *Arterioscler Thromb Vasc Biol* **20**, 2175-2183 (2000).
131. Turrens, J.F. Mitochondrial formation of reactive oxygen species. *J Physiol* **552**, 335-344 (2003).
132. Castello, P.R., David, P.S., McClure, T., Crook, Z. & Poyton, R.O. Mitochondrial cytochrome oxidase produces nitric oxide under hypoxic conditions: implications for oxygen sensing and hypoxic signaling in eukaryotes. *Cell Metab* **3**, 277-287 (2006).
133. Lu, D., Maulik, N., Moraru, II, Kreutzer, D.L. & Das, D.K. Molecular adaptation of vascular endothelial cells to oxidative stress. *Am J Physiol* **264**, C715-722 (1993).
134. de Belder, A.J., MacAllister, R., Radomski, M.W., Moncada, S. & Vallance, P.J. Effects of S-nitroso-glutathione in the human forearm circulation: evidence for selective inhibition of platelet activation. *Cardiovasc Res* **28**, 691-694 (1994).

135. Lusis, A.J. Atherosclerosis. *Nature* **407**, 233-241 (2000).
136. Suwa, T., *et al.* Particulate air pollution induces progression of atherosclerosis. *J Am Coll Cardiol* **39**, 935-942 (2002).
137. Gimbrone, M.A., Jr. Vascular endothelium, hemodynamic forces, and atherogenesis. *Am J Pathol* **155**, 1-5 (1999).
138. Tabas, I., Williams, K.J. & Boren, J. Subendothelial lipoprotein retention as the initiating process in atherosclerosis: update and therapeutic implications. *Circulation* **116**, 1832-1844 (2007).
139. Boren, J., *et al.* Identification of the principal proteoglycan-binding site in LDL. A single-point mutation in apo-B100 severely affects proteoglycan interaction without affecting LDL receptor binding. *J Clin Invest* **101**, 2658-2664 (1998).
140. Dai, G., *et al.* Distinct endothelial phenotypes evoked by arterial waveforms derived from atherosclerosis-susceptible and -resistant regions of human vasculature. *Proc Natl Acad Sci U S A* **101**, 14871-14876 (2004).
141. Glass, C.K. & Witztum, J.L. Atherosclerosis. the road ahead. *Cell* **104**, 503-516 (2001).
142. Hansson, G.K. & Libby, P. The immune response in atherosclerosis: a double-edged sword. *Nat Rev Immunol* **6**, 508-519 (2006).
143. Radomski, A., *et al.* Nanoparticle-induced platelet aggregation and vascular thrombosis. *Br J Pharmacol* **146**, 882-893 (2005).

144. Radomski, M. & Moncada, S. An improved method for washing of human platelets with prostacyclin. *Thromb Res* **30**, 383-389 (1983).
145. Radomski, A., Stewart, M.W., Jurasz, P. & Radomski, M.W. Pharmacological characteristics of solid-phase von Willebrand factor in human platelets. *Br J Pharmacol* **134**, 1013-1020 (2001).
146. Radomski, A., *et al.* Identification, regulation and role of tissue inhibitor of metalloproteinases-4 (TIMP-4) in human platelets. *Br J Pharmacol* **137**, 1330-1338 (2002).
147. Jurasz, P., Alonso, D., Castro-Blanco, S., Murad, F. & Radomski, M.W. Generation and role of angiostatin in human platelets. *Blood* **102**, 3217-3223 (2003).
148. Worle-Knirsch, J.M., Pulskamp, K. & Krug, H.F. Oops they did it again! Carbon nanotubes hoax scientists in viability assays. *Nano Lett* **6**, 1261-1268 (2006).
149. Malinski, T. & Taha, Z. Nitric oxide release from a single cell measured in situ by a porphyrinic-based microsensor. *Nature* **358**, 676-678 (1992).
150. Xue, J., Ying, X., Chen, J., Xian, Y. & Jin, L. Amperometric ultramicrosensors for peroxynitrite detection and its application toward single myocardial cells. *Anal Chem* **72**, 5313-5321 (2000).

151. Livak, K.J. & Schmittgen, T.D. Analysis of relative gene expression data using real-time quantitative PCR and the 2(-Delta Delta C(T)) Method. *Methods* **25**, 402-408 (2001).
152. Jurasz, P., *et al.* Matrix metalloproteinase 2 in tumor cell-induced platelet aggregation: regulation by nitric oxide. *Cancer Research* **61**, 376-382 (2001).
153. Alonso-Escolano, D., Strongin, A.Y., Chung, A.W., Deryugina, E.I. & Radomski, M.W. Membrane type-1 matrix metalloproteinase stimulates tumour cell-induced platelet aggregation: role of receptor glycoproteins. *British Journal of Pharmacology* **141**, 241-252 (2004).
154. Chung, A.W., Jurasz, P., Hollenberg, M.D. & Radomski, M.W. Mechanisms of action of proteinase-activated receptor agonists on human platelets. *British Journal of Pharmacology* **135**, 1123-1132 (2002).
155. Radomski, A., Stewart, M.W., Jurasz, P. & Radomski, M.W. Pharmacological characteristics of solid-phase von Willebrand factor in human platelets. *British Journal of Pharmacology* **134**, 1013-1020 (2001).
156. Jurasz, P., *et al.* Role of von Willebrand factor in tumour cell-induced platelet aggregation: differential regulation by NO and prostacyclin. *Br J Pharmacol* **134**, 1104-1112 (2001).

157. Abrams, C.S., Ellison, N., Budzynski, A.Z. & Shattil, S.J. Direct detection of activated platelets and platelet-derived microparticles in humans. *Blood* **75**, 128-138 (1990).
158. Murdock, R.C., Braydich-Stolle, L., Schrand, A.M., Schlager, J.J. & Hussain, S.M. Characterization of nanomaterial dispersion in solution prior to in vitro exposure using dynamic light scattering technique. *Toxicol Sci* **101**, 239-253 (2008).
159. Li, N., Xia, T. & Nel, A.E. The role of oxidative stress in ambient particulate matter-induced lung diseases and its implications in the toxicity of engineered nanoparticles. *Free Radic Biol Med* **44**, 1689-1699 (2008).
160. Corbalan, J.J. Trinity College Dublin (2009).
161. Mroz, R.M., *et al.* Nanoparticle carbon black driven DNA damage induces growth arrest and AP-1 and NFkappaB DNA binding in lung epithelial A549 cell line. *J Physiol Pharmacol* **58 Suppl 5**, 461-470 (2007).
162. Eder, W., Ege, M.J. & von Mutius, E. The asthma epidemic. *N Engl J Med* **355**, 2226-2235 (2006).
163. Jaffe, E.A., Nachman, R.L., Becker, C.G. & Minick, C.R. Culture of human endothelial cells derived from umbilical veins. Identification by morphologic and immunologic criteria. *J Clin Invest* **52**, 2745-2756 (1973).

164. Thomassen, L.C., *et al.* Synthesis and characterization of stable monodisperse silica nanoparticle sols for in vitro cytotoxicity testing. *Langmuir* **26**, 328-335 (2010).
165. Ehrenberg, M.S., Friedman, A.E., Finkelstein, J.N., Oberdorster, G. & McGrath, J.L. The influence of protein adsorption on nanoparticle association with cultured endothelial cells. *Biomaterials* **30**, 603-610 (2009).
166. Chavanpatil, M.D., Khair, A. & Panyam, J. Nanoparticles for cellular drug delivery: mechanisms and factors influencing delivery. *J Nanosci Nanotechnol* **6**, 2651-2663 (2006).
167. Conner, S.D. & Schmid, S.L. Regulated portals of entry into the cell. *Nature* **422**, 37-44 (2003).
168. He, Q., Zhang, Z., Gao, Y., Shi, J. & Li, Y. Intracellular localization and cytotoxicity of spherical mesoporous silica nano- and microparticles. *Small* **5**, 2722-2729 (2009).
169. Giraldo, L.F., *et al.* Mesoporous Silica Applications. *Macromol. Symp.* **258**, 129-141 (2007).
170. Shi, X.L., Dalal, N.S., Hu, X.N. & Vallyathan, V. The chemical properties of silica particle surface in relation to silica-cell interactions. *J Toxicol Environ Health* **27**, 435-454 (1989).
171. Mao, Y., Daniel, L.N., Whittaker, N. & Saffiotti, U. DNA binding to crystalline silica characterized by Fourier-transform infrared spectroscopy. *Environ Health Perspect* **102 Suppl 10**, 165-171 (1994).

172. Saffiotti, U., *et al.* Mechanisms of carcinogenesis by crystalline silica in relation to oxygen radicals. *Environ Health Perspect* **102 Suppl 10**, 159-163 (1994).
173. Nan, A., Bai, X., Son, S.J., Lee, S.B. & Ghandehari, H. Cellular uptake and cytotoxicity of silica nanotubes. *Nano Lett* **8**, 2150-2154 (2008).
174. Napierska, D., *et al.* Size-dependent cytotoxicity of monodisperse silica nanoparticles in human endothelial cells. *Small* **5**, 846-853 (2009).
175. Edgell, C.J., McDonald, C.C. & Graham, J.B. Permanent cell line expressing human factor VIII-related antigen established by hybridization. *Proc Natl Acad Sci U S A* **80**, 3734-3737 (1983).
176. Stöber, W., Fink, A., Bohn, E. . Controlled growth of monodisperse silica spheres in the micron size range. *Journal of Colloid and Interface Science* **26**, 62 - 69 (1968).
177. Laaksonen, T., *et al.* Failure of MTT as a toxicity testing agent for mesoporous silicon microparticles. *Chem Res Toxicol* **20**, 1913-1918 (2007).
178. Lin, Y.S. & Haynes, C.L. Impacts of mesoporous silica nanoparticle size, pore ordering, and pore integrity on hemolytic activity. *J Am Chem Soc* **132**, 4834-4842 (2010).
179. Slowing, II, Wu, C.W., Vivero-Escoto, J.L. & Lin, V.S. Mesoporous silica nanoparticles for reducing hemolytic activity towards mammalian red blood cells. *Small* **5**, 57-62 (2009).

180. Malinski, T., Radomski, M.W., Taha, Z. & Moncada, S. Direct electrochemical measurement of nitric oxide released from human platelets. *Biochem Biophys Res Commun* **194**, 960-965 (1993).
181. Vallance, P., *et al.* Direct measurement of nitric oxide in human beings. *Lancet* **346**, 153-154 (1995).
182. Shono, T., *et al.* Involvement of the transcription factor NF-kappaB in tubular morphogenesis of human microvascular endothelial cells by oxidative stress. *Mol Cell Biol* **16**, 4231-4239 (1996).
183. Bowie, A.G., Moynagh, P.N. & O'Neill, L.A. Lipid peroxidation is involved in the activation of NF-kappaB by tumor necrosis factor but not interleukin-1 in the human endothelial cell line ECV304. Lack of involvement of H₂O₂ in NF-kappaB activation by either cytokine in both primary and transformed endothelial cells. *J Biol Chem* **272**, 25941-25950 (1997).
184. Barnes, C.A., *et al.* Reproducible comet assay of amorphous silica nanoparticles detects no genotoxicity. *Nano Lett* **8**, 3069-3074 (2008).
185. Chen, F., Sun, S.C., Kuh, D.C., Gaydos, L.J. & Demers, L.M. Essential role of NF-kappa B activation in silica-induced inflammatory mediator production in macrophages. *Biochem Biophys Res Commun* **214**, 985-992 (1995).

186. Gojova, A., *et al.* Induction of inflammation in vascular endothelial cells by metal oxide nanoparticles: effect of particle composition. *Environ Health Perspect* **115**, 403-409 (2007).
187. Rot, A., *et al.* Some aspects of IL-8 pathophysiology. III: Chemokine interaction with endothelial cells. *J Leukoc Biol* **59**, 39-44 (1996).
188. Cho, M., *et al.* The impact of size on tissue distribution and elimination by single intravenous injection of silica nanoparticles. *Toxicol Lett* **189**, 177-183 (2009).
189. Park, E.J. & Park, K. Oxidative stress and pro-inflammatory responses induced by silica nanoparticles in vivo and in vitro. *Toxicol Lett* **184**, 18-25 (2009).
190. Bihari, P., *et al.* Single-walled carbon nanotubes activate platelets and accelerate thrombus formation in the microcirculation. *Toxicology* **269**, 148-154 (2010).
191. Li, X., *et al.* Platelet compatibility of PLGA, chitosan and PLGA-chitosan nanoparticles. *Nanomedicine* **4**, 735-746 (2009).
192. Moro, M.A., *et al.* The formation of nitric oxide donors from peroxynitrite. *Br J Pharmacol* **116**, 1999-2004 (1995).